Conceptual Design of a Pile Installation Frame with Adjustable Footprint

P.J. Stins

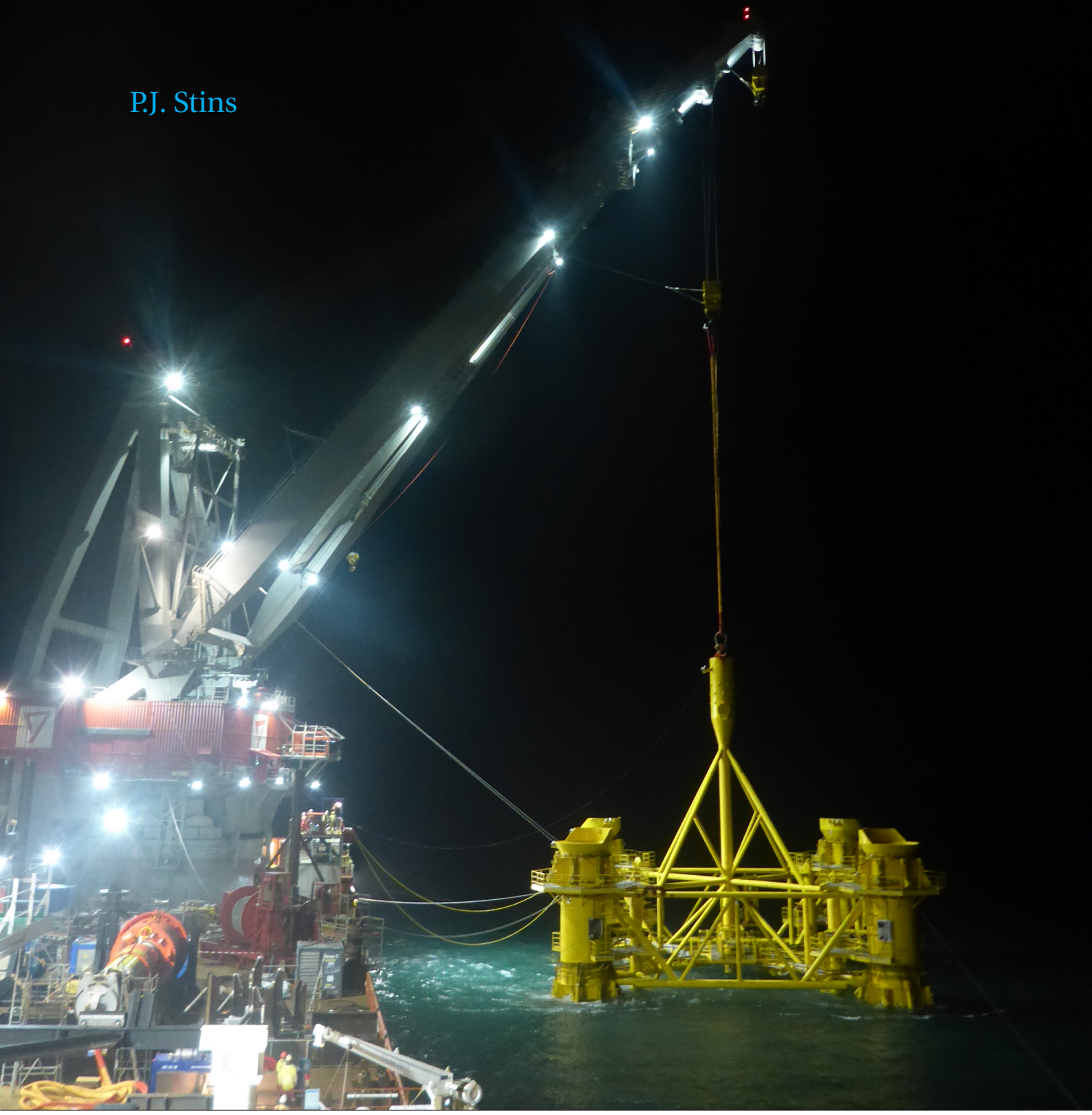

TU Delft Delft University of Technology

Seaway Heavy Lifting

Challenge the future

Conceptual Design of a Pile Installation Frame with Adjustable Footprint

by

P.J. Stins

in partial fulfilment of the requirements for the degree of

Master of Science

in

Offshore and Dredging Engineering
Bottom Founded Structures, Arctic and Wind

to obtain the degree of Master of Science at the Delft University of Technology, to be defended publicly on Wednesday December 19, 2018 at 10:30 AM.

Student number: 4386604

Thesis committee:

ir. P.G.F. Sliggers,	TU Delft, chairman
dr. ir. K.N. van Dalen,	TU Delft
ir. P.C. Meijers,	TU Delft
ir. A. Shahbazkhani,	Seaway Heavy Lifting

TU Delft Delft University of Technology

Seaway Heavy Lifting

Preface

The New York Times, September 2017: "Caribbean Devastated as Irma Heads Toward Florida"[11]. Irma is one of the most powerful ocean hurricanes ever recorded. This is one of the consequences of the widely discussed "Global Warming".

Since this century, global warming is accepted as a major problem and gradually governments work on solutions to restrain this. Finally, the whole world faces the problem and made commitments about the emissions during the Paris Climate Conference (COP21) in December 2015. The agreement with 195 countries sets out a plan to reduce the global warming below 2°C [5]. A couple of solutions are possible, reduce the energy consumption and/ or generate energy by sustainable methods. To achieve the commitments most governments increases the investments in sustainable energy, what induces an up-trend, which is also noticeable in the offshore wind industry.

Seaway Heavy Lifting participate in the offshore wind industry with their installation services. Thanks to this company I got the chance to do my master thesis project related to the renewable industry, and contribute on small scale to the reduction of the greenhouse gases. In combination with my passion for heavy steel structures, the topic about the pile installation frame was a nice opportunity.

Thanks to the helpful people in the office, I was able to solve all kind of challenges and questions. In particular, I want to thank Amin Shahbazkhani, which was always willing to discuss about solutions and the interpretation of the results during the project. Thereby, I also want to thanks Shafiek Suliman and Pellegrino Guerriero for the support with the software SACS.

Especially, I would like to thank Peter Meijers who had the role of university supervisor. During the whole project I faced various difficulties, which I could talk through and finally makes more easy with his help.

Thereby, I would like to express my acknowledgement towards my committee members, ir. P.G.F. Sliggers, (and once again) ir. P.C. Meijers and ir. A. Shahbazkhani, for their guidance and support.

P.J. Stins
Zoetermeer, December 2018

Table of Contents

Summary

An offshore wind turbine is placed on a so called “foundation” to gain height above the sea surface level. One of the used foundations is the jacket structure, which is kept in place by pre-piled supports. The piles are hammered into the seabed first, after which the jacket legs are stabbed into the piles. A template is used to guide the piles during installation and to secure the relative distances as well as the straightness and depth of the piles with respect to each other. This template is called the Pile Installation Frame (PIF).

Seaway Heavy Lifting has designed a PIF with a fixed footprint for the Beatrice offshore wind farm project. However, there is a need to make the PIF adjustable in order to use it in different situations (e.g. environmental conditions, pile designs and jacket configurations). Therefore, this thesis investigates the following two questions: “How can the current PIF be altered in order to make the footprint adjustable for various footprints?”, and: “What are the influences of variations in pile designs and conditions?”.

A trade-off method is used to find the most feasible conceptual design. Resulted in interchangeable frames connected between the original pile supports and the center base frame (with equipment and a lifting point). The integrity of the concept is checked for one of the operational scenarios, namely, “the in-place scenario”, i.e., the PIF is at the seabed and the piles are stabbed into the sleeves with a hydraulic hammer on top of one of the piles.

A model of the concept design is made with the structural simulation software SACS, that does not account for the second order bending effect of the pile. Therefore, a new calculation model is developed. This model calculates the reaction forces from the piles onto the PIF, and it is based on the linear wave theory, a linearised approached current profile, and the Morrison equation. The bending of the pile is computed using the Euler-Bernoulli beam theory, which is iteratively solved to take into account the second order bending effect.

The PIF is checked for the minimum square footprint of 20 m, 24 m and the maximum of 32 m for a representative reference condition (Beatrice offshore wind farm). From the check, the maximum stress level in the members and braces is below half of the maximum allowable stress. Furthermore, the deformations at the pile supports in the sleeve are in the same order of magnitude than the current PIF. Hence, these are not critical for the installation tolerances in the same conditions.

To show the influences of the variations per project in pile design and conditions, an analysis is executed. From the analysis, it is concluded that the forces on the frame are maximum when the hammer is at the seawater level. Moreover, a pile diameter of 2.2 meter is the optimum for the reference condition. It is also observed that, the influence of the pile thickness is not considerable with respect to the forces onto the frame.

The forces in the members and braces of the frame are mainly caused by the pile reaction forces transferred to the PIF. Therefore, the calculation model can be used for a first estimation of the PIF integrity. When the reaction forces are lower than for the reference conditions, the PIF can be used; when they are higher, an additional analysis with SACS is required.

1 Introduction

Seaway Heavy Lifting (SHL) is an offshore contractor in the Oil & Gas and Renewable Industry and operate through the whole world. The company offers Transport and Installation solutions (T&I) as well as Engineering, Procurement, Construction and Installation solutions (EPCI). Two monohull crane vessels, Stanislav Yudin and Oleg Strashnov, are in full ownership of SHL. These vessels have significant lift capacities of maximum 2,500 and 5,000 tonnes and are well known for the exceptional working characteristics. Seaway Heavy Lifting owns all kinds of support equipment like: rigging, hammers, pile handling- and pile installation tools.

The support structure of an offshore wind turbine, like the word says, supports the wind turbine to gain enough height above the sea surface level. Currently, the following support structures are applied (installed share): Monopile (80.8%), Gravity (7.5%), Jacket (6.6%), Tripod (3.2%), Tripile (1.9%), Floating (0.02%)[8]. The monopile is the most applied substructure. The new offshore wind farm projects moves to deeper waters and further offshore, leading to larger wind turbines, therefore jacket substructures become more popular.

A jacket structure is kept in place at the seabed by piled foundations. The installation of the piles depends on the design of the jacket, for some jacket installations the piles are installed first after which the jacket legs are stabbed in the piles, also called pre-pile installation (A sketch of a pre-pile jacket stabbed into the piles is given in figure 1.1).For the installation of the piles a template is used to secure the distances as well as the straightness and depth of the piles into the soil. This template, named the Pile Installation Frame (PIF) is the topic of this Master Thesis.

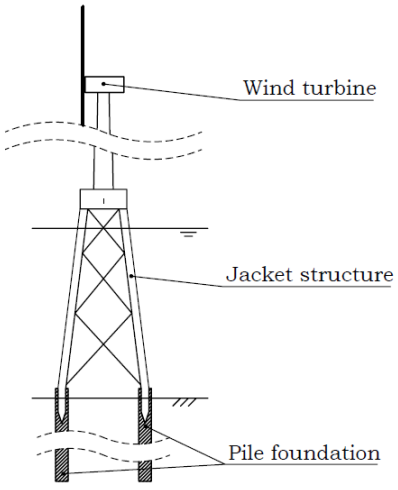

Figure 1.1: Pre-piled jacket substructure

Figure 1.2: Pile installation frame for Beatrice OWF (with worker mid-right)

Seaway Heavy Lifting has designed the current PIF (figure: 1.2) specially for the Beatrice offshore wind farm (OWF) project, located at the coast of Scotland in the Northern North Sea. This PIF is more than 30 meters height, which equals approximately 17 full grown people on top of each other. The Beatrice wind farm includes 84 turbines of 7 MW and two substations, both with pre-piled jacket structures. These turbines will provide energy equivalent to the needs of roughly 450,000 homes [3], and covers an area comparable to 26,000 football fields, in water depths from 35 meter up to 55 meter [1]. The responsibility of Seaway Heavy Lifting for this project, was the installation of the pile foundations and the jacket structures.

Because of a relatively short design period, SHL decided to make a fixed framing, which makes the PIF suitable for only the particular footprint of 24 meter center to center. Since the project is finished SHL wants to use the PIF for future projects in different situations.

Therefore, this thesis investigates the following two questions:
"How can the current PIF be altered in order to make the footprint adjustable for various footprints?", and:
"What are the influences of the variations in pile designs and conditions?".

In order to answer these questions, the structure of the report is as follows, with the relations between the chapters given in figure 1.3. Firstly, in chapter (2), a brief background of the current PIF is given with the operational procedure. In chapter 3 the design requirements and criteria are given. Chapter 4 answers the question: "What conceptual design is most feasible to work out further". Followed by chapter 5, where the description of the developed model is given, to calculate the forces from the piles onto the PIF. In the subsequent chapter 6, the question is answered: "Is the conceptual resistant to the reference conditions, and does it satisfy all the requirements?". Chapter 7 contains an analyses, about the influence of the variations in pile designs and conditions. The report ends with the conclusions and recommendations in chapter 8.

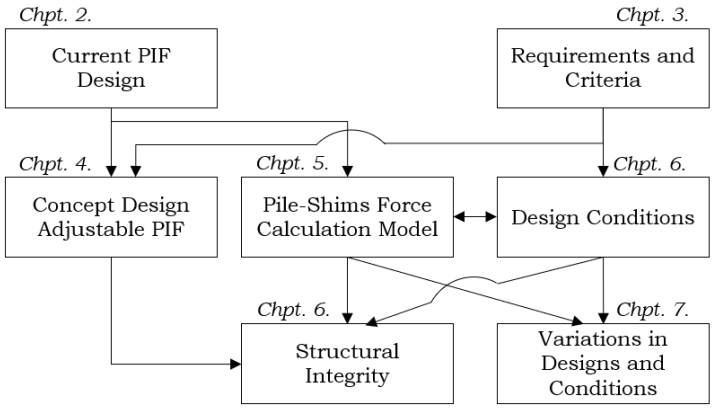

Figure 1.3: Project overview

2

Background: Current Pile Installation Frame

In this chapter, a background is given of the current Pile Installation Frame (PIF) design and about the operational procedure.

2.1. Design of the Current PIF

As mentioned in the introduction the current PIF is specially designed for the Beatrice offshore wind farm, in order to install the piles for the pre-piled jacket structures. The main requirement for this project, were the installation tolerances of the piles. In particular, the center to center distances of 24 meters and the straightness both horizontally and vertically with respect to each other.

The configuration of the PIF is a square tubular frame, which connects the sleeves and other components to each other. A drawing of the current PIF is given in figure 2.1 with the main components indicated. These are briefly described in the following list:

- ILT-bucket
  The Internal Lifting Bucket is a casing where a lifting tool can be placed; this is the same lifting tool as is used for lifting of the piles.
- Centre platform
  The centre platform contains a hydraulic powerpack, electronics and sensors for monitoring.
- Sleeves
  The sleeves are cylinders of 3.6 meter diameter, at the corners of the PIF. These are designed, to place and center the pile in. The sleeves contains hydraulic shims, monitoring sensors and cameras.
- Mudmats
  The mudmats prevent the PIF from sinking into soft unconsolidated soil on the seabed.
- Inclination sensors
  The Inclination sensors, are used to monitor the inclination of the PIF, and consequently, also the straightness of the piles.

As you can imagine, the seabed is not smoothly and straight. So, when the PIF is placed onto the seabed, this should be compensated, in order to satisfy the installation tolerances of the piles. Therefore, the PIF is performed with a hydraulic system to compensate for this irregularities. According to the requirements, this system together with the sleeves and mudmats should be reused for the new design. Therefore, this part of the current PIF is shown in more detail in figure 2.2.

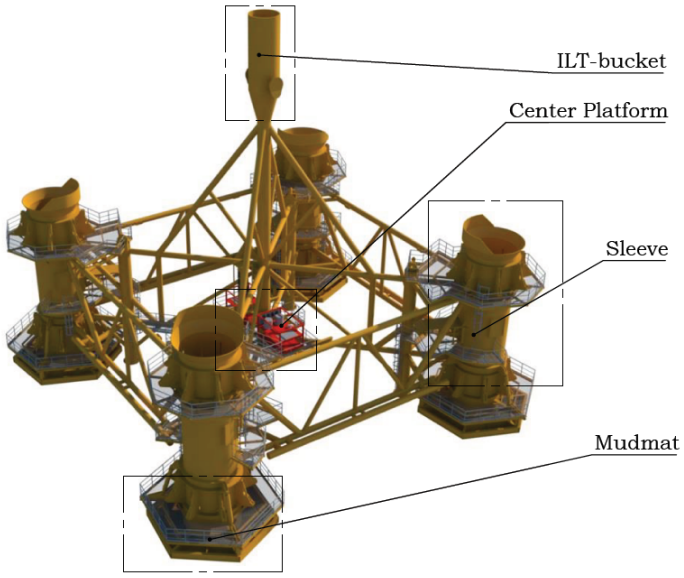

Figure 2.1: Current PIF with the main components indicated

The lower part of the sleeve with the mudmat and hydraulic cylinders, are shown in figure 2.2b. The mudmat is connected to the sleeve with three hydraulic cylinders. These cylinders can be extended to push the sleeves upwards. By extending the individual sleeves and measuring the inclination, the PIF can be levelled straight.

The shims are located at the bottom and the top of the sleeve as indicated in figure 2.2a. These can be extended hydraulically to center the pile in the middle of the sleeve (see top view figure 2.2c). The shims can also be retracted, to be able to go into the sleeves with a wider hammer. This is nesceserry to reach the target penetration of the pile. In other words, the piles should be penetrated into the soil further than the top shims.

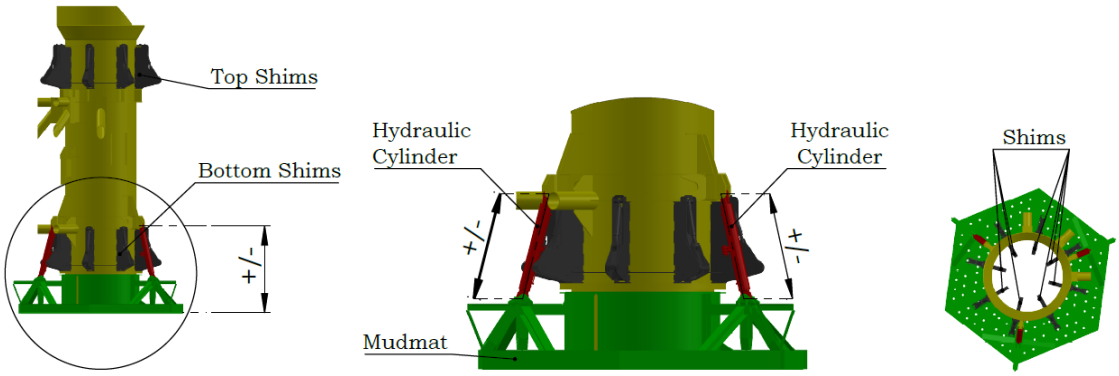

(a) Sleeve (b) detail view (c) Top view

Figure 2.2: Sleeve (yellow) with mudmat (green) shims (grey) and hydraulic levelling cylinders (red)

2.2. Procedure to Install the Piles

The procedure to install the piles with the pile installation frame is explained in this section. The following list gives the steps of the procedure (with related sketches given in figure 2.3):

1. Transport the PIF to the desired location with the Heavy Lift Vessel
2. Lift PIF to the seabed with the internal lifting tool
3. Level to horizontal with hydraulic levelling system
4. Stab Piles into the sleeves
5. Drive the piles to target penetration into the seabed
6. Retrieve the PIF to the Heavy Lift Vessel

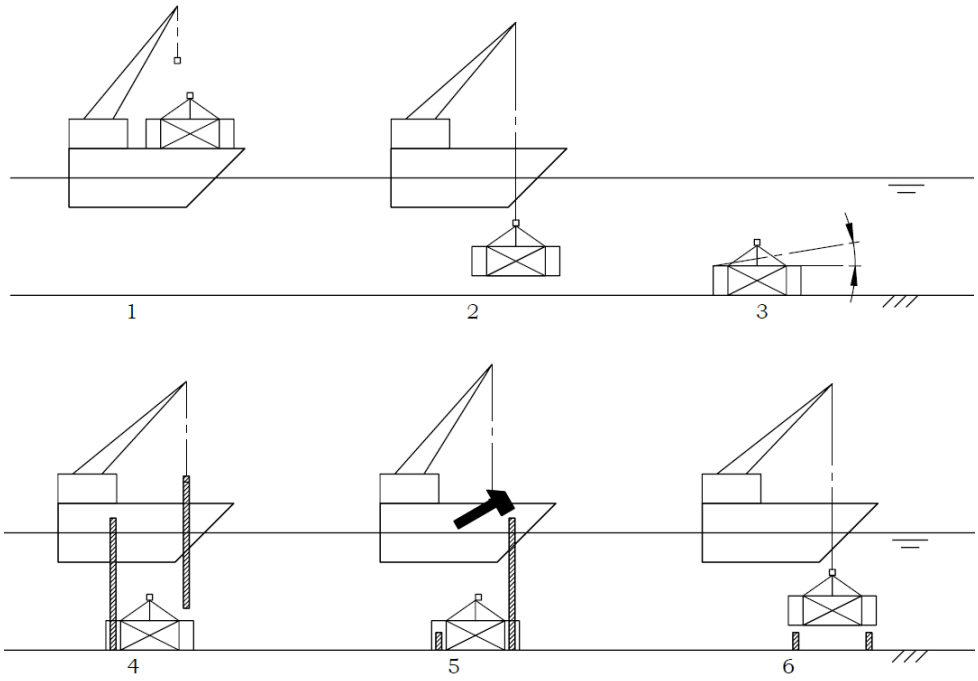

Figure 2.3: Pile installation procedure

Subsequently, these steps of the procedure are explained in more detail.

1. Transport the PIF to the desired location with the heavy lift vessel

   First, the frame is transported to the desired location on deck of a Heavy Lift Vessel (HLV). The frame is bolted to a specially fabricated structure which is connected on deck to secure it for sea conditions. To reduce the required deck space and to sail with the crane boom in the transport mode, the PIF is placed out of center of the HLV, as can be seen in figure 2.4. When the HLV has arrived at the location to install the piles, the sea-fasting is released.

2. Lift PIF to the seabed with the Internal Lifting Tool

   The next step is to hook the PIF to the crane. As mentioned in section 2.1 an internal lifting tool is used. This tool is inserted into the ILT-bucket, after which it hydraulically clamps itself. The same tool is also used for lifting the piles. So, without changing of equipment the lift procedure can be continued.

3. Level to horizontal with hydraulic levelling system

   Every individual sleeve is connected to an mudmat with three hydraulic cylinders. By extending these cylinders, the PIF can be levelled horizontally, up to a seabed slope to 2 degrees. With measurement equipment the straightness of the PIF is perceived.

4. Stab Piles into the sleeves

   When the PIF is placed at the right location and levelled straight, the piles can be stabbed into the sleeves. The piles are lifted from a barge, through the waterline, into the sleeves. For a controlled operation, the pile tip is observed by cameras on a Remotely Operating Vehicle (ROV: unmanned underwater robot). Such, that the crane operator can see the operation under water.

5. Drive the piles to target penetration into the seabed

   The internal lifting tool is placed on deck and the hydraulic impact hammer is lifted on top of the pile. Then the piles are hammered one by one to target penetration.

6. Retrieve the PIF to heavy lift vessel

   When the piles are at the required position and depth, the PIF can be retrieved back on deck of the HLV. The internal lifting tool is hooked again, and the PIF can be lifted to the deck. At the deck the PIF is sea-fastened again. After the internal lifting tool is placed on deck and the crane boom is in transport mode, the HLV is can sail to the next location.

Figure 2.4: Current PIF on deck of with ILT in slings of the crane

3

Design Requirements and Criteria

In the total organisation of an offshore wind farm design, a lot of parties are involved. These all have requirements and criteria that should be met for any particular part of the design and/ or installation process. In this chapter these requirements and criteria are listed and explained.

A distinction is made, between design requirements and criteria. The definition of design requirements: "state the important characteristics that your design must meet in order to be successful" [4], these are the characteristics which are measurable and should be checked. The unmeasurable characteristics to meet, are classified by the criteria.

First, the list of requirements and criteria are presented. Then, these are discussed in more detail.

3.1. List of Requirements and Criteria

Requirements

1. The design should be capable to install the piles within the prescribed tolerances.
2. The frame should be adjustable to three and four leg footprint configurations with a center to center distance varying from 20 meter to 32 meter.
3. The integrity of the PIF against the environmental conditions should be higher than the maximum operable sea states of the Stanislav Yudin to do the installation.
4. The maximum gross weight of the design should not reach the maximum lifting capacities of the heavy lift vessels.
5. Lifting with an internal lifting tool.
6. The following parts of the current PIF should be reused:
   (a) Sleeve with the mudmat and levelling system.
   (b) Equipment of the center platform.
7. Transport on deck of the heavy lift vessel (HLV).
8. Adjustment of the footprint on deck of the HLV.
9. The framing and equipment of the PIF should be accessible to inspect and repair.

Criteria

1. The design should satisfy the ISO codes for the petroleum and natural gas industries: 1990X.
2. Safety during fabrication, operation and maintenance.

3.2. Requirements in Detail

1. The design should be capable to install the piles within the prescribed tolerances.

   The designer of the jacket foundation structure assumed reasonable tolerances for the pile installation to base the jacket design on. If the installation of the piles are out of tolerance, the jacket cannot be placed onto the piles.
   The pile installation tolerances of the Beatrice offshore wind farm are assumed to be representative for future projects as well. These are given in table 3.1, and clarified with help of figure 3.1.

Description	Tolerances
Centre pile to centre pile	+/- 100 mm
Absolute vertical position w.r.t. target elevation	+/- 100 mm
Relative pile top height between lowest and highest pile	100 mm
Final inclination w.r.t. vertical	0.5°

Table 3.1: Installation tolerances

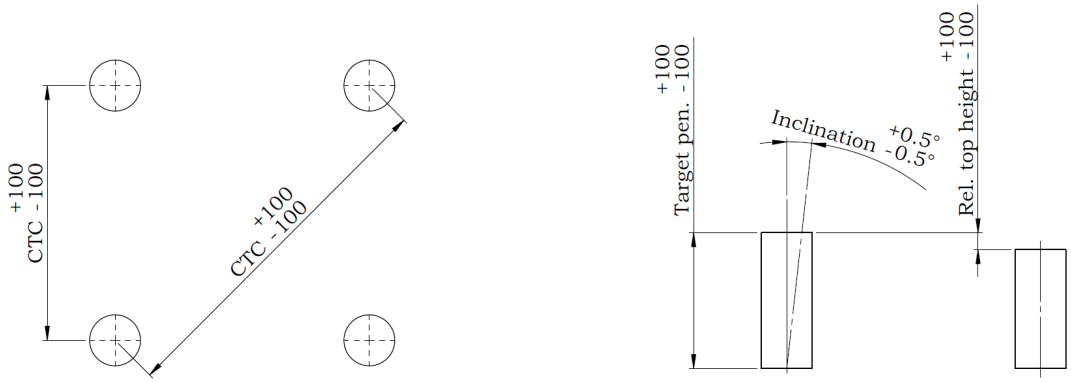

(a) Top view (b) Front view

Figure 3.1: Drawing of the square footprint with the pile installation tolerances (dimensions in mm)

2. The frame should be adjustable to an three and four leg footprint configurations with an center to center distance varying from 20 meter to 32 meter.

   The configuration of the PIF is depended on the footprint of the foundation structure design. These footprints variates per location and sometimes even within one project. Based on the prospectives and current project request for pile installation projects, the minimum and maximum variations are set for both an three legged as an four legged footprint.

3. The integrity of the PIF against the environmental conditions should be higher than the maximum operable sea states of the Stanislav Yudin

   Seaway Heavy Lifting wants to install the piles with theirs own heavy lift vessel, the Stanislav Yudin, at all potential wind farm locations. Since every location has different environmental conditions, the operability of the Stanislav Yudin is taken as the limiting factor. The limiting sea states are from a dynamic analysis, with ANSYS simulation software. This is executed by the naval engineering department, for the current PIF. The maximum operable sea states are given in table 3.2, together with the survival condition.
   Seaway Heavy lifting wants to be able to leave the PIF at the seabed in any unexpected or emergency situation. For instance, the environmental conditions are worse than was predicted. For this, Seaway Heavy Lifting has a general assumption of the maximum survival sea state.
   According to the ISO Code [2], the maximum wave height can be calculated from the significant wave height: $H_{max} = 1.87 \cdot H_s$.

Table 3.2: Maximum operational and survival wave conditions for the Stanislav Yudin with the current PIF

		Operational								**Survival**
t_p	(s)	4	5	6	7	8	9	10	11	8.2
H_s	(m)	1.11	1.8	2.43	1.89	1.13	0.7	0.52	0.45	3.50
H_{max}	(m)	2.08	3.37	4.54	3.53	2.11	1.31	0.97	0.84	6.50

4. The maximum weight of the design should not reach the maximum lifting capacities of the heavy lift vessels.

   The installation of the piles should be done with the heavy lift vessels of Seaway Heavy Lifting. Therefore, the lifting capacities should not be exceeded. The lifting capacities depends on the distance the crane has to reach to the side of the vessel. The limiting load capacities are given in figure 3.2.

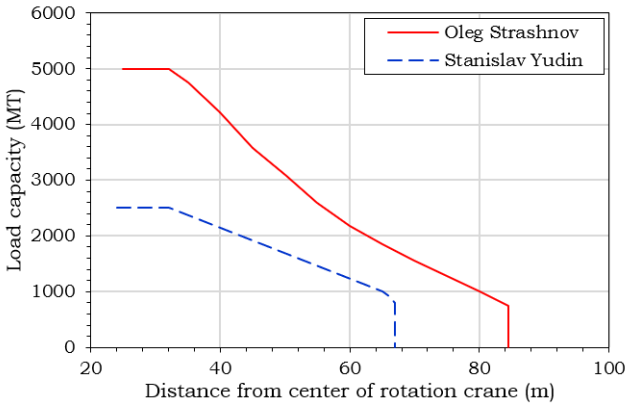

Figure 3.2: Load capacity over the distance from the center of rotation of the crane for both HLVs

5. Lifting with an internal lifting tool.

   Seaway Heavy Lifting wants to use a internal lifting tool to lift the piles and the PIF, as the current internal lifting tool had performed well in previous projects.

6. Reuse of the sleeve, mudmat, levelling system and the equipment of the center platform.

   The sleeve with the mudmat and levelling system are the most expensive parts of the current PIF. Since the current PIF installed all the piles within the tolerances, Seaway Heavy Lifting wants to reuse these components for the new design.

7. Transport on deck of the heavy lift vessels.

   Seaway Heavy Lifting wants to place and transport the new design PIF on deck of both heavy lift vessels.

8. Adjustment of the footprint on deck of the heavy lift vessels.

   For some pile installation projects multiple footprints should be installed. Therefore, the footprint should be changed on deck of the heavy lift vessels, so the installation can be continued as quickly as possible.

9. The framing and equipment of the PIF should be accessible for inspection, repair and maintenance.

   The PIF shall be used multiple times within an offshore wind farm project. To avoid down time, the reliability of the PIF should be checked in between installations, and if necessary also repaired and maintained.

3.3. Criteria in Detail

1. The design should satisfy the ISO codes for the petroleum and natural gas industries: 1990X.

   The PIF should be designed by standards/codes for the offshore industry. Worldwide mainly three standards/codes are used, namely: DNV GL, API RP 2A and ISO 1900X. The standard/ code to use depends on the government and authorities, the developer and main contractor. The design brief of the Beatrice offshore wind farm required to design according to the LRFD (load resistance factor design) principle. The ISO code is widely accepted and therefore preferred.

   For special tools like the PIF, no specific codes are available. Therefore, is suggested to the classification company DNV to use the code for fixed steel structures. The DNV, which is responsible for the certification of the PIF, approved this suggestion. Consequently, the PIF should be designed according to the ISO for fixed steel structures.

2. Safety during fabrication, operation and maintenance.

   Seaway Heavy Lifting works according to an incident and injury free program, which drives continuous improvement and demands full compliance with national and international regulatory requirements.

4

Design Concept Generation

This chapter covers the generation of the conceptual design for a PIF with an adjustable footprint. The concept generation process, answers the question as stated in the introduction: "How can the current PIF be altered in order to make the footprint adjustable for various footprints?".

First, is explained way a frame is needed, followed by a trade off between different concepts to adjust the PIF. Then an explanation is given, how the sleeve connections with the frame should be modified. Next, the material and profiles are defined. And concluded, the configuration is given of the concept design with adjustable footprint.

4.1. Install Piles at Different Footprints

In this section is explained why a pile installation frame is needed, while other options also may be possible. First two other options are introduced, followed by the pile installation frame.

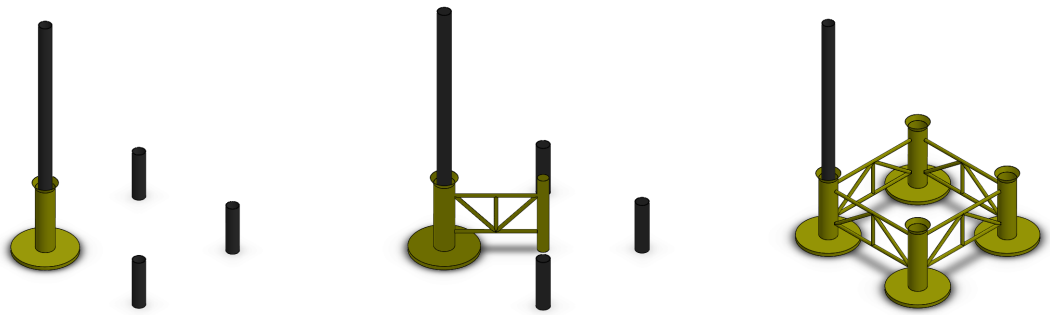

(a) One-by-one (b) Rotate (c) Frame

Figure 4.1: Methods to Install the Piles

a. Replace Sleeve one-by-one
Installation of the piles with one sleeve (one-by-one; figure 4.1a), makes it is possible to install the piles at any place. And, thus is applicable for all possible footprints. Also, this concept takes little deck space, and requires little fabrication, since no framing is needed. Although, the installation of the piles with one sleeve has difficulties to achieve the installation tolerances of the piles. Firstly, because the sleeve should be replaced for every pile, which makes it challenging to do relative measurements between the piles. Secondly, the overturning moment due to the external load should be counteracted by only one mudmat. To keep the pile vertical, undoubtedly the mudmat should be redesigned. As stated in the requirements, the sleeve with mudmat and levelling system needs to be reused. Furthermore, the installation procedure takes relatively much time, because of the multiple replacement for one footprint. Overall, this option is not feasible with respect to the requirements.

Option b. Rotate Sleeve around middle
One sleeve is connected with a frame to the middle of the footprint. There it is secured in the soil, and the sleeve can be rotated around it (figure 4.1b). The secured middle act as a reference point for the relative pile measurements, also to ensure the right distance of the piles with respect to the middle. Although, to install the next pile of the footprint, the sleeve should be lifted over the pile. Resulting in a relative time consuming installation procedure, and in significant technical and structural design challenges. When the environmental load is perpendicular to the frame, the single mudmat should counteract the overturning moment of the pile. Therefore, also for this option, an other mudmat design is needed. All in all, also this method is not feasible with respect tot the requirements.

c. Pile Installation Frame
The pile installation frame exist of three or four sleeves connected to each other. This is introduced, because all piles of a footprint can be installed when the frame is on the seabed. Resulting in a relative short installation time, and consequently, in lower operational costs. In contrast, it takes more deck space and has higher fabrication costs. The pile installation frame is based on proven technology (current PIF), that preciously fulfilled the installation tolerances successfully. Therefore can be stated, that the PIF is feasible. Since the frame is desirable for different projects, the footprint should be adjustable. The adjustable concepts of the PIF are introduced in the next section 4.2.

4.2. Adjustable PIF Conceptual Design

The adjustable PIF is needed for the design as concluded from the previous section. The sleeves are connected to each other with frames. This gives the following problem to solve: What configuration of the framing can be used to connect the sleeves, ILT-bucket and equipment to each other, and can be adjusted to various footprints?

4.2.1. Concepts

Four concepts are introduced and sketched in the figures. Figure 4.2 shows the meaning of the sketched figures.

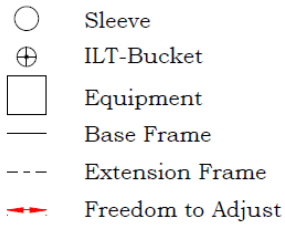

Figure 4.2: Legend for figures

The sleeve, ILT-bucket and equipment are introduced in section 2.1. With base frame is meant, the frame that is the basis of the adjustable PIF, this part is used for all footprints without modifications. The extension frames are the frames that can be adjusted.

Concept a: Star-Frame
The star frame concept (figures 4.3 & 4.4) can be used for a three and four legged footprint using the same base frame.

The operation to adjust the footprint exist of: loosen the connections of the extension pieces, loosen the connections of the hoses and cables, lift the extension pieces, lift the sleeves at the right distances with respect to each other, lift the different extension pieces between the base frame and the sleeves, connect the extension pieces. And, re-connect the hoses and cables from the base frame to the sleeves.

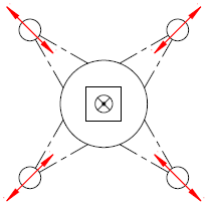

Figure 4.3: Star-Frame square

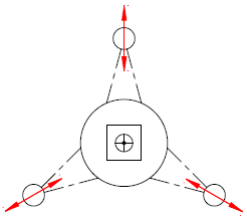

Figure 4.4: Star-Frame triangular

In summary operational (per sleeve to adjust):
- 3x lift
- Middle frame at position during adjustment
- Reconnect hoses and cables

Structural:
- 1 extension piece (per sleeve)
- 3 and 4 legged footprint with one base frame
- The extension piece should be able to take torsional loads
- Different footprints requires different extension pieces

Technical:
- Connections at sleeves, extension pieces and base frame.
- Connections between hoses and cables

Concept b: Sliding Sleeve
Offshore operation of the Sliding Sleeve is considered, because of a time saving adjusting principle. Adjusting the footprint can be done at ease by using an existing mechanism in the frame (figures 4.5 & 4.6 & 4.7).

The adjustment of the footprint is executed as follows: The sleeves are unlocked, then the sleeve will be slid to the right location and locked again.

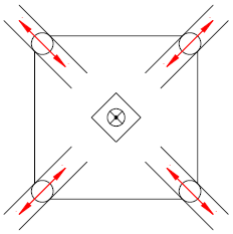

Figure 4.5: Slide-frame square

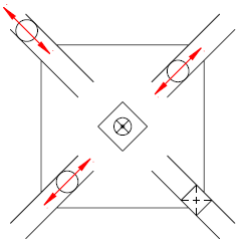

Figure 4.6: Slide-frame square for three piles

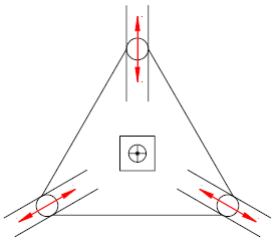

Figure 4.7: Slide-frame triangular

In summary operational (per sleeve to adjust):
- Slide to position
- Unlock and lock sleeve at position

Structural:
- Sliding system
- Locking system
- Mass of frame is constant for all footprints

Technical:
- Push/ pull system to slide the sleeve
- Connections between hoses and cables

Concept c: OX-Frame
The OX-Frame (figures 4.8 & 4.9) is mentioned, as a similar existing frame is used for the Beatrice offshore wind farm project.

The operation to adjust the footprint, is similar to the star frame, except from lifting and connect/ reconnect more extension pieces.

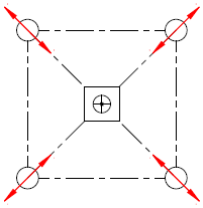

Figure 4.8: OX-frame square

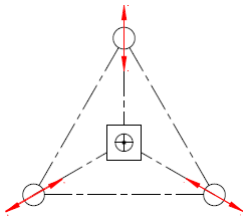

Figure 4.9: OX-frame triangular

Operational (per sleeve to adjust):
- 5x lift
- Reconnect hoses and cables

Structural:
- 2 extension piece (per sleeve)
- Redesign of extension pieces for all footprints
- Use current framing at sleeve

Technical:
- Connections at sleeve, extension piece and base frame
- Different angle to connect sleeve with extension pieces for three and four legged footprint
- Different angle to connect base frame to extension pieces for three and four legged footprint
- Connections between hoses and cables

Concept d: O-Frame
The O-Frame concept (figures 4.10 & 4.11) contains four/ three extension frames, that connect the sleeves to each other.

The operation to adjust the footprint, is similar to the star frame. The main difference for this concept is the ILT-bucket, which is pre-rigged with slings to the frame. This results in an additional operation. Namely, the ILT-bucket should be placed in upwards position, to be able to put the internal lifting tool into it. Upward positioning can be done for instance at the seabed or at the frame.

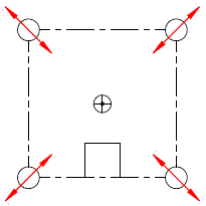

Figure 4.10: O-frame square

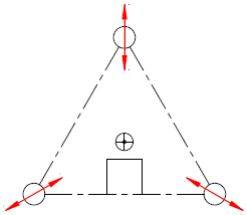

Figure 4.11: O-frame triangular

Operational (per sleeve to adjust):
- 3x lift
- Reconnect hoses and cables
- Pre-rigged ILT-bucket for lift

Structural:
- 1 extension piece (per sleeve)
- Center of gravity is out of center
- Redesign of extension pieces for all footprints
- Use current framing at sleeve

Technical:
- Connections at sleeve, extension piece and base frame
- Different angle to connect sleeve with extension pieces for three and four legged footprint
- ILT-bucket upwards when PIF is at the seabed
- Connections between hoses and cables

4.2.2. Trade-off

The selection of the concept is done according to a trade-off. The concepts are evaluated by rating on four sub-categories: operational, structural, technical and commercial. The commercial subcategory is divided into: operational costs (OPEX), initial costs CAPEX and maintenance costs. The ratings are shown in table 4.1, the higher the number the better the appreciation. Explanation of the ratings are given below.

Table 4.1: Concept ratings

	Weight	**Star** a	**Slide** b	**OX** c	**O** d
Operational	0.25	3	4	2	1
Structural	0.25	1	3	4	4
Technical	0.25	4	1	3	2
Commercial	0.25	2.31	1.98	2.64	1.98
Capex	*0.33*	*2*	*1*	*4*	*3*
Opex	*0.33*	*3*	*4*	*2*	*1*
Maintenance	*0.33*	*2*	*1*	*2*	*2*
Total	1	2.58	2.50	2.91	2.25

Operational/OPEX:
Concept b. can be adjusted within the least time, since no lifting is required. The sleeve only need to be unlocked, slid to the right position, and locked again. With the other concepts, the connections should be loosened, and multiple lifting operations are required to adjust the footprint. Concept d. is lifted with a pre-rigged ILT-bucket, which makes the installation procedure of the piles relatively time consuming, and therefore the operational costs higher.

Structural/CAPEX:
For concept c. and d. the existing sleeve needs the least modifications, since the tubular members are connected at the same positions. Therefore, it needs less investment costs. The design of the slide frame contains no extension pieces.

Technical/CAPEX:
The slide frame is the most sophisticated method to adjust the footprint. This concept requires a the sliding system, resulting in relatively high initial costs.

Maintenance: Concept b. requires more maintenance due to the existence of the sleeve sliding system. For the other three concepts the same inspection and maintenance procedures are assumed.

Concept c. the OX-frame has the lowest initial costs, since the least modifications to the current PIF are needed. Since offshore operational costs are relatively expensive, concept b the slide frame, becomes more interesting when the PIF will be adjusted more often. For this thesis concept c. is worked out further.

4.3. Modification of Sleeve Connection

A requirements is that the sleeve with the mudmat and levelling system should be reused in the new design. It is convenient to reuse as much connected framing at the sleeves as possible. Figure 4.13 shows where the framing is cut from the current PIF. The reused sleeve including connected framing, for the adjustable PIF is given in figure 4.12.

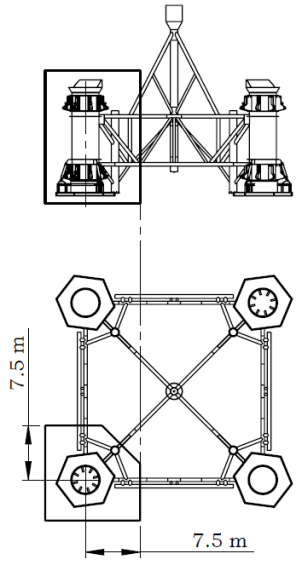

Figure 4.12: Cut lines current PIF

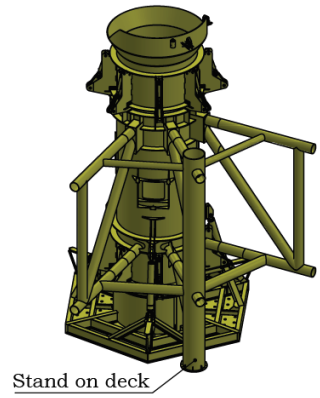

Figure 4.13: Cut sleeve with connected members

4.4. Center Base Frame with Equipment

The base frame in the center, contains the equipment needed for the systems. The base frame will be reused for all the square configurations. A design with additional connection points mikes it possible to use it also for a triangular configuration (not included in this report). The center frame contains enough space for the equipment, this is shown in figure 4.14, where the major equipment is randomly placed. Also the ILT is connected, above the COG of the frame. The outer dimensions of the base frame are such, that for the smallest footprint (20 x 20 meters), no interchangeable frames are needed to connect the center frame to the sleeves.

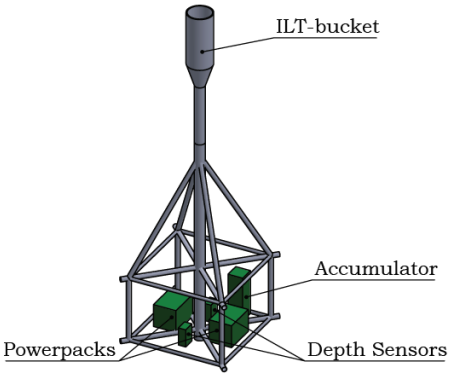

Figure 4.14: Center base frame with equipment

4.5. Material and Profile

In this section is decided which material and profiles to use for the adjustable PIF design. Steel is a widely used material in the offshore industry, and the ISO code is predominately dedicated to steel offshore structures with tubular members. The connected profiles at the sleeve also contains tubular members. Therefore, it is convenient to use the same steel tubular members for the adjustable PIF. The most commonly used steel for offshore structures is S355, which is also used for this concept design. Table 4.2 shows the applied members with its properties.

The main advantage of tubular members is that the resistance to bending in all directions is equally. Steel S355 is relatively easy to machine and weld with respect to more high strength steels.

Table 4.2: Member Properties

Property		**Unit**	**Main Members**	**Cross Members**
Outer Diameter	D	(mm)	457	323
Wall Thickness	t	(mm)	12.7	12.7
Yield Strength	ρ_{steel}	(kg/m^2)	7800	7800
Youngs Modulus	E	(N/mm^2)	205,000	205,000
Shear Modulus	S	(N/mm^2)	82,000	82,000
Yield Strength	f_y	(N/mm^2)	355	355

4.6. Conclusion and Recommendation

The Pile Installation Frame (PIF), with interchangeable connections between the original sleeves and the center base frame, is the most feasible conceptual design to alter the existing PIF design. This concept, shown in figure 4.15, contains eight interchangeable frames. Moreover, the center base frame (with equipment and a lifting point) is usable for all footprint configurations. According to the trade-off, this concept requires the least investment costs for the modifications, because the existing sleeve connections are reused. However, the operational time to adjust the footprint is relatively time consuming. Assuming the footprint is not adjusted on a regular base, this is of secondary importance.

The members of the interchangeable frames are tubular from steel S355. The total operational procedure is the same as for the current PIF, which is described given in section 2.2.

The PIF should be transported on deck of the heavy lift vessels. In appendix A.1 the maximum footprint configuration is shown on deck of the vessels. For the Stanislav Yudin the additional members (green) should be taken off during transport, because of a conflict with the crane boom in transport mode.

When the footprint of the PIF should be adjusted on a regular basis, the operational costs become more important than the investment costs. In that case the conceptual design, where the sleeves can slide to all positions, should be considered. The adjustment of this concept is less time consuming during offshore operation. So, the more the frame needs to be adjusted, the more interesting this concept becomes.

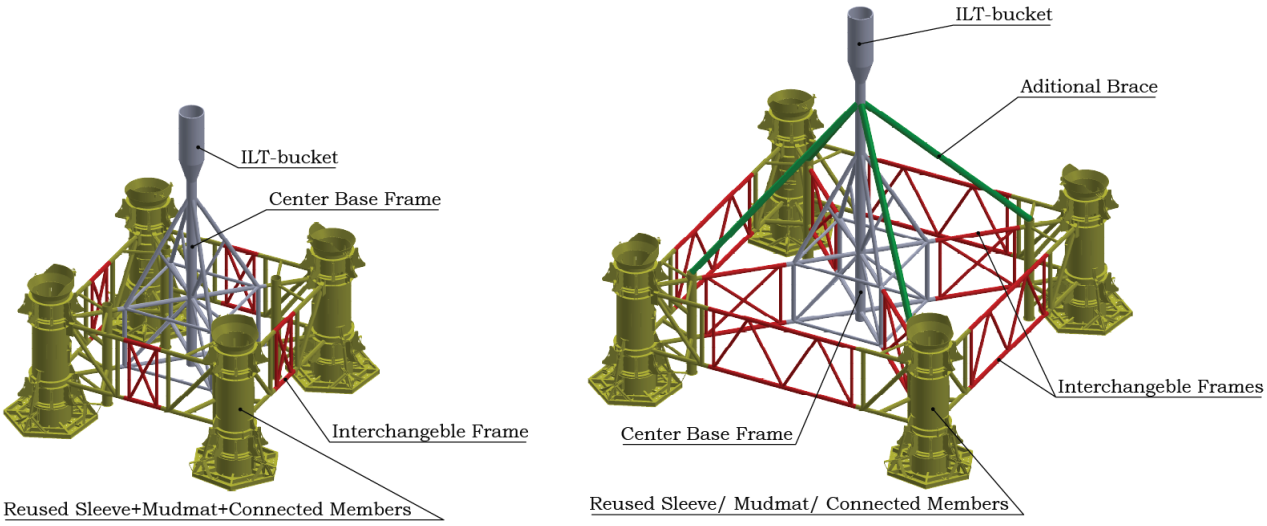

(a) concept minimum footprint: 20x20 meter

(b) concept maximum footprint 32x32 meter

Figure 4.15: Sketches of adjustable frame in minimum and maximum square footprint configuration

5

Pile-Shims Force Calculation Model

In this chapter, the model is described to calculate the reaction forces from the piles onto the shims in the sleeve. This new model is introduced for three reasons. Firstly, the structural simulation software SACS is not capable of taking the second order bending effects into account. Secondly, the pile bending due to the environmental forces is calculated directly within the model, so no additional calculation with SACS is needed. Thirdly, for the current PIF a calculation method was used with rough approximations.

In the subsequent sections, first the calculation procedure is explained, followed by the representation of the model, and the theoretical framework. Then and the individual calculation steps are explained. Concluded by a verification of the model and a conclusion and discussion.

5.1. Calculation Procedure

In this section the procedure is explained to calculate the static forces onto the shims. The procedure is shown in the flowchart of figure 5.1.

The main reason of generating the calculation model is the second order effect. The definition of the second order effect is: "The second order effect, also called P-delta effect, are those caused by eccentric applied loads. When an axial compressive force simultaneous occurs with eccentricity, this creates additional bending in the member, causing the internal moments to be higher.".

The input of the model exist of the design of the pile, the design of the hammer, the wave and current motions, and the gaps between the shims and pile.

The gaps and the environmental load results in eccentricity of the pile, hence also displacement of the pile top ($v_{A1,initial}$). Consequently, the hammer on top of this pile and the pile itself, are eccentric applied loads. Since the pile bends further by this second order effect ($v_{A1,2nd}$), this calculation is repeated till the results converges.

The output of the model is than calculated by adding the reaction forces due to the second order effect ($R_{2,2nd}$, $R_{3,2nd}$) and the environmental loads ($R_{2,env}$, $R_{3,env}$) together. This gives the total reaction forces at the top shim (R_2) and bottom shim (R_3). From the model also the reaction forces due to second order effect are gained and the total displacement of the pile top (v_{A1}).

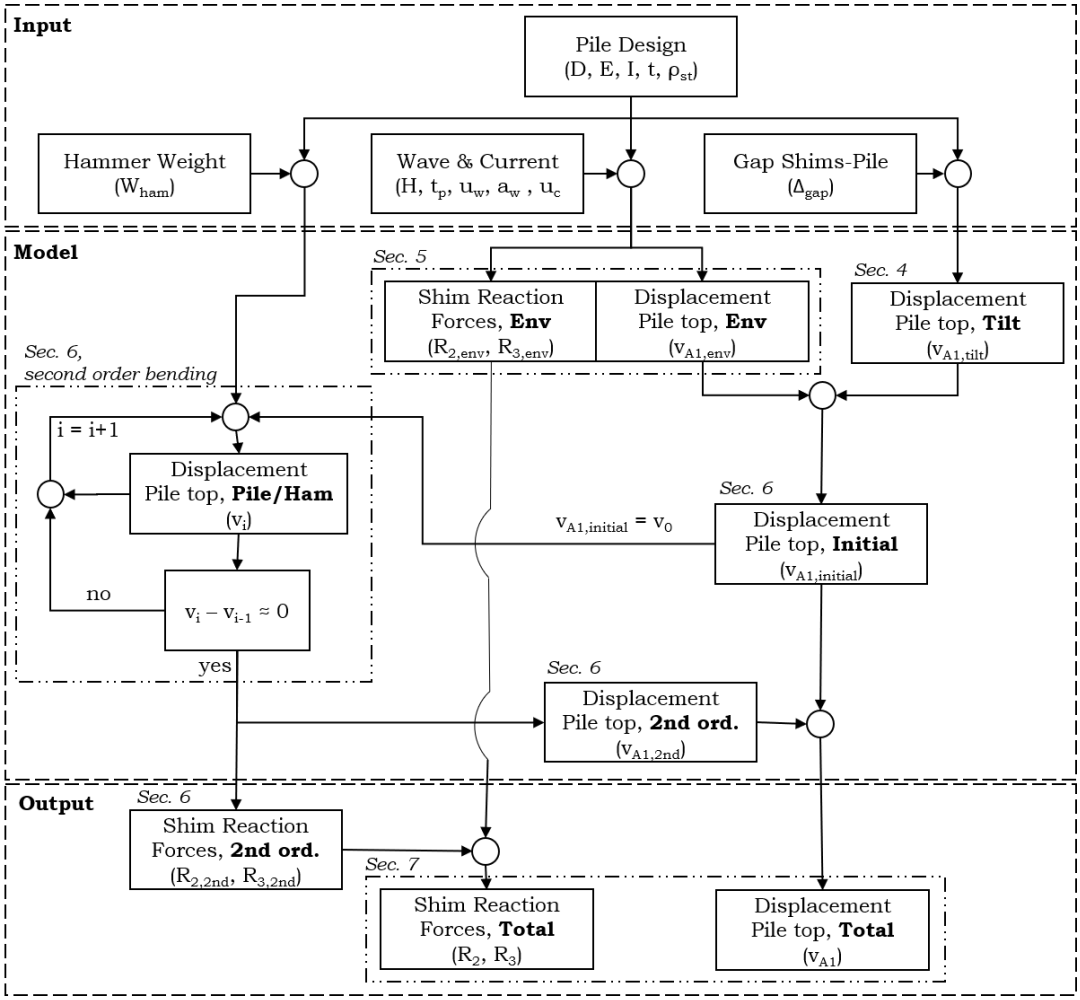

Figure 5.1: Calculation procedure of the Pile-Shims calculation model

5.2. Model Representation of the Pile-Sleeve

This section contains the model representation of the pile and sleeve.

5.2.1. Free Body Diagram

As mentioned in the introduction, the sleeve is designed to guide the piles straight into the soil. In figure 5.3 a section view of the sleeve is given, where the shims are visible. The shims are at the bottom and the top of the sleeve. The free body diagram is shown in figure 5.2 with the assumption explained in the text.

The pile into the sleeve is supported in horizontal direction by the top (2) and bottom (3) shims. Along these shims the pile can slide freely into the soil. Therefore, the shims are modelled as freely supported hinges in z-direction with a fixed relative distance. The distance between the top and bottom shims (L_B) is constant. Because the shims are fixed in the sleeve.

The initial pile penetration is a result of the self-weight of the pile. When the pile is stabbed into the sleeve, it goes into the soil until the soil gives enough frictional resistance to support the pile. The soil can be modelled as distributed horizontal, vertical, and rotational springs. For a conservative calculation, the initial penetration is assumed to be small. The less penetration depth, the more pile above the top shim, what results in higher environmental loads, and consequently higher reaction forces.

This minimal penetration also means, that the soil stiffness against rotation is negligible. Because, there is little soil to counteract the rotation of the pile. Moreover, the influence of the distributed springs are small, since these act on a small pile length. From this can be concluded, that for conservative calculation the soil can be modelled as a hinge freely supported in x direction. Although, to be able to say something about soil stiffness, the distributed horizontal springs are assumed as one spring at the tip of the pile.

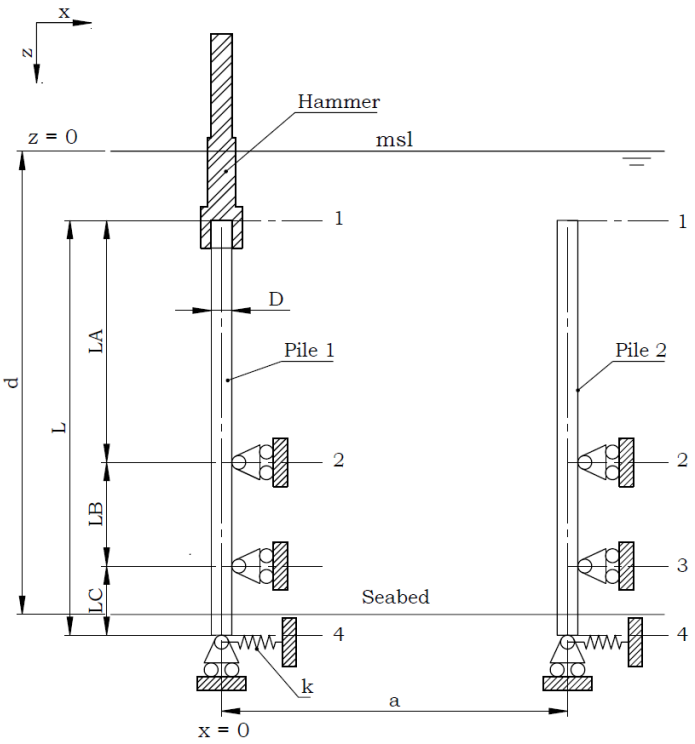

Figure 5.2: Free body diagram pile - sleeve

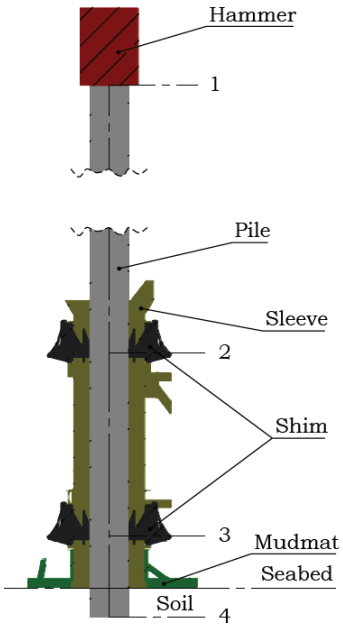

Figure 5.3: Section view: sleeve, pile, hammer

5.2.2. Boundary and Interface Conditions

To identify the locations of the boundary and interface conditions, the pile is divided in three sections: A, B and C. The sections are between the nodes: 1, 2, 3 and 4. An overview of the nodes and sections is given in figure 5.4. Node 1 is at the top of the pile, node 2 at the upper shim. Node 3 is at the lower shim, with and node 4 at the tip of the pile (4).

For the calculation model the boundary and interface conditions of the pile at the nodes are needed. These are given in expressions 5.1 up to 5.13 [10].

Definition of the subscripts:

- $X_{"\mathbf{A}"1}$: the character represent the section of the pile
- $X_{A"\mathbf{1}"}$: the number represent a location at the node of the pile

Boundary conditions at node 1 $z = 0$

$$S_{A1} = S_{A1-ham} = (S_1) \tag{5.1}$$
$$M_{A1} = M_{A1-ham} = (M_1) \tag{5.2}$$

Interface conditions at node 2 at $z = L_A$

$$S_{A2} - S_{B2} = R_2 \tag{5.3}$$
$$M_{A2} = M_{B2} = (M_2) \tag{5.4}$$
$$\varphi_{A2} = \varphi_{B2} \tag{5.5}$$
$$v_{A2} = v_{B2} = 0 \tag{5.6}$$

Interface conditions at node 3 at $z = L_A + L_B$

$$S_{B3} - S_{C3} = R_3 \tag{5.7}$$
$$M_{B3} = M_{C3} = (M_3) \tag{5.8}$$
$$\varphi_{B3} = \varphi_{C3} \tag{5.9}$$
$$v_{B3} = v_{C3} = 0 \tag{5.10}$$

Boundary conditions at node 4 at $z = L$

$$S_{C4} - k \cdot V_{C4} = R_4 \tag{5.11}$$
$$M_{C4} = 0 \tag{5.12}$$
$$v_{C4} = \frac{R_4}{k} \tag{5.13}$$

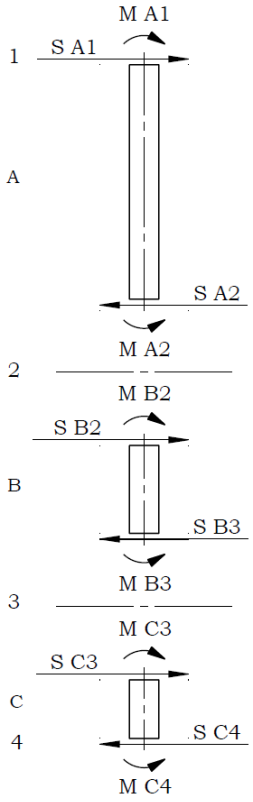

Figure 5.4: Internal force/ moment equilibrium at nodes

5.3. Theoretical Framework

This section contains the theoretical framework of the model, consisting of the bending theory, wave theory, and the current velocity profile approach.

5.3.1. Bending Theory

The model is based on the Euler-Bernoulli beam theory [7]. This theory is applicable to only small bending of a beam subjected to perpendicular forces. Assumed is, that the beam is totally homogeneous without imperfections. The Euler-Bernoulli equation describes the relation between the applied loads and the deflection of the beam and is modelled as a one dimensional object. The Euler-Bernoulli equation:

$$\frac{d^2}{dz^2}\left(EI\frac{d^2v}{dz^2}\right) = q \quad \text{with } EI(z) \text{ constant gives:} \quad EI\frac{d^4v}{dz^4} = q \quad [N/m] \tag{5.14}$$

In which $v(z)$ is the deflection of the beam in the x-direction at position z, q is a distributed load, E is the elastic modulus and I is the second moment of area of the cross section of the pile.

By integration of the distributed force on the pile over z, the shear force is calculated (S), followed by double integration to find the bending moment (M), triple integration gives the rotation (φ) and with four times integration the deflection v is found.

Performing these integration steps for the loads on pile section A:

$$-S_A = EI\int \frac{d^4v}{dz^4}dz = \int q dz \quad [N] \tag{5.15}$$

$$-M_A = EI\iint \frac{d^4v}{dz^4}dz^2 = \int -S dz = EI\cdot\frac{d^2v}{dz^2} \quad [Nm] \tag{5.16}$$

$$\varphi_A\cdot EI = EI\iiint \frac{d^4v}{dz^4}dz^3 = \int -M dz = EI\cdot\frac{dv}{dz} \quad [rad] \tag{5.17}$$

$$v_A\cdot EI = EI\iiiint \frac{d^4v}{dz^4}dz^4 = \int \varphi dz \quad [m] \tag{5.18}$$

For pile section B the internal moment expression is generated, and differentiated to find the shear force. Followed by two times integration of the internal moment expression to find the bending. This gives the following equations for section B:

$$-S_B = -\frac{M_2}{L_B} + \frac{M_3}{L_B} \tag{5.19}$$

$$-M_B = \frac{M_2}{L_C}(L_B - z_B) + \frac{M_3}{L_B}z_B = M_2 - \frac{M_2 z_B}{L_B} + \frac{M_3 z_B}{L_B} \tag{5.20}$$

$$\varphi_B\cdot EI = M_2 z_B - \frac{1}{2}\frac{M_2 z_B^2}{L_B} + \frac{1}{2}\frac{M_3 z_B^2}{L_B} + C_3 \tag{5.21}$$

$$v_B\cdot EI = \frac{1}{2}M_2 z_B^2 - \frac{1}{6}\frac{M_2 z_B^3}{L_B} + \frac{1}{6}\frac{M_3 z_B^3}{L_B} + C_3 z_B + C_4 \tag{5.22}$$

Every integration step, gives a constant. These constants can be solved with the boundary and interface conditions, given in subsection 5.2.2.

Calculation of the constant C_4 by submitting interface condition 5.6 into equation 5.22:

$$v_{B2} = 0 \quad \rightarrow \quad C_4 = 0 \tag{5.23}$$

Calculation of the constant C_3 by submitting interface condition 5.10 into equation 5.22:

$$v_{B3} = 0 \quad \rightarrow \quad C_3 = -\frac{1}{3}M_2 L_B - \frac{1}{6}M_3 L_B \tag{5.24}$$

The internal moment expression for section C is generated, and differentiated to find the shear force. Followed by two times integration of the internal moment expression to find the bending. This gives the general equations for section C:

$$-S_C = -\frac{M_3}{L_C} \tag{5.25}$$

$$-M_C = \frac{M_3}{L_C}(L_C - z_C) = M_3 - \frac{M_3 z_C}{L_C} \tag{5.26}$$

$$\varphi_C \cdot EI = M_3 z_C - \frac{1}{2}\frac{M_3 z_C^2}{L_C} + C_5 \tag{5.27}$$

$$\nu_C \cdot EI = \frac{1}{2}M_3 z_C^2 - \frac{1}{6}\frac{M_3 z_C^3}{L_C} + C_5 z_C + C_6 \tag{5.28}$$

Calculation of the constant C_6 by submitting interface condition 5.10 into equation 5.28:

$$\nu_{C3} = 0 \quad \rightarrow \quad C_6 = 0 \tag{5.29}$$

Calculation of the constant C_5 by solving interface condition 5.9:

$$\varphi_{B3} = \varphi_{C3} \quad \rightarrow \quad C_5 = \frac{1}{6}M_2 L_B + \frac{1}{3}M_3 \tag{5.30}$$

Calculation of ν_4 with formula 5.28:

$$\nu_4 = \frac{-EI - \frac{1}{3}kL_C^3 - \frac{1}{3}kL_C^2 L_B}{\frac{1}{6}M_2 L_B L_C} \tag{5.31}$$

From this the the moment at node three can be calculated:

$$M_3 = k\nu_4 L_C \tag{5.32}$$

By knowing M_3, the constants and the expressions for all pile sections can be solved for a load onto pile section A.

5.3.2. Environmental Load Theory

The ISO code [2] requires to use the Morrison equation 5.33 to calculate the load due to waves and current motions. The Morrison equation:

$$F_M(x,z,t) = \underbrace{C_m \rho_f \frac{\pi}{4} D^2 a_w}_{Inertia} + \underbrace{C_D \rho_f \frac{1}{2} D(u_w + u_c)|u_w + u_c|}_{Drag} \quad \text{(per meter lenght)} \tag{5.33}$$

With C_m is the inertia constant; C_D the drag constant; a_w the wave acceleration (equation 5.35); u_w the wave velocity (equation 5.34); u_c the current velocity (equation 5.37); D the diameter.

The empirical inertia and drag constants from the ISO code for different diameter piles are shown in appendix A.2.

5.3.3. Selection of the Model Wave Theory

The ISO code requires the Dean graph to select the design wave theory. The maximum operable wave conditions are included in the Dean graph for the water depths of the reference condition, given in figure 5.5. The reference condition is a representative condition for offshore wind farm projects, gained from the Beatrice offshore wind farm, given in appendix A.4.

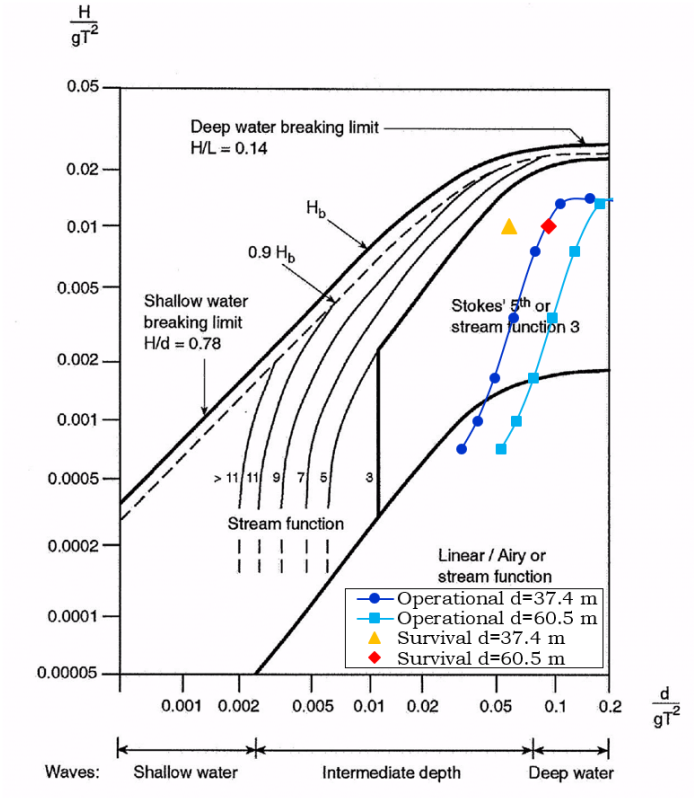

Figure 5.5: Dean graph for the maximum operable wave conditions

From this graph is concluded, that the most relevant wave conditions requires the Stokes fifth order wave theory. The Stokes fifth order wave theory is complicated to include in the model. Therefore, is checked whether it is valid to use an other theory. This is done by comparing the differences between the classic airy wave theory, the airy wave theory and the Stokes fifth order wave theory (for the reference conditions).

The simulation software SACS is used to compare the different wave theories. This program is an offshore structure analysis and design software, based on international design codes, and is able to predict offshore structural performance within environmental conditions. A SACS model similar to the new generated model is used to calculate the reaction forces these wave theories, see figure 5.6.

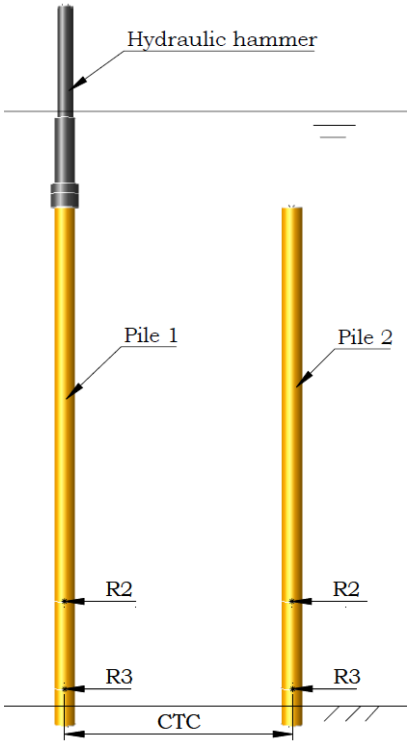

Figure 5.6: SACS model of pile 1 and pile 2

The results from the SACS model are shown in figure 5.7.

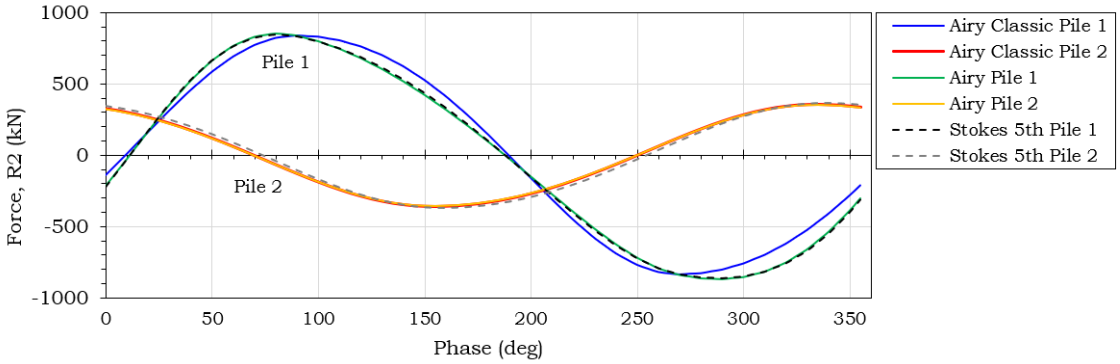

Figure 5.7: Comparison wave theories with SACS for one wave cycle

From this graph is concluded, that the airy Classic theory is a little out of phase, though the maximum reaction force in the same order as the other theories. The Stokes theory and airy theory are almost similar. Calculated for the maximum reaction force, the difference is less then one percent, namely: $\frac{845.5-853.5}{853.5} < 1\%$.

In conclusion, the maximum reaction force of the top shim are in the same order for the mentioned theories. The results of the airy wave theory 5th order theory are similar, therefore it is valid to use the airy wave theory.

5.3.4. Airy (Classic) Wave Theory

As stated in the previous subsection, the model is based on the airy theory, also called Linear wave theory. In this section this theory is explained.

The water particle velocities and accelerations of the airy theory are based on the velocity potential theory [9]. Form these the equations of the wave motions are derived:

$$u_w(x,z,t) = \sin(\omega t - kx) \cdot \omega a \frac{\cosh(k(d-z))}{\sinh(kd)} \tag{5.34}$$

$$a_w(x,z,t) = \frac{d\,u_w(x,z,t)}{dt} = \cos(\omega t - kx) \cdot \omega^2 a \frac{\cosh(k(d-z))}{\sinh(kd)} \tag{5.35}$$

With k the wave number (equation 5.36), ω angular speed related to the peak period $\omega = \frac{2\pi}{t_p}$, a the wave amplitude, d the water depth and z the distance with respect to the mean sea water level.

These formulas are applicable for all water depths. The wave particle accelerations are 90 degree out of phase with the particle velocities. Due to pile bending and tilt, the pile is not exactly eccentric. This eccentricity is small, therefore the calculation of the wave motions is based on the assumption that the pile is exactly straight. In other words, the whole pile over the depth is at $x = 0$.

The distributions of the wave velocity and acceleration over the water depth are shown in figure 5.8a and 5.8b.

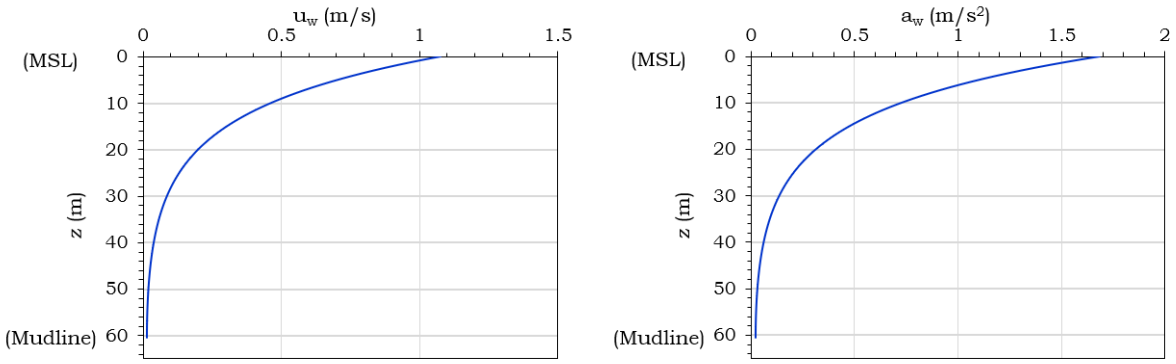

(a) Wave velocity in x direction

(b) Wave acceleration in x direction

Figure 5.8: Profile of wave velocity and acceleration over the water depth z

The figures shows, that the maximum velocity and accelerations are at the mean sea water level (MSL).

The difference between the classic airy wave theory and airy wave theory, are the boundary conditions at the water surface. The classic airy wave theory is calculated up to the mean sea water level ($z = 0$). And the airy wave theory up to the water surface ($z = \eta$ with $\eta(x,t) = a\sin(\omega t - kx)$).

The required wave number is calculated with the Eckhart method, and a refinement of Fenton [9]:

$$k \approx \frac{1}{d} \cdot \frac{\alpha + \beta^2 \left(\cosh\beta\right)^{-2}}{\tanh\beta + \beta\left(\cosh\beta\right)^{-2}} \quad \text{with} \quad \alpha = \omega^2 d/g \quad \text{and} \quad \beta = \alpha \tanh(\alpha)^{-1/2} \tag{5.36}$$

5.3.5. Current Profile Approach

The current velocity over the depth is given in equation 5.37 by a power law. This empirical formula is prescribed in the ISO code [2]. The velocity profile is pictured in figure 5.9. The figure shows also the approach which is used in the SACS simulation software, and the linearised approach for this model.

$$u_c(z) = u_c(0)\left(\frac{d-z}{d}\right)^{1/7} \tag{5.37}$$

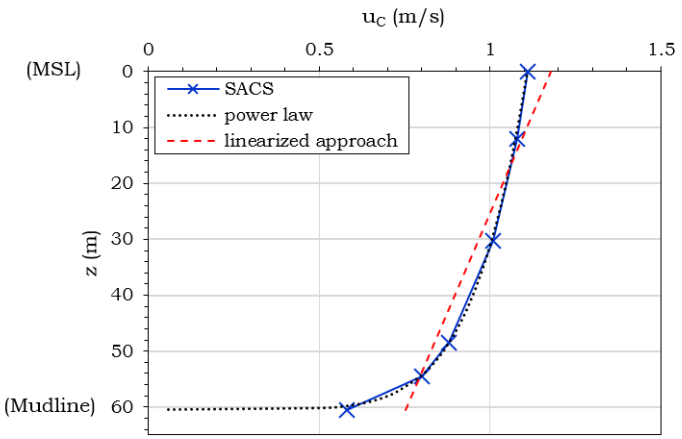

Figure 5.9: Current profile over the water depth

The linearised approach is introduced, because various numerical calculation software programs (Maple, Matlab, Wolfram Alpha, www.integral-calculator.com) were not able to find the integral of the Morrison equation with the power law. To simplify the equation, a linear approximation of the current velocity (u_c) is assumed, according to the linear regression equation. The expression for the linear approximation is given in equation 5.38. This method is based on a linear approximation of individual results, n times the power law is calculated equally over the water depth at locations z.

$$u_c(z, u_c(0)) = ez + f \tag{5.38}$$

The constants e and f are found with equation 5.3.5.

$$e = \frac{n\Sigma(z \cdot u_c)(\Sigma z^2) - (\Sigma z)(\Sigma u_c)}{n(\Sigma z^2) - (\Sigma z)^2} \quad \text{and} \quad f = \frac{(\Sigma u_c)(\Sigma z^2) - (\Sigma z)(\Sigma z \cdot u_c)}{n(\Sigma z^2) - (\Sigma z)^2}$$

With n is the number of calculations. $\Sigma(z \cdot u_c)$ is the summation of the z locations for which the power law is calculated, multiplied by the result of the power law at that z locations (u_c). Σz^2 is the summation of the square of the z locations for which the power law is calculated. Σz is the summation of the z locations for which the power law is calculated. And Σu_c is the summation of the results of the power law for all z locations, for which the power law is calculated.

5.4. Displacement: due to Gap between Pile and Shims

The stabbed pile into the sleeve contains a gap with the shims. The reason of the gap, is that the pile can slide smoothly through the shims, even when a pile contains a small fabrication deviation. These gaps result in an initial tilt of the pile, which is depicted in figure 5.10. In the model is assumed that the tilt of the pile is in the same direction as the environmental load, since this scenario gives the highest forces onto the shims.

The initial gap is 40 mm at the top and bottom shim. For the base case scenario the tilt is 0.245 deg gives an out of center at the top of 180 mm,

The tilt angle is:

$$\theta_{tilt} = \arctan\left(\frac{2 \cdot \Delta_{gap}}{L_B}\right) \tag{5.39}$$

This gives a displacement of the pile top of:

$$v_{A1,tilt} = \sin(\theta_{tilt})\left(L_A + \frac{1}{2}L_B\right) \tag{5.40}$$

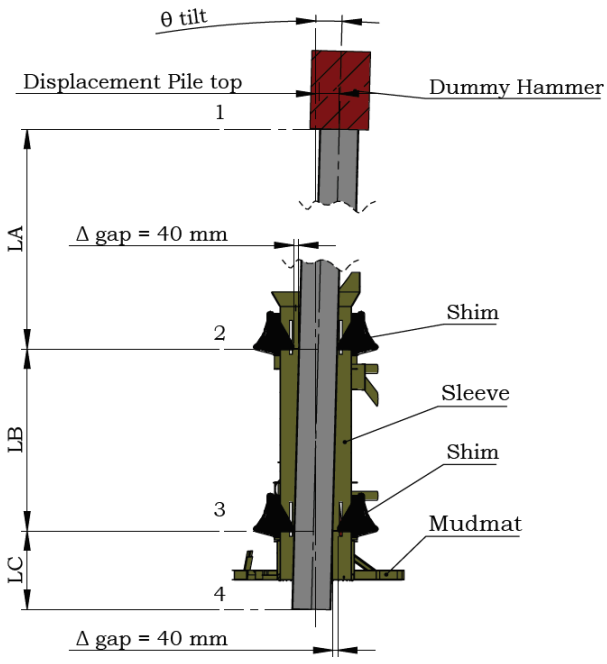

Figure 5.10: Section view of sleeve with tilted pile

5.5. Displacement and Reaction Forces due to: Environmental Load

In this section, the method is explained to calculate the displacement of the pile top and the reaction forces in the shims due to the environmental load. Wave and current motions induces a load on the stabbed piles (and hammer if present) and will therefore bend. This results in an eccentricity of the piles and reaction forces at the shims.

The expressions of the full expressions are too long to present in the report, therefore only the method to find the expressions is presented.

The displacement of the pile top is:

$$v_{A1,env} = \iiiint F_M(z, t = t_{max})(dz)^4 \tag{5.41}$$

The constants from the result of the integration are solved using the boundary and interface conditions of subsection 5.3.1.

The reaction forces at the shims are:

$$R_{2,env} = S_{2B} - S_{2A} \quad \text{and} \quad R_{3,env} = S_{3C} - S_{3B} \tag{5.42}$$

5.5.1. Integration of Environmental Load over the Pile

The environmental load is calculated with the Morrison equation from subsection 5.33.

Since the pile is covered by the sleeve, the force onto the pile due to the environment is only on pile section A.

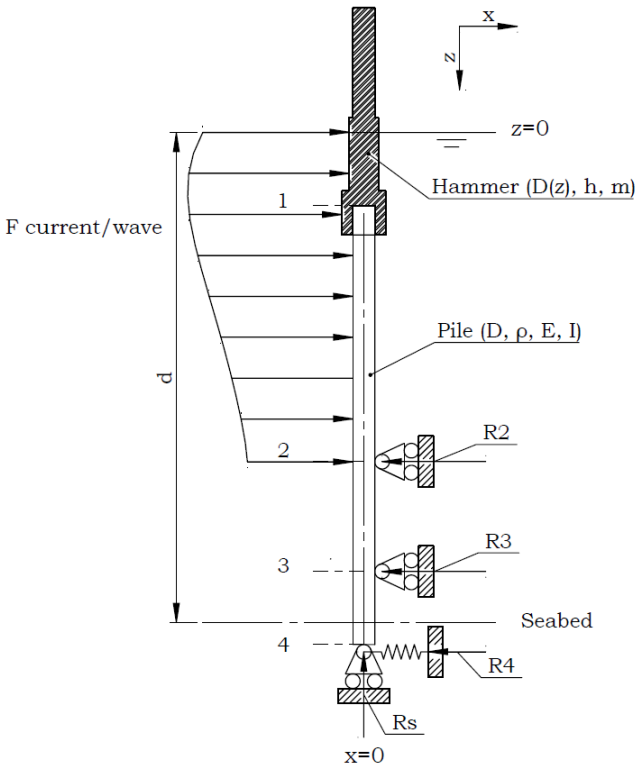

Figure 5.11: FBD of pile with hammer with environmental load

The Morrison equation with the wave motions and current profile substituted gives:

$$\begin{aligned} F_M(z=\eta,t) &= \frac{1}{2}C_D D\rho_f\left(\sin(\omega t-kx)\cdot\omega a\frac{\cosh(k(d-z))}{\sinh(dk)}+\mathrm{e}z+f\right) \\ &\quad\cdot\left|\sin(\omega t-kx)\cdot\omega a\frac{\cosh(k(d-z))}{\sinh(dk)}+\mathrm{e}z+f\right| \\ &\quad+\frac{\pi}{4}D^2\rho_f C_I\cos(\omega t-kx)\cdot\omega^2 a\frac{\cosh(k(d-z))}{\sinh(dk)} \quad \text{(per meter lenght)} \end{aligned} \tag{5.43}$$

The unit of the Morrison equation is in force per meter length. So, this represents a distributed force over the height for a particular diameter ($q(z)=F_M(z,t=t_{max})$. As can be seen in figure 5.11 the pile and hammer has different diameters. Therefore, the forces and moments of each diameter section should be calculated individually. The calculation boundaries depends on the water level with respect to these sections.

The distributed force of the Morrison equation can be substituted into the Euler-Bernoulli equation to calculate the shear forces, moments, angle and displacement of the pile (and hammer).

The method to calculate the shear forces and moments at the hammer is elaborated in the appendix section A.5. The interface between the hammer and the pile is assumed to be a fixed connection, so the total shear force and moment is transferred to the pile top, so : $S_{A1}=-S_{H,4}$, and $=M_{A1}=-M_{H,4}$. This is assumed, because the hammer is heavy; the pile diameter wide; and the pile bending is small, therefore the hammer will not rotate and shift with respect to the pile top.

The environmental load is from the water level (integration boundary a) until the top shim (node 2), (defined in equation 5.47). Calculation of the environmental force on pile:

$$-S_A=\int_{z_2}^{a}F_M dz+S_1 \tag{5.44}$$

$$-M_A=\int_{z_2}^{a}-S_A dz+M_1 \tag{5.45}$$

$$\varphi_A\cdot EI=\int_{z_2}^{a}-M_A \tag{5.46}$$

With:

$$a=\begin{cases} z_1 & \text{if} z_1\geq 0 \\ 0 & \text{if } z_1<0 \end{cases} \tag{5.47}$$

The deformation of the pile depends on the environmental force, so the deformation is up until water level. If the pile top (z_1) is higher than the water level, the part of the pile above water level will have a constant angle with respect to vertical. This is shown in equation 5.48 and 5.49

$$v_A\cdot EI=\int_{z_2}^{z_1}\varphi_A dz \quad \text{if } z_1\geq 0 \tag{5.48}$$

$$v_A\cdot EI=\begin{cases} \int_{z_2}^{z_1}\varphi_A dz & \text{for } z\geq 0 \\ v_a(z_1)+\varphi A(0)\cdot z_1 & \text{for } z<0 \end{cases} \quad \text{if} z_1<0 \tag{5.49}$$

Substitution of these results into equations 5.19 until 5.32 to calculate the reaction forces at the shims with equation 5.42 and the displacement of the pile top with equation 5.41.

5.5.2. Maximum Environmental Load in in Time and Space

The Morrison equation is dependent on time (t) and space (x). To calculate the maximum force, the moment in time the force is maximum shall be found. In this model, the highest force on the first pile is calculated at $x = 0$.

The distribution of the force variates over the water depth. As you can notice from figures 5.8 and 5.9, the velocity and acceleration profile (at a particular time and space) are maximum at sea level, and consequently also the force is maximum. Therefore, the moment in time that the force is maximum at water level, is the same moment in time, the total force over the whole water depth is maximum.

To find the moment in time at which the force is maximum, the first derivative of the Morrison equation with respect to time, equals to zero is solved:

$$\frac{dF_x(z=0,t)}{dt} = 0 \quad \rightarrow \quad t_{max} \tag{5.50}$$

The derivative of the Morrison equation with help of numeric software is:

$$\begin{aligned}\frac{dF_M(z=0,t)}{dt} = &\frac{aD\rho_f\omega^2\cosh(k(d-z))}{4\sinh(dk)} \\ &\cdot\left(4C_D\cos(kx-t\omega)\left|\frac{a\omega\cosh(l(d-z))\sin(kx-t\omega)}{\sinh(dk)} - ex - f\right| + \pi C_I D\omega\sin(kx-t\omega)\right)\end{aligned} \tag{5.51}$$

In figure 5.12 the inertia part (F_I), the drag part(F_d) and the sum(F_m) of these forces are plotted for $z = \eta$, as well as the derivative of the total force (dF_m/dt). As you can see the derivative has an abrupt change at $t \approx 4$ seconds. This is because of the absolute velocity part in the Morrison equation.

The first set up of the model was according to the classic airy wave theory, where t_{max} is calculated at z = 0. Since the model is extended to the airy wave theory , t_{max} have to be found for z = η. η Is dependent on time, so the first derivative of the Morrison equation will change, and therefore t_{max} possibly changes. In the model t_{max} is still calculated for the classic airy wave theory. Therefore, the model additionally calculates the summation of the force over the pile for $t_{99} = 0.99\,t_{max}$ and $t_{101} = 1.01\,t_{max}$. If one of these gives a higher force than t_{max}, the time is manually tuned until the maximum force is found.

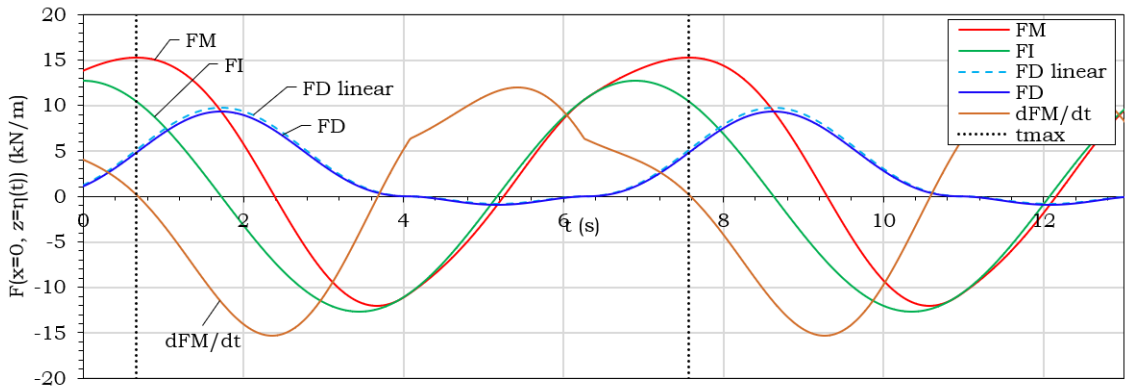

Figure 5.12: Force per meter length at $z = \eta$ over time

5.6. Displacement and Reaction Forces: due Second Order Effects

Definition: "The *second-order effects* are those caused by eccentric applied loads. When an axial compressive force simultaneous occurs with eccentricity, this creates additional bending in the member, causing the internal moments to be higher."

The tilt of the pile in combination with bending, due to environmental load, gives an initial eccentricity. The vertical load of the hammer is concentrated at the top of the pile, and the self-weight of the pile is distributed over the whole length of the pile. These vertical loads in combination with the eccentricity gives the second order effect. Since internal moments becomes higher, the pile will bend further, giving an extra eccentricity, and again higher internal moments, and so on. This is a non-linear effect, and is calculated iteratively until the difference of the result with the previous iteration step converges to zero. The output of this calculation step of the model is: eccentricity of the pile and the shim reaction forces due to second order effects.

Output:

The displacement of the pile top is (with C_2 an integration constant solved in subsection 5.6.3):

$$v_{A1,2nd} = \frac{C_2}{-EI} \tag{5.52}$$

The reaction forces at the shims are:

$$R_{2,2nd} = S_{2B} - S_{2A} \quad \text{and} \quad R_{3,2nd} = S_{3C} - S_{3B} \tag{5.53}$$

Input:

The initial displacement is the summation of the tilt (result of equation 5.40 and environmental load (result of equation 5.41 on the pile:

$$v_0 = v_{A1,initial} = v_{A1,env} + v_{A1,tilt} \tag{5.54}$$

In the subsequent subsections, the bending due to the hammer weight and self-weight of the pile is elaborated.

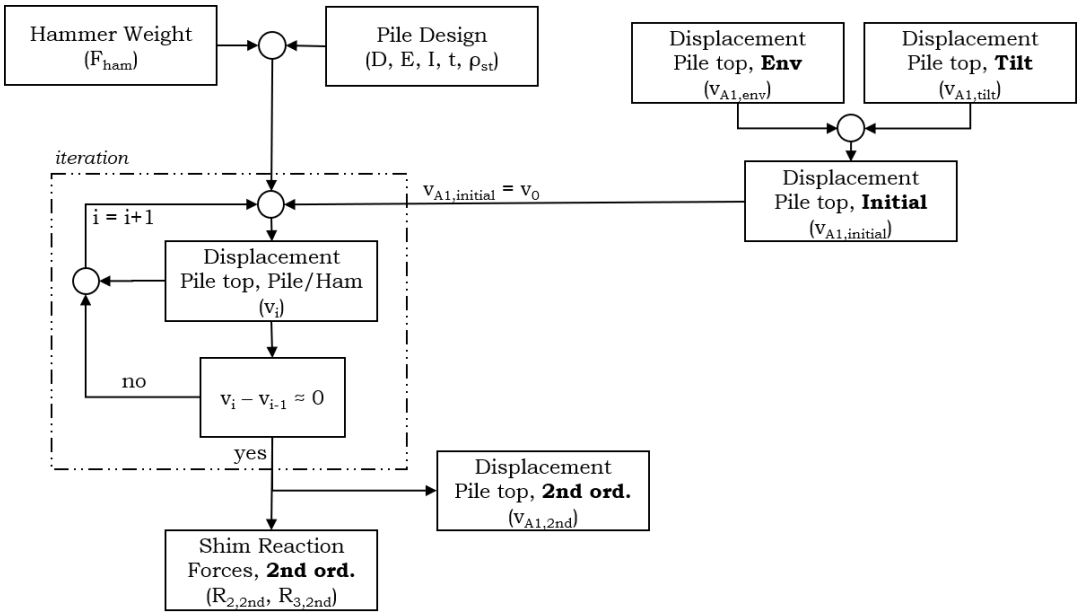

Figure 5.13: Flowchart second order effect (part of flowchart: figure 5.1)

5.6.1. Hammer Weight on the Pile

The moment and shear force due to the hammer weight are given in this subsection. Figure 5.14 shows, how the pile bends due to eccentricity, and how this modelled. Since the model is based on small pile bending, assumed is, that the vertical level of node 1 is constant independent of the bending.

The bending moment into the pile at section A (between node 1 and 2) due to the hammer weight is:

$$M_A = F_{ham} \tan(\theta_i) z_A \tag{5.55}$$

Differentiation with respect to z gives the shear force:

$$S_A = F_{ham} \tan(\theta_i) \tag{5.56}$$

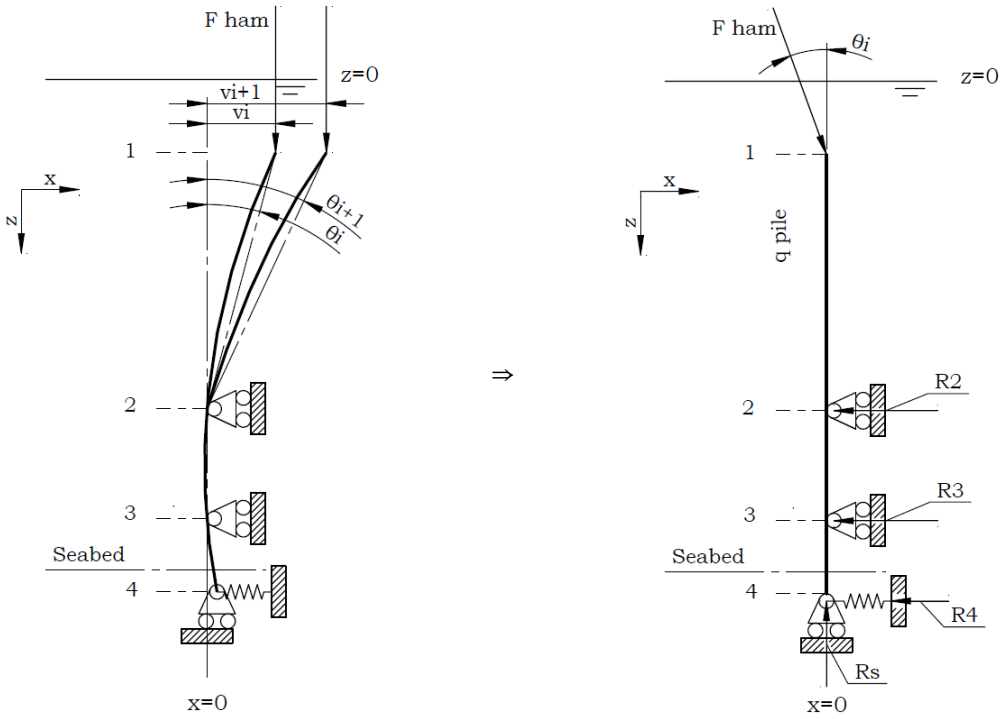

(a) Pile bending due to hammer weight

(b) Bended pile due to loads

Figure 5.14: Profile of the maximum wave velocity and acceleration at moment of time over the water depth z

5.6.2. Self-Weight of the Pile

The moment and shear force due to the self-weight of the pile are given in this subsection. In figure 5.15 is shown, how the pile bends due to eccentricity, and how this is modelled. Since the model is based on small bending, assumed is a constant internal rotation of the pile. In other words assumed as a straight line from node 2 to node 1 as shown with the intermittent line in figure 5.15). This means the force is assumed equally distributed over the pile. The forces due to self weight of the pile are expected to be relatively low, so this assumption will introduce a small error with respect to the non-linear distribution profile. Also is assumed, that the vertical level of node 1 is constant independent of the bending.

The self-weight of the pile for a part of z is:

$$W_{pile} = \rho g A \Delta z \quad \text{with} \quad A = \frac{\pi}{4}(D_O^2 - D_I^2) \tag{5.57}$$

The bending moment into the pile between of section A (between node 1 and 2) due to the hammer weight is:

$$M_A = \frac{1}{2}\rho g A z_A \tan(\theta_i) z_A \tag{5.58}$$

Differentiation with respect to z gives the shear force:

$$S_A = \rho g A z_A \tan(\theta_i) \tag{5.59}$$

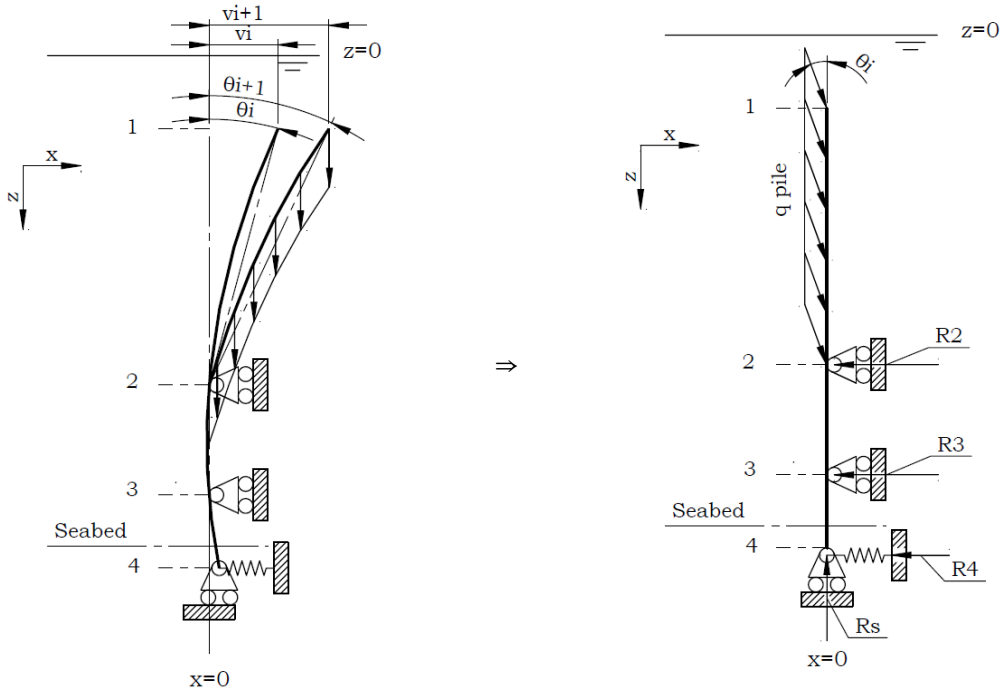

(a) Pile bending due to hammer weight

(b) Bended pile due to loads

Figure 5.15: Profile of the maximum wave velocity and acceleration at moment of time over the water depth z

5.6.3. Equations for Bending due to Hammer Weight and Self-Weight of the Pile

Previous subsections showed how the shear forces and internal moments are determined. With the Euler-Bernoulli theory, described in subsection 5.3.1, the angle and bending of the pile is calculated for a particular angle θ_i. Because this angle is getting bigger due to the second order effect, this calculation steps are performed multiple times.

The equations for pile section A in between node 1 and 2 are:

$$S_A = F\tan(\theta_i) + \rho g A \tan(\theta_i) z_A \tag{5.60}$$

$$M_A = F\tan(\theta_i) z_A + \frac{1}{2}\rho g A \tan(\theta_i) z_A^2 \tag{5.61}$$

$$-EI\varphi_A = \frac{1}{2}F\tan(\theta_i) z_A^2 + \frac{1}{6}\rho g A \tan(\theta_i) z_A^3 + C_1 \tag{5.62}$$

$$-EI v_A = \frac{1}{6}F\tan(\theta_i) z_A^3 + \frac{1}{24}\rho g A \tan(\theta_i) z_A^4 + C_1 z_A + C_2 \tag{5.63}$$

Constant C_2 is computed by substituting boundary condition 5.12 into equation 5.63:

$$v_{A2} = 0 \quad \rightarrow \quad C_2 = -\frac{1}{6}S_{A1}L_A^3 - C_1 L_A \tag{5.64}$$

And constant C_1 by solving interface condition 5.10:

$$\varphi_{A2} = \varphi_{B2} \quad \rightarrow \quad C_1 = -\frac{1}{2}S_{A1}L_A^2 - \frac{1}{3}M_2 L_B - \frac{1}{6}M_3 L_B \tag{5.65}$$

The displacement of the pile top (v_1) is found as follows: Substitution of L_A into equation 5.61 for z_A gives the moment at node 2($M_{A2} = M_2$). Followed by substitution of M_2 into equation 5.31, and substitute this into equation 5.32 gives the moment at node 3 (M_3). By knowing M_2 and M_3, the bending profile of pile section A can be found with equation 5.63. For $z_A = 0$, equation 5.63 gives v_1.

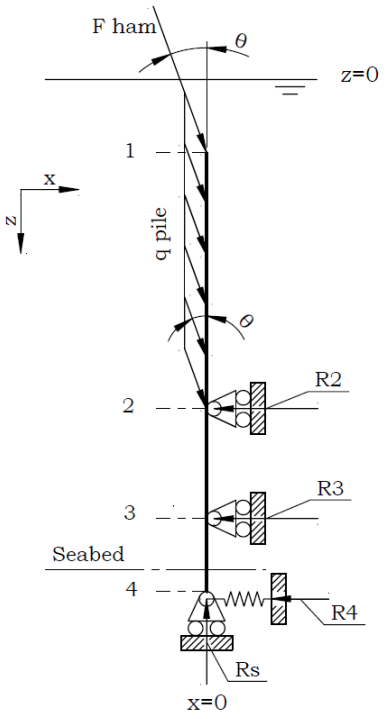

Figure 5.16: Bended pile due to loads

5.7. Reaction Forces: Pile Two, Three and Four

In this section is explained how the reaction forces of pile two, three and four are calculated.

Pile one contains a hammer on top, as shown in figure 5.17. This hammer results in higher forces onto the shims, and consequently also in the members of the PIF. Because of the higher reaction forces due to the hammer, t_{max} is calculated for pile one. The other piles are calculated at the same time (t_{max}) at a distance x.

The wave velocities and accelerations are dependent on time and distance, see Morrison equation 5.33. The distance of the other piles with respect to pile one, aligned with the environmental load, varies per direction. These distances are given in table 5.1. As a result the reaction forces of the other piles also varies per exposed direction. The footprint dimension is defined as "a".

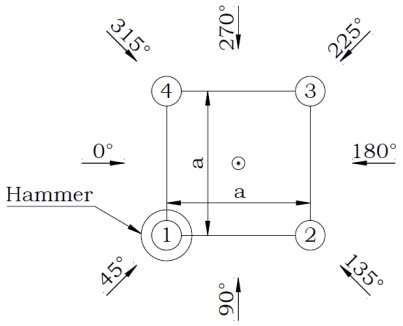

Figure 5.17: Environmental conditions from eight directions spaced at 45° interval

Table 5.1: Distance with respect to pile one, aligned with the environmental load direction

Direction →	**0°**	**45°**	**90°**	**135°**	**180°**	**225°**	**270°**	**315°**
Pile 1	0	0	0	0	0	0	0	0
Pile 2	a	$\frac{1}{2}\sqrt{2a^2}$	0	$-\frac{1}{2}\sqrt{2a^2}$	$-a$	$-\frac{1}{2}\sqrt{2a^2}$	0	$\frac{1}{2}\sqrt{2a^2}$
Pile 3	a	$\sqrt{2a^2}$	a	0	$-a$	$-\sqrt{2a^2}$	$-a$	0
Pile 4	0	$\frac{1}{2}\sqrt{2a^2}$	a	$\frac{1}{2}\sqrt{2a^2}$	0	$-\frac{1}{2}\sqrt{2a^2}$	$-a$	$-\frac{1}{2}\sqrt{2a^2}$

When the piles are stabbed in the sleeves, the direction of the pile tilt due to the gaps is random. Assumed is, that the tilt of pile one is in the same direction as the environmental load, while the initial tilt of the other piles are in the contrary direction. With this assumption the compression force in the top member becomes the highest, and the tension force in the bottom member the lowest, see figure 5.18.

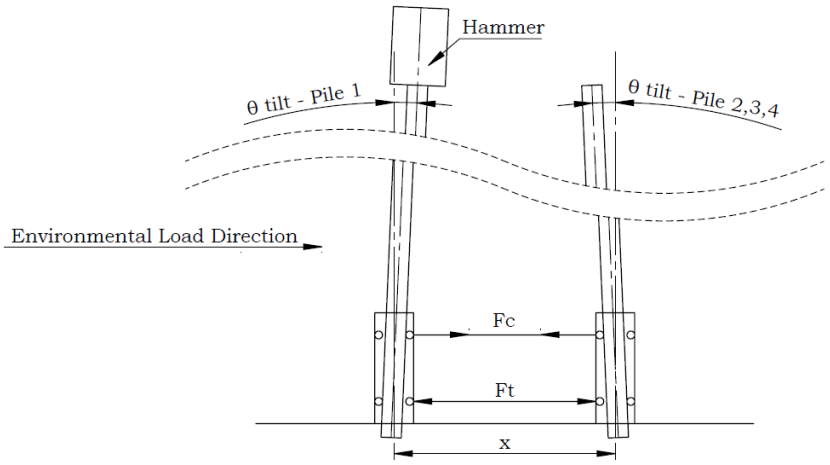

Figure 5.18: Tilt of piles due to gabs into sleeves

5.8. Model Verification

In this section the calculation model is verified, by comparing the results with the same SACS model as given in figure 5.6. First the model is verified per individual load, followed by the environmental load through time.

5.8.1. Individual Loads

The model is verified per individual load to show the difference per load between the Shim-Force calculation model with the SACS model. The individual loads on the SACS model are shown in appendix A.6.

First, the model is exposed to current, after that, to waves, followed by the combination of these at t_{max}. The SACS software does not take into account the second order bending effect. Therefore is the hammer modelled as a horizontal force at the top of the pile, and the pile self-weight as a horizontal distributed forces.

The bending of the pile is the last integration step in the model. Therefore, the pile top displacement is compared for the model verification. In table 5.2 the results of both models are given.

Table 5.2: Comparison of the pile tip displacement calculation model with SACS model

Input			**SACS** (cm)	**Model** (cm)	**1 - Model/ SACS** (%)
Current	u_c	1.1 m/s	1.836	1.921	0.19%
Wave	H_{max} & t	4.7 m & 6.9 s	10.917	10.820	-0.90%
Wave & Current	H_{max} & t, u	4.7 m & 6.9 s, 1.1 m/s	13.461	13.356	-0.79%
Hammer	F_{hortop}	500 kN	36.31	36.31	0.00%
Pile	q_{hor}	50 kN/m	60.37	60.38	0.01%

From this, one can conclude, that the forces onto the shims due to the hammer and pile self-weight are the same. The differences in bending due to the environmental forces are within one percent. This is assumed to be acceptable.

* *Note: The SACS model is also based on the Euler-Bernoulli theory and the Morrison equation.*

Figure 5.19 shows the convergence of the pile tip displacement, by illustrating the difference between each iteration. Clearly, the solution becomes stable after multiple iteration steps. From this is conclude, the whole computation converges, including the bending moments.

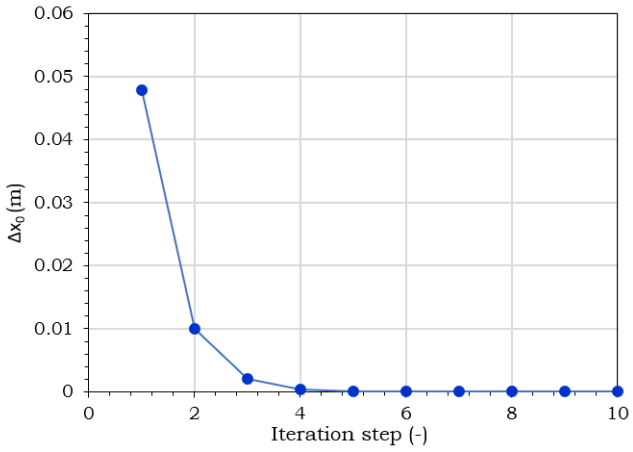

Figure 5.19: Iteration convergence of second order effect

5.8.2. Environmental Load through Time

The classic airy theory and the airy theory are verified for pile one and two, for one wave length in the 0 degree direction including current. The weight of the pile and hammer are not included.

In figure 5.20 the results of the classic airy wave theory for both models are shown. The difference in theories between the models is the current profile, which is linear approximated into the calculation model.

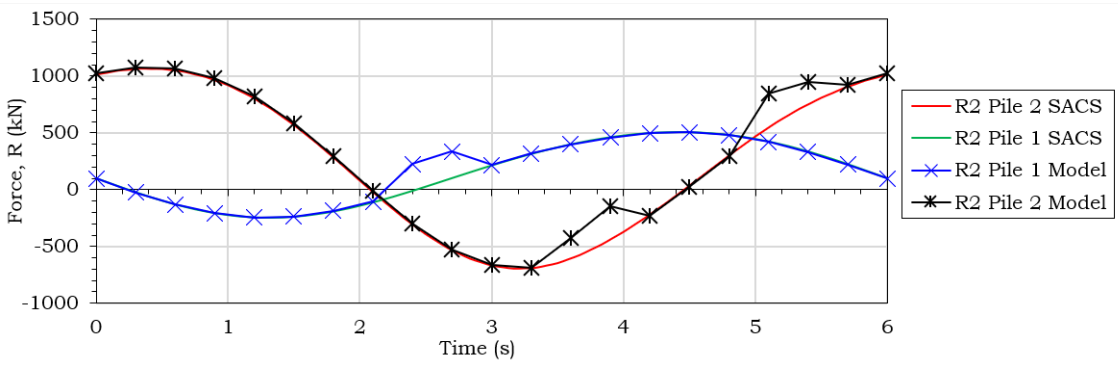

Figure 5.20: Comparison classic airy wave theory with Model and SACS including current velocity for one wave cycle

Noticeable is the result from the model at approximately 2.5 s and 5 s. This offset of the calculation model occurs when the particle velocity at the seawater level change signs. Since only the maximum force at t_{max} = 0.66 seconds is used for the integrity check of the PIF, this offset does not influence the results.

Figure 5.21 shows the results of the airy wave theory for both models. The differences between the models are the current stretching methods up to the water surface.

The calculation model contains the Wheeler stretching method; the power law current profile is stretched till the water surface $z = \eta$, as shown in figure A.4. In the model the stretched current profile is linear approximated as shown in figure 5.9.

The SACS model contains approached power law as current profile over the water depth, as shown in figure 5.9. This current profile is stretched by the extrapolating stretching method; when the wave is above mean sea water level (MSL), the current velocity is assumed constant, and below MSL the current velocity is cut off until the surface, see figure A.3.

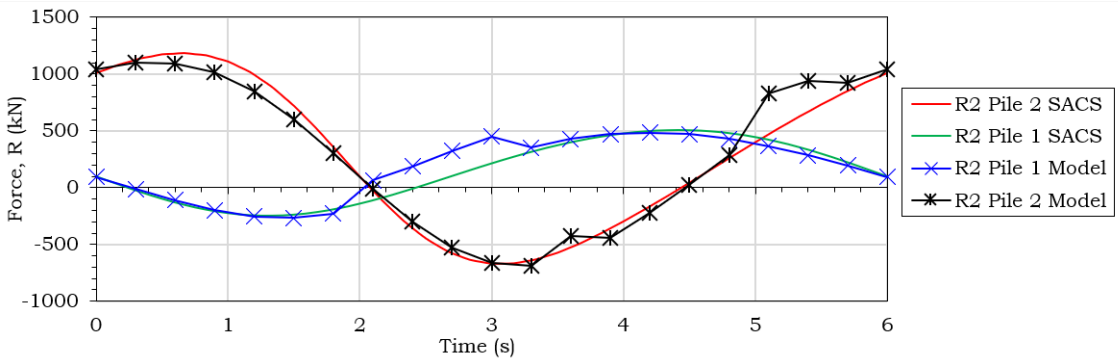

Figure 5.21: Comparison airy wave theory with Model and SACS including current velocity for one wave cycle

The airy wave theory contains the same offset as described preciously. The different stretching methods give also differences in the results of the models. The calculation model has a lower maximum reaction force and earlier in time. Since the velocities of the extrapolated method are higher for the maximum wave elevation, also the maximum reaction forces are higher. These higher velocities also results in a more drag dominated environmental force. Since the drag and inertia force components are 90 degree out of phase, the maximum force is at an other moment in time.

5.8.3. Comparison Calculation of Second order Bending Effect with Currently used Method

The calculation model results of the second order bending effect are compared with the currently used method by Seaway Heavy Lifting. The comparison is executed for the reference condition. In the tables 5.3 the differences of the reaction forces in the shims are shown. For two water depths with a single pile and a pile with hammer on top. The free body diagram of the current calculation method is shown in figure 5.22.

The differences of the currently used method with the new calculation model are:

- An additional step is needed, the bending due to environmental load is extracted from a SACS model
- Assumed is that all six degrees of freedom are fixed half way of section b between node 2 and 3
- The bending of the pile beneath the upper shim is not taken into account
- The reaction moment (M_r) at the fixity, is equally divided over the upper and lower shims

The calculation method is explained in appendix A.7

Table 5.3: Reaction forces into the shims of the current method the new calculation model

Scenario				Reaction Force		
Nr.	**Model rep.**	**Water Depth** (m)	**Shim**	**Current Method** (kN)	**Model** (kN)	**Model/ Current Method - 1** (%)
1	Pile + Ham	60.5	R2	241.4	271.0	12.3%
	Pile + Ham	60.5	R3	-241.4	-211.8	-12.3%
2	Pile	60.5	R2	21.3	25.3	18.6%
	Pile	60.5	R3	-21.3	-17.5	-18.0%
3	Pile + Ham	37.4	R2	165.6	185.4	12.0%
	Pile + Ham	37.4	R3	-165.6	-145.8	-11.9%
4	Pile	37.4	R2	19.4	22.9	18.0%
	Pile	37.4	R3	-19.4	-16.0	-17.6%

Table 5.3 shows that the currently used model underestimate the reaction forces at the top shims (R_2) and overestimate at the lower shims (R_3).

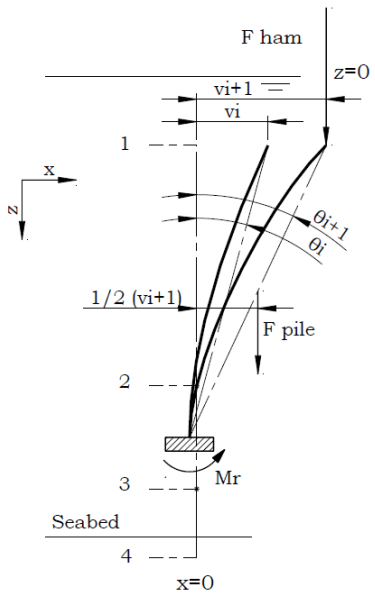

Figure 5.22: FBD of current bending calculation method

5.9. Model Conclusion/ Discussion

With the new generated pile-shims force calculation model, the reaction forces at the shims are calculated. These forces results from the load due to waves and current, the hammer weight and self-weight of the pile.

In the calculation model the airy wave theory is used, for which the results are close to the required 5th Stokes theory. From the Pile-Shims calculation model, only the reaction force due second order effect are implemented in the SACS model of the total adjustable PIF, to check the integrity. In this SACS model the required wave theory is used. Therefore, the already neglectable deviation of the pile-shims force calculation model becomes relative to the total reaction forces, even lower.

The model contains an offset in calculating the reaction forces of the environmental load over time. These offsets occurs when the particle velocities at sea water level change signs. Since only the maximum force is used for the integrity check of the PIF, this offset does not influence the results.

The model results of the different integration steps of the load on the pile (for the reference condition) are: the distributed load in figure 5.24, shear force in figure 5.25, internal moment in figure 5.26, rotation in figure 5.27 and deflection in figure 5.28.

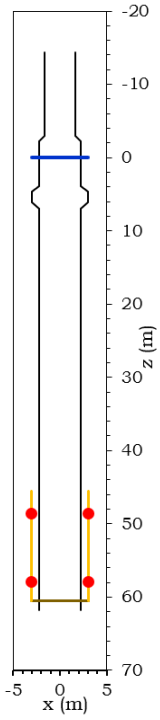

Figure 5.23: Pile sleeve representation

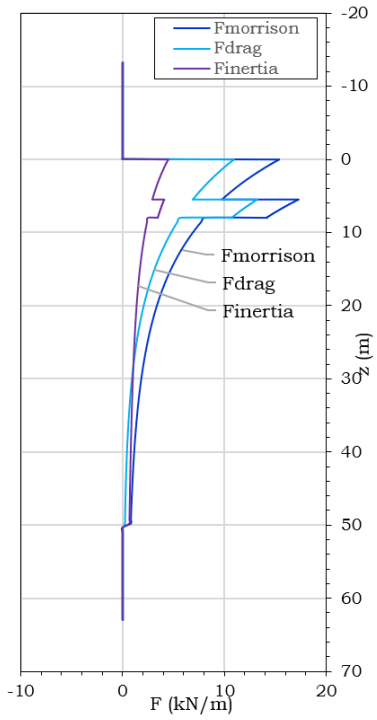

Figure 5.24: Distributed load

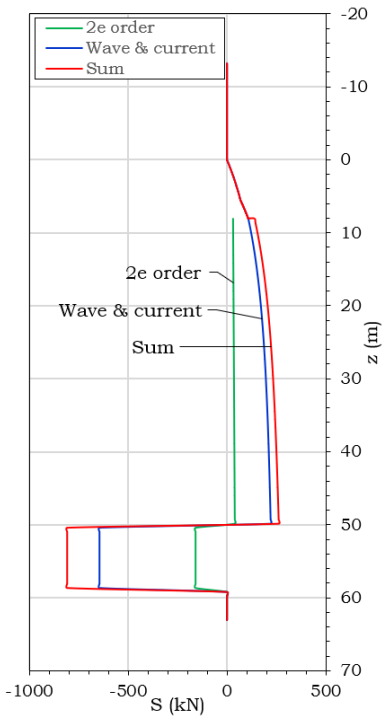

Figure 5.25: Shear force

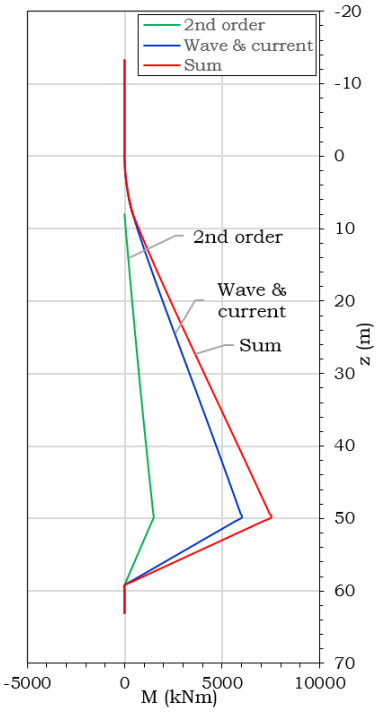

Figure 5.26: Internal moment

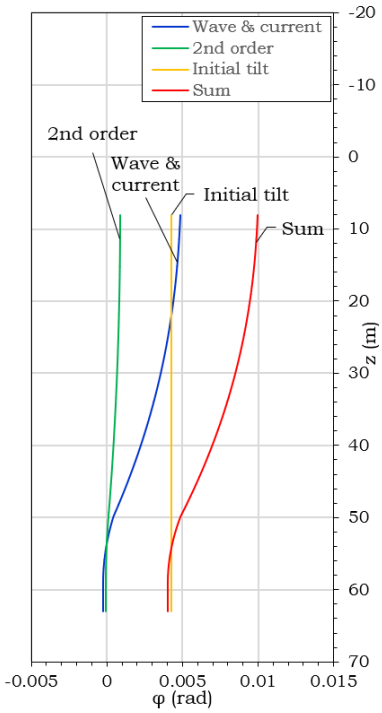

Figure 5.27: Rotation

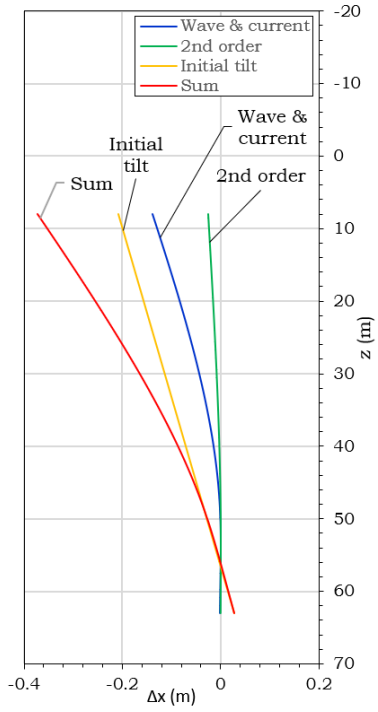

Figure 5.28: Deflection

6

Structural Integrity

In this chapter the structural integrity of the conceptual design is checked with the structural simulation software SACS. The following questions are investigated: "Is the frame strong enough to withstand the external loads", and: "What are the deflections of the PIF, and are these critical for the installation tolerances?", and last: "Should the sleeve be rechecked for the adjustable PIF?".

First the design loads are introduced, followed by the load combinations, and how these are systematically reduced to manageable numbers.

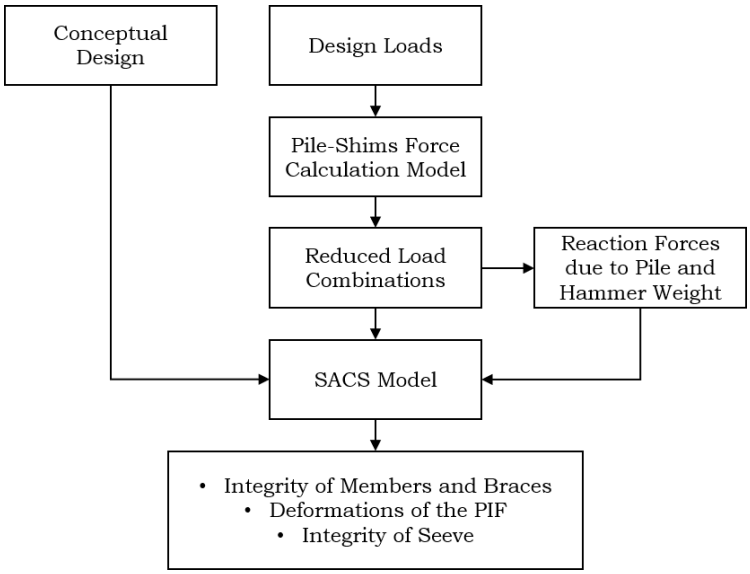

Figure 6.1: Environmental conditions from eight directions spaced at 45° interval

6.1. Design Loads

This section explains for what design conditions and combinations the integrity of the conceptual PIF is checked. The new designed PIF should be capable to install piles at all conditions of planned offshore wind farms. It is not possible to check the integrity for all conditions, therefore the representative reference condition is considered, which is given in the appendix section A.4.

6.1.1. Operational Load Scenarios

The PIF will be exposed to different load scenarios during offshore operation. These follows from the installation procedure, which is equal for the adjustable PIF as described in the background chapter 2. The integrity check should be performed for the following scenarios:

- Transport
- Lifting
  - in air
  - through the splash zone
  - under water-surface
- In-place condition
  - operational
  - survival

In this report is focused on the in place condition, because this condition is the most critical for the current PIF design. Both the operational as the survival conditions are considered. The differences between these scenarios are: the survival condition is exposed to harsher environmental loads, and no hammer is on top of a pile.

6.1.2. Conditions for the In-Place Scenario

The reference conditions are summarized in table 6.1. Additionally, the maximum and minimal reasonable conditions for other offshore wind farms are shown. The maximum operable wave conditions are mentioned in the requirements in table 3.2.

Table 6.1: Conditions for the in-place scenario

Condition	Unit	Reference	Min	Max	(source)
Footprint CTC	(m)	24	20	32	(Requirement)
Water Depth	(m)	37.4 - 60.5	25	75	(Tender department)
Current Velocity	(m/s)	1.11	0	1.5	(Tender department)
Hammer Weight	(MT)	390	330	460	(IHC-Hydro-hammer)
Pile Length	(m)	55	40	70	(Tender department)
Pile thickness Ratio D/t	(-)	44	15	60	(Tender department)
Pile diameter	(m)	2.2	1	3.5	(Sleeve limitations)

The PIF should be able to placed on the seabed in any direction with respect to the waves and current. For the integrity check eight directions with 45° interval are considered as depicted in figure 5.17. Assumed that waves and currents are aligned.

6.1.3. Load Combinations

The integrity of the PIF should be checked for all combinations of the load conditions. In table 6.2 the number of the load combinations are given. Since some combinations clearly results in lower loads, these have not to be considered.

Table 6.2: nr of load combinations

Load conditions	**nr. of conditions**	
	initial	reduced
Wave height/ Peak period	9	1
Water depth	2	1
Direction of wave and current	8	8
Parial load factors (ISO code)	3	1
Frame footprint	3	3
Total combinations	1296	24

According to the requirements nine maximum wave conditions should be considered, for both the maximum and minimum water depth, in eight directions. According to the ISO code, all conditions should be checked with additional action factors existing of three combinations, shown in table 6.2. Since the PIF is adjustable, all possible footprints should be checked. Representative is to considerer three square footprints: the maximum and minimum required footprint, and the reference footprint to compare the results with the current PIF.

Table 6.3: Partial action factors for calculating internal forces according to the ISO-code ([2])

Combination	**Partial action factor**	
	γ_G	γ_E
1	1.3	1.0
2	1.1	1.35
3	0.9	1.35

The significant load combinations are found by using the pile-shims force calculation model. The results of the model are representative for the whole PIF, since the main loads into the members of the PIF comes from the pile-shims reaction forces. This is shown in section 7.1. The results of the individual load combinations are compared for only the top shims, because the ratio between the top and bottom shims is constant (for the reference conditions).

First, the reaction forces are calculated for the operable wave conditions, for both the maximum and minimum water depth, including the reference current velocity and pile and hammer. The results of these calculations are shown in figure 6.2 without the ISO action factors.

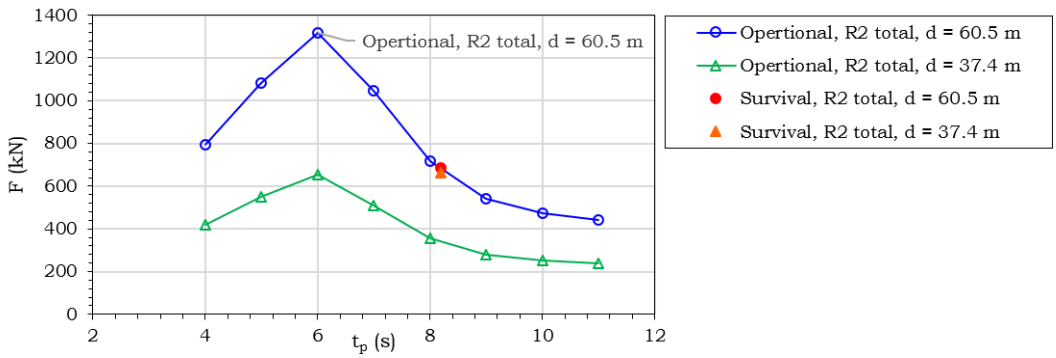

Figure 6.2: Reaction force at top shims for the maximum operable waves

The maximum reaction forces are at a peak period (t_p) of 6 seconds with the maximum wave height of 4.54 m and the deepest water depth of 60.53 meters (blue circles). Though the survival condition is exposed to a

"rougher sea state" ($h_s = 3.5\ m$, $t_p = 8.2\ s$), the reactions forces are significantly lower. This is because of the absence of the hammer on top of the pile.

Figure 6.3 shows the results of the different action factor at the maximum load combination of figure 6.2.

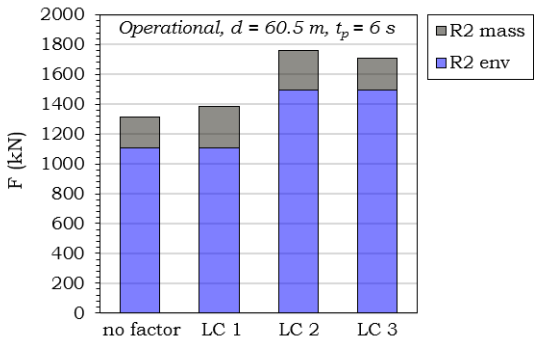

Figure 6.3: Action factor combinations on governing load combination

Clearly is noticed that action factor combination 2 (LC2) gives the highest reaction forces. This is because of the following: The wave loads induces a bending of the pile; the higher the wave loads; the more bending; and consequently the higher the second order moments due to the weight of the pile and the hammer. Since both the environmental loads as the mass loads are enlarge by action factor combination 2, this is the governing load case.

All environmental directions should be considered. This is a result of the different distances from piles two three and four are has with respect to pile one for different environmental directions, as explained in section 5.7.

In conclusion, the integrity of the three PIF footprints should be checked for the operational scenario in 8 environmental direction; in the the deepest water depth of 60.53 meter; exposed to a wave with a peak period of 6 seconds and 4.54 meter high; with action factor combination 2.

6.2. Results of Shims-Force Calculation Model for the Governing Load Combinations

The shim reaction forces due to the second order bending effect are calculated with the calculation model introduced in chapter 5. In this chapter the results for the governing load combinations are shown. These results have to be include in the SACS models of the adjustable PIF.

The reaction forces of the four piles at the top and bottom shim, for three different footprints, are given in tables 6.4, 6.5 and 6.6.

Table 6.4: Square footprint of 20 meter, reaction forces at top and bottom shims for different environmental directions

Pile	**Shim**	**Environmental Direction, θ_{env}**							
		0°	45°	90°	135°	180°	225°	270°	315°
P1	**R2**	262.8	262.8	262.8	262.8	262.8	262.8	262.8	262.8
	R3	-205.4	-205.4	-205.4	-205.4	-205.4	-205.4	-205.4	-205.4
P2	**R2**	-19.0	-16.3	-13.6	-13.6	-16.5	-13.6	-10.7	-16.3
	R3	13.2	11.3	9.4	9.4	11.4	9.4	7.4	11.3
P3	**R2**	-19.0	-19.6	-19.0	-10.7	-16.5	-19.7	-16.5	-10.7
	R3	13.2	13.6	13.2	7.4	11.4	13.6	11.4	7.4
P4	**R2**	-10.7	-16.3	-19.0	-16.3	-10.7	-13.6	-16.5	-13.6
	R3	7.4	11.3	13.2	11.3	7.4	9.4	11.4	9.4

Table 6.5: Square footprint of 24 meter, reaction forces at top and bottom shims for different environmental directions

Pile	**Shim**	**Environmental Direction, θ_{env}**							
		0°	45°	90°	135°	180°	225°	270°	315°
P1	**R2**	262.8	262.8	262.8	262.8	262.8	262.8	262.8	262.8
	R3	-205.4	-205.4	-205.4	-205.4	-205.4	-205.4	-205.4	-205.4
P2	**R2**	-19.9	-17.8	-15.0	-15.0	-18.4	-15.0	-10.7	-17.8
	R3	13.8	12.3	10.4	10.4	12.7	10.4	7.4	12.3
P3	**R2**	-19.9	-17.6	-19.9	-10.7	-18.4	-19.6	-18.4	-10.7
	R3	13.8	12.2	13.8	7.4	12.7	13.6	12.7	7.4
P4	**R2**	-10.7	-17.8	-19.9	-17.8	-10.7	-15.0	-18.4	-15.0
	R3	7.37	12.30	13.75	12.30	7.37	10.38	12.71	10.38

Table 6.6: Square footprint of 32 meter, reaction forces at top and bottom shims for different environmental directions

Pile	**Shim**	**Environmental Direction, θ_{env}**							
		0°	45°	90°	135°	180°	225°	270°	315°
P1	**R2**	262.8	262.8	262.8	262.8	262.8	262.8	262.8	262.8
	R3	-205.4	-205.4	-205.4	-205.4	-205.4	-205.4	-205.4	-205.4
P2	**R2**	-18.5	-19.7	-17.8	-17.8	-19.9	-17.8	-10.7	-19.7
	R3	12.8	13.6	12.3	12.3	13.8	12.3	7.4	13.6
P3	**R2**	-18.5	-12.3	-18.5	-10.7	-19.9	-14.6	-19.9	-10.7
	R3	12.8	8.5	12.8	7.4	13.8	10.1	13.8	7.4
P4	**R2**	-10.7	-19.7	-18.5	-19.7	-10.7	-17.8	-19.9	-17.8
	R3	7.4	13.6	12.8	13.6	7.4	12.3	13.8	12.3

From this tables can be noticed, that the reaction forces for the pile 1 with hammer are significantly higher than the other piles without hammer.

6.3. SACS Model of the Adjustable PIF

The structural integrity of the PIF is executed with a model of the adjustable PIF in the simulation software SACS, as shown in figure 6.4. The model exist of nodes connected to each other with members. The members are defined in the model with the properties of table 4.2. To make the model as realistic as possible, the most equipment, framing and walkways are modelled. The smaller parts are included as external forces or moments onto the frame, these are shown in the appendix in figures A.14 up to A.32).

The governing load combinations and the second order reaction forces are an input in the SACS model. As concluded from the Dean Graph (5.5) the fifth order Stokes theory is required to model the wave motions.

The input of the reaction forces in SACS are in x and y direction. Therefore, the results of section 6.2 for each direction are recalculated to a force in x an y direction, with the following equations:

$$x = R\cos(\theta_{env}) \tag{6.1}$$

$$y = R\sin(\theta_{env}) \tag{6.2}$$

The outputs of the SACS models are:

- Ratio between the applied and allowable stress of members
- Total stiffness of the frame, expressed by the deflections measured at the locations of the shims
- The axial forces in the members connection to the sleeve

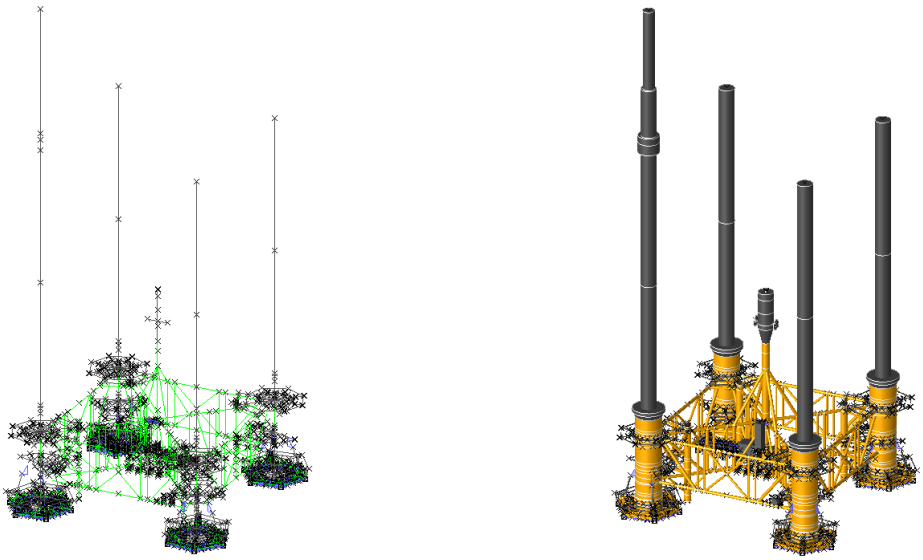

(a) Nodes connected (b) Members defined

Figure 6.4: SACS model of the adjustable PIF with a 24 meter x 24 meter footprint

6.4. Ratio between Applied and Allowable Stress of Members

The the maximum ratio between the applied and allowable stresses of the members, also called unity check, is executed with the SACS model according to the ISO code [2]. In this section, the maximum unity check of the members are shown for the three footprints. From the SACS model is concluded that the maximum unity check is at the same location for these footprints, with the most critical member shown in figure 6.5.

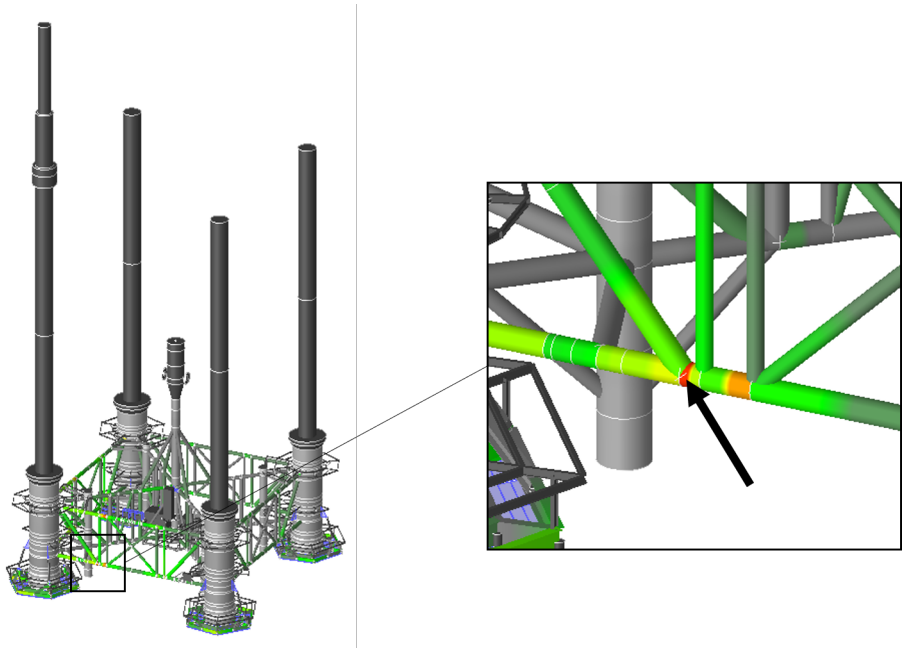

Figure 6.5: Unity check of the adjustable PIF with 24 meter footprint

The unity checks are calculated on:

- Tension
- Compression
- Bending
- Shear
- Hydrostatic pressure

And combinations of these. The governing unity check is for the combination of compression, bending and hydrostatic pressure. The results of the maximum unity checks are shown in 6.7

Table 6.7: Maximum ratio between the applied and allowable stresses of the members of the different footprints

Footprint	**Maximum Ratio applied/ allowable stress**
(m)	(-)
20	0.377
24	0.395
32	0.315

When the unity check is below 1, the members does not fail. So, from this can be concluded that all the footprints of the PIF will survive the reference condition.

The SACS report with the calculation results of the unity checks are given in the appendix section A.11. To verify the results from SACS, the calculation is also done by hand for the most critical member of the 24 meter footprint configuration. These calculations are shown in appendix section A.10. Information of the member with highest unity check are given in table 6.8.

Table 6.8: Member properties

Total Length	L	(m)	0.41
Outer Diameter	D	(mm)	457
Wall Thickness	t	(mm)	12.7
Youngs Modulus	E	(N/mm^2)	205,000
Shear Modulus	S	(N/mm^2)	82,000
Yield Strength	f_y	(N/mm^2)	355
Effective Length Factor*	K	(-)	0.7

The water depth at the member including wave elevation, for which the unity check is maximum, is $H_z = 63.625m$.

To be able to calculate the unity checks, the forces and moments in the member should be known. These are gained by the SACS model, given in table 6.9.

Table 6.9: Moments and forces at member with maximum unity check

Torsional Moment x	M_x	(kNm)	-6.0095
Bending Moment y	M_y	(kNm)	-177.4442
Bending Moment z	Mz	(kNm)	-0.5021
Axial Force x	f_x	(kN)	-579.4655
Shear Force y	V_y	(kN)	2.441
Shear Force z	V_z	(kN)	355.1502

The ISO code [2] requires the following resistance factors to apply over the stresses of the member, these are given in table 6.10.

Table 6.10: Resistance Factors (ISO code [2])

Tension	$\gamma_{R,t}$	1.05
Compression	$\gamma_{R,c}$	1.18
Bending	$\gamma_{R,b}$	1.05
Shear	$\gamma_{R,s}$	1.05
Hoop Buckling	$\gamma_{R,h}$	1.25

The results of the calculated unity checks for the 24 meter footprint are given in table 6.11.

Table 6.11: Summary of unity check

Stress due to	**Ratio applied/ allowable stress**
Compression	0.158
Bending	0.237
Shear	0.248
Hydrostatic	0.003
Comp. + Bend. + Hydr.	0.395

Overall can be concluded, that the maximum unity check of the adjustable PIF for all footprints is not critical.

6.5. Sleeve Integrity

The integrity of the sleeve is reviewed by comparing the axial forces into the members at the sleeve of the adjustable PIF with the existing PIF design. The results are gained from the SACS model of the adjustable PIF and the results from the design report of the current PIF [6]. This comparison is valid since the connected members at the sleeves are preserved for the adjustable PIF.

The result of the comparison, for the governing load combinations, are given in figure 6.6. The results are compared by dividing the axial forces in the members from the adjustable PIF with the current PIF.

Some of the forces into members are relatively low, therefore small differences between the forces gives high percentages. To reduce this effect the percentages of the forces of the adjustable PIF are divided by the maximum force. $(F_{adj}/F_{cur} - 1) \cdot F_{adj}/F_{max}$

In figure 6.7 a top view and front view of sleeve 1 is shown, with the names of the members defined. Combination of the names of the top view with front view is the name of the individual members.

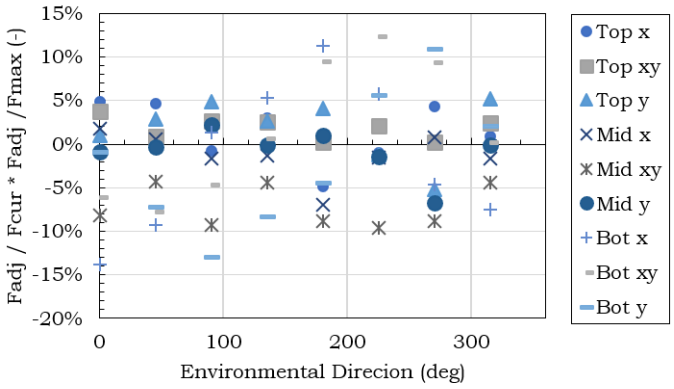

Figure 6.6: Comparison axial forces in the members connected to the sleeve

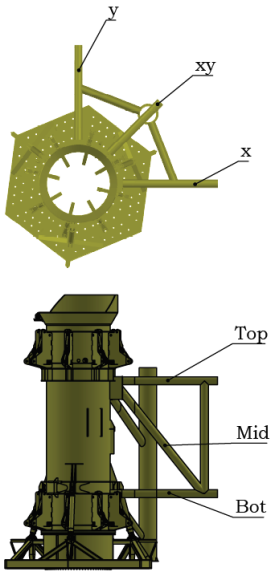

Figure 6.7: Member name define

From this is concluded, that the axial forces in the members at the sleeve of the adjustable PIF are either lower(-%) as higher(+%), than the current PIF. Therefore, the sleeve should be re-checked for the adjustable PIF, whether it can resist the different loads from the members to the sleeve.

6.6. Deflection of the PIF

Stiffness is resistance to deflection. So, the degree of deflection of the PIF gives is representative to the stiffness of the total frame. The stiffness of the frame is required to install the piles within the required tolerances. Therefore, the displacements at the top and bottom shims are gained from the SACS model.

With these deflections the tilt of the pile is calculated with the following equation:

$$\theta_{def} = \arctan\left(\frac{B}{\sqrt{\left(\Delta_{top,x}+\Delta_{bot,x}\right)^2+\left(\Delta_{top,y}+\Delta_{bot,y}\right)^2}}\right) \tag{6.3}$$

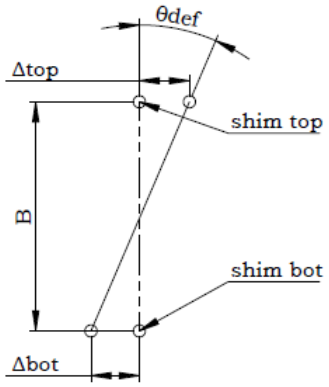

Figure 6.8: Displacement of the Shims

In table 6.12 the angle due to the deflections and the tilt due to the gaps between the shims are given.

Table 6.12: Resulted pile angle due to deflections and tilt

PIF configuration	θ_{def} (deg)	θ_{total} (deg)	**Environmental Direction** (deg)
Current 24	0.0804	0.3261	315
Adjustable 20	0.0690	0.3147	315
Adjustable 24	0.0876	0.3334	315
Adjustable 32	0.0846	0.3303	315

From this can be concluded, that the stiffness of the adjustable frame with respect to the current frame is equivalent. Also, is noticed that the tilt of the pile due to deflections is a small with respect to the total tilt.

The current PIF managed to install the piles just within the tolerances. Therefore, can be stated that the different footprints of the adjustable PIF design also satisfies the required tolerances.

Figure 6.9: Deflections of the adjustable PIF model

6.7. Conclusions

The ratio between the maximum stress and allowable stress of the members are in the same order for the different footprints. The maximum ratio is under 0.4 for the representative reference condition, which is the Beatrice offshore wind farm.

The deflections at the pile supports (shims), for the in-place condition are relatively small. This deflections are not critical for the pile installation tolerances, since these are in the same order than the current PIF.

The members connected to the sleeve are both higher and lower than was designed for. Therefore, the sleeve should be rechecked for the adjustable PIF, and if nesceserry modified.

7

Influence of Variations in Design Conditions

Offshore wind farms with pre-piled jackets are planned at various locations around the world. In chapter 6 the integrity of the adjustable PIF is only executed for the reference load conditions. Therefore, this chapter investigates the question: "What is the influence of variations in pile designs and conditions"; it is based on the before mentioned reference condition with one parameter varied per analysis. The results are shown in graphs, in which the results of two scenarios are depicted: one with only the pile; and one with the hammer on top of the pile.

For the scenario, pile with hammer on top, the results are shown for the reaction forces due to the weight of the pile and the hammer, the environmental load, and the total reaction forces.

For the scenario with only the pile, only the total reaction forces are shown. Because the contribution of the pile weight on the total reaction force is relatively low, as concluded in section 6.2. Consequently, the total reaction forces are almost equal to the reaction forces due to the environmental load.

Throughout this chapter, the following symbols and abbreviations are used:

- R_2 - reaction force at top shim (node 2)
- R_3 - reaction force at bottom shim (node 3)
- P&H - pile and hammer
- P - pile
- tot - total reaction force due to environment and weight of pile and hammer
- env - reaction force due to environment
- mass - reaction force due to weight of pile/ hammer

In the subsequent analyses, the graphs contains a intermittent horizontal line, representing the maximum pile-shims reaction force of the reference condition. The vertical intermittent lines shows the representative boundaries for reasonable offshore wind farm projects, which are presented in table 6.1.

7.1. Influence of Piles and Hammer on Forces in the Members

This section contains the influence of the piles and hammer on the axial forces into the members, connected to the sleeve, see figure 6.7. The SACS model of the adjustable PIF exposed to the reference conditions (including second order effect) is used for the results. Two scenarios are compared: adjustable PIF with piles and hammer, and, only the adjustable PIF.

The results of the axial forces in the members are shown in table 7.1 for both scenarios. Only the axial forces of the Top x, Mid x and Bot x members are given, because the PIF is practically symmetrical in x and y direction.

The axial forces in the members for the "only PIF" scenario, are about 6% with respect to the axial forces of the PIF with pile and hammer, meaning that the forces in the members are mainly caused by the pile-shims

Table 7.1: Axial forces into the members connected to the sleeve

Name	Model description	Top x Force (kN)	Mid x Force (kN)	Bot x Force (kN)
a.	PIF with pile and hammer	975	596	-1133
b.	Only PIF	59.2	16.6	-68
b./a.	Percentage	6.1%	2.8%	6.0%

reaction forces for the reference condition.

In combination with the conclusions of chapter 6, the frame of the PIF is capable to withstand the reference condition, and to install within the installation tolerances. It can be assumed that: if the pile-shims reaction forces are below these of the reference conditions the PIF can be used. Consequently, the direct results of the pile-shims calculation force model (including environmental load) can be used for a first estimation of the PIF integrity.

7.2. Environmental Conditions Influences

In this section the influence of the environmental conditions with respect to the pile-shims reaction forces are analysed.
The variation in environmental parameters are:

- Water depth
- Current velocity
- Soil stiffness
- Wave conditions

The influence of variations in wave conditions are not considered, since the maximum operable wave conditions of the Stanislav Yudin with the PIF are equal at all locations. Therefore, the maximum operable wave condition is used for all analyses, and it is found in section 6.1.3: $t_p = 6$ s and $h_{max} = 4.54$ m.

7.2.1. Water Depth

The influence of the water depth to the reaction forces at the shims are given in figure 7.1.

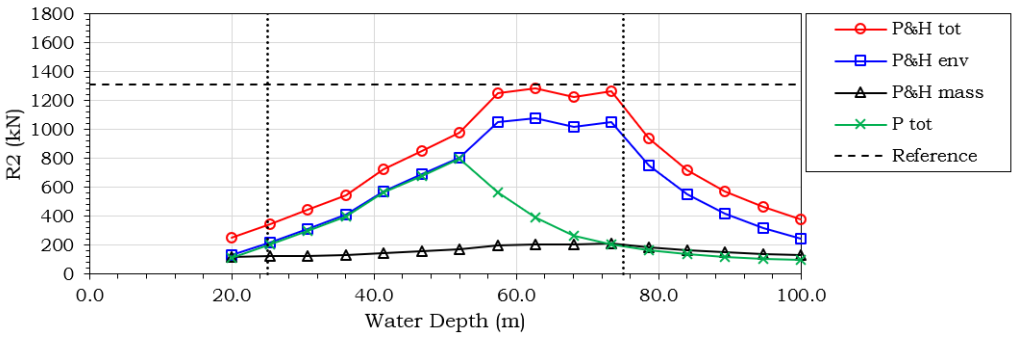

Figure 7.1: Reaction forces at top shims, with respect to the water depth

The environmental force of both the pile and the pile with hammer increase with the water depth until they are fully submerged. With increasing water depth, more of the pile/hammer is exposed to the water. When fully submerged, the reaction force decreases because of lower environmental loads. The current velocity and wave velocity and accelerations are maximum at sea water level, and decreases over the water depth. Therefore, the reaction force for only the pile increases until 55 meter water depth, followed by decreasing, when fully submerged.

The hammer on top of the pile has different diameters, see the sketch of hammer in figure A.6); this results in

irregularities in the forces between 55 m and 75 m. The force on a cross section depends on the diameter, just as the drag and inertia constants. So, with increasing water depth, another diameter is at the water surface level, resulting in abrupt reaction force changes.

The reaction force due to the weight of the pile increases when the environmental load increase. The bending of the pile increase with environmental loading, resulting in higher second order effects. Consequently, the internal moment due to the hammer weight becomes higher, and therefore also the reaction force at the top shims.

The reaction forces at the shims within the pile length boundary conditions are all below the maximum reaction force of the reference condition.

7.2.2. Current Velocity

The influence of the current velocity on the reaction forces at the shims are given in figure 7.2.

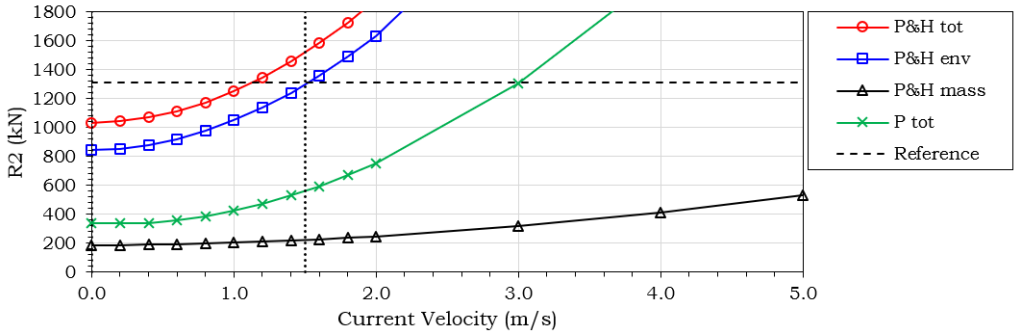

Figure 7.2: Reaction forces at top shims, with respect to the current velocity

The load increase with the current velocity squared, see Morrison equation 5.33. Consequently, the pile bends with the velocity squared. Therefore, the initial pile top displacement is larger, and the pile bends further, resulting in higher reaction force due the second order effect. However, the increase in reaction force due to the mass is marginal for the representative velocities (under 1.5 m/s).

A higher current velocity gives higher reaction forces; this means that the PIF can not be used for the reference conditions with an increased current velocity.

7.2.3. Soil Stiffness

The influence of the spring (representing the soil stiffness) on the reaction forces at the shims are given in figure 7.3.

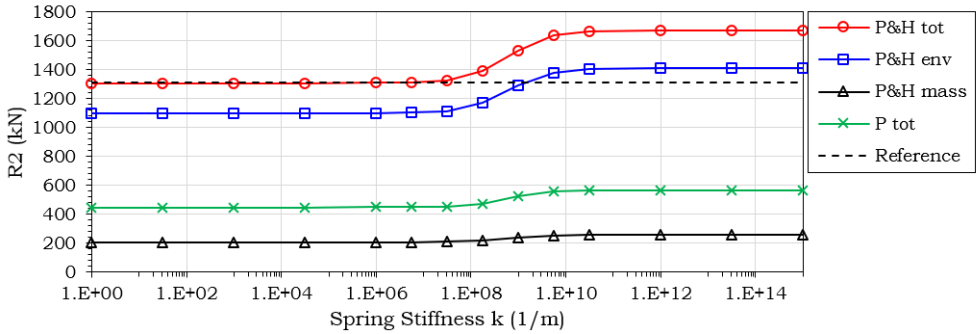

Figure 7.3: Reaction forces at top shims, with respect to the replaced soil spring stiffness

The reaction force is constant for a spring stiffness below 10^7 1/m. For a stiffer soil, the displacement of the pile tip becomes lower, and the soil will act as a hinged connection fixed in x direction, resulting in an increase

of the shim force at the top shim.

Because the interaction with the soil changes with the stiffness, also the ratio between the reaction force of the top and bottom shims becomes different. The ratio between the reaction force of the top and bottom shims with respect to the replaced soil spring stiffness is given in figure 7.4.

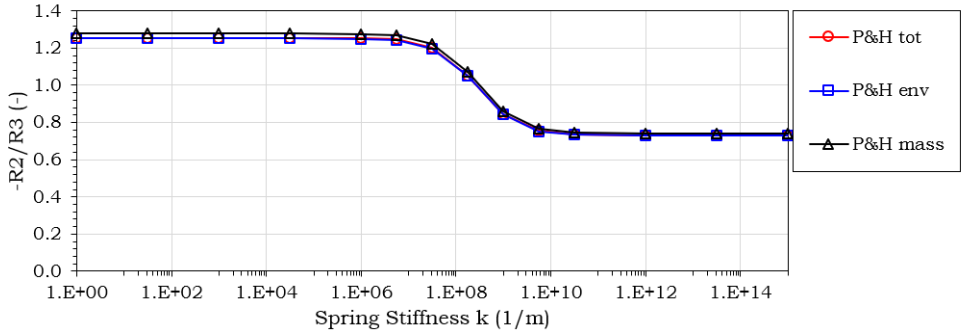

Figure 7.4: Ratio between the reaction force of top and bottom shims with respect to the replaced soil spring stiffness

When the stiffness of the soil becomes higher, the pile bending changes, therefore the ratio between the top and bottom shims also changes. The initial pile penetration is assumed small. Consequently, the replaced soil spring will below 10^7 1/m.

The constant ratio below the spring stiffness of 10^7 1/m is calculated, by assuming is an infinitely stiff pile (no bending) and a soil stiffness of zero (freely supported hinge), for a force at the top of the pile. A sketch is given in figure 7.5.

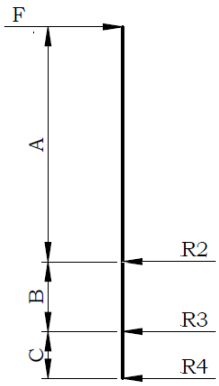

Figure 7.5: Pile

For no soil stiffness, $R_4 = 0$ is assumed to be zero. The relation between the top and bottom shims can be calculated by solving the static balance for the forces and moments:

$$\Sigma M_2 = 0: \quad F \cdot A + R_3 \cdot B = 0 \quad \rightarrow \quad F = -\frac{R_3 \cdot B}{A} \tag{7.1}$$

$$\Sigma F = 0: \quad F - R_2 - R_3 = 0 \quad \rightarrow \quad \frac{R_2}{-R_3} = 1 + \frac{B}{A} \tag{7.2}$$

For the reference condition: A = 41.8 m, B = 9.325 m, this gives $-R_2/R_3 = 1.22$. This equals the result of the model.

7.3. Pile Design Influence

In this section the influence of pile design on the reaction forces onto the shims are analysed.

The variation in pile design parameters are:

- Length
- Diameter
- D/t ratio
- Hammer weight

7.3.1. Length

The influence of the pile length on the reaction forces at the shims are given in figure 7.6.

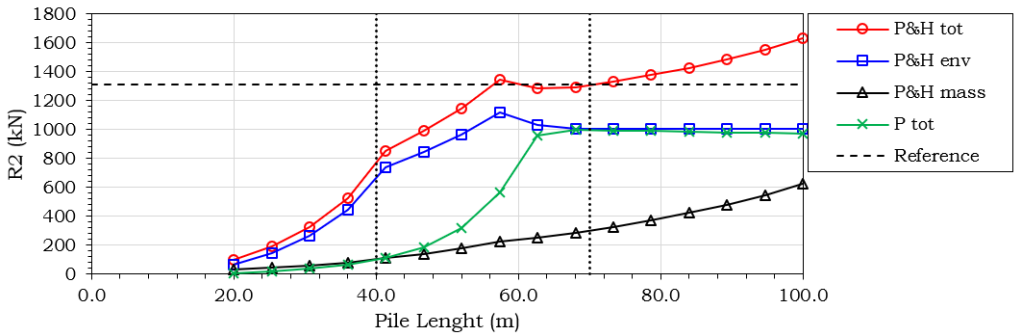

Figure 7.6: Reaction forces at top shims, with respect to the length of the pile

The reaction forces increase with the pile length due to both, the environmental load and bending due to mass. The environmental load is the highest at the sea water level, as explained in subsection 7.2.1. When the pile length becomes longer, it reaches above the sea water level, then the environmental load stays constant.

The weight of the pile and hammer increases with the length of the pile. The longer the pile, the bigger the initial displacement of the pile top due to tilt. The larger the displacement the higher the internal moment, and consequently higher reaction force at the shims.

Within the reasonable boundary conditions, the reaction forces for all pile lengths are approximately beneath the maximum reference condition. So, the variation in pile length will not be a show-stopper.

7.3.2. Diameter

The influence of the pile diameter on the reaction forces at the shims are given in figure 7.7.

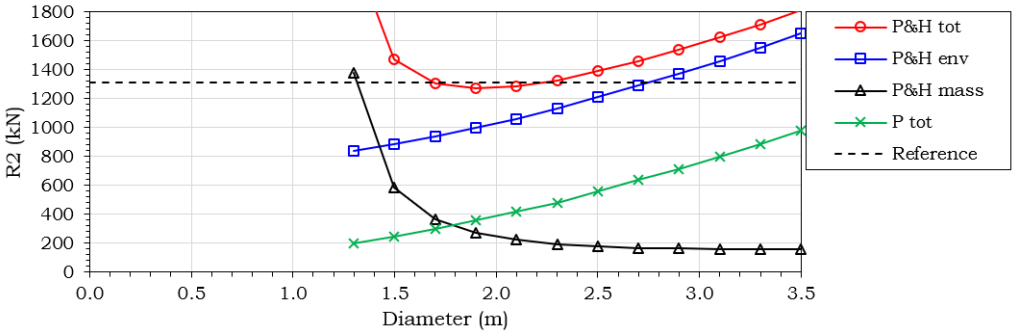

Figure 7.7: Reaction forces at top shims, with respect to the current velocity

The diameter of the pile is varied from 1.3 meters, because with lower diameters the pile bends infinitely, in other words the pile fails. The maximum diameter is 3.5, because a larger diameter cannot be installed with the current sleeves.

The environmental load depends linearly on the pile diameter, see Morrison equation 5.33. Also, the inertia and drag coefficients increase with the diameter. So, the environmental load increases with the diameter.

The second moment of inertia depends on the diameter to the power four. Meaning, the smaller the diameter, the less resistance against bending. This results further pile bending, consequently the internal moment, because of the mass of the hammer and self-weight, becomes higher. By increasing the diameter, the second moment of inertia increases by the power four, and therefore the influence of the mass decreases.

Overall, increasing the diameter results in higher environmental load, and lower influence of the pile and hammer weight. Moreover, an optimum is at 2.2 meter diameter, which equals the pile diameter of the reference conditions.

7.3.3. D/t Ratio

The influence of the ratio between the diameter and the thickness on the reaction forces at the shims are given in figure 7.8.

The diameter is kept constant, the thickness is varied.

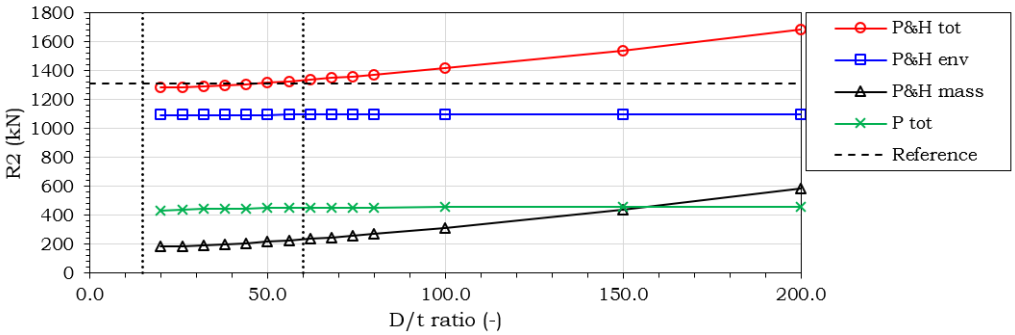

Figure 7.8: Reaction forces at top shims, with respect to the pile diameter

The higher the D/t ratio, means a smaller pile thickness for a constant diameter. A smaller pile thickness results in a lower second moment of inertia, so the resistance against bending decreases. This means that the pile bends further, resulting in a higher internal moment, and the reaction forces increase.

The additional bending for reasonable d/t ratio's as given in the box are approximately constant. So, the influence of the pile thickness is not considerable with respect to the reaction forces.

7.3.4. Hammer Weight

The influence of hammer weight on the reaction forces at the shims are given in figure 7.9.

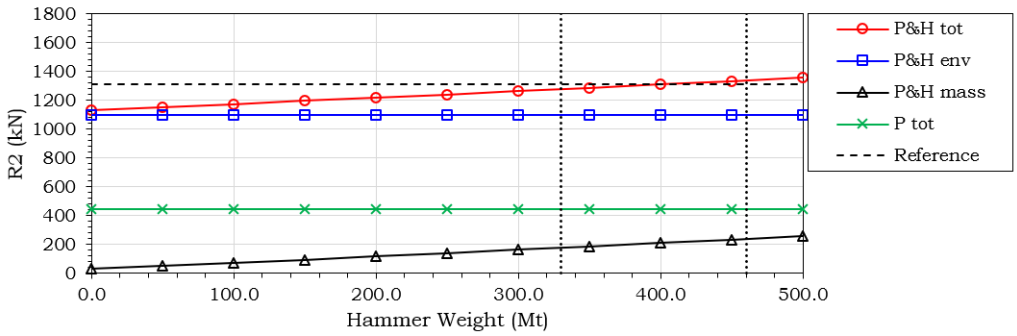

Figure 7.9: Reaction forces at top shims, with respect to the pile diameter

The reaction force increases with the weight of the hammer. The higher the hammer weight, the higher internal moment, and therefore higher reaction forces at the shims. Although, for the current used hammer weights, the differences are not significant.

8

Conclusions and Recommendations

8.1. Conclusions

The Pile Installation Frame (PIF), with interchangeable connections between the original sleeves and the center base frame, is the most feasible conceptual design to alter the existing PIF design. This concept, shown in figure 8.1, contains eight interchangeable frames. Moreover, the center base frame (with equipment and a lifting point) is usable for all footprint configurations. According to the trade-off, this concept requires the least investment costs for the modifications, because the existing sleeve connections are reused. However, the operational time to adjust the footprint is relatively time consuming. Assuming the footprint is not adjusted on a regular base, this is of secondary importance.

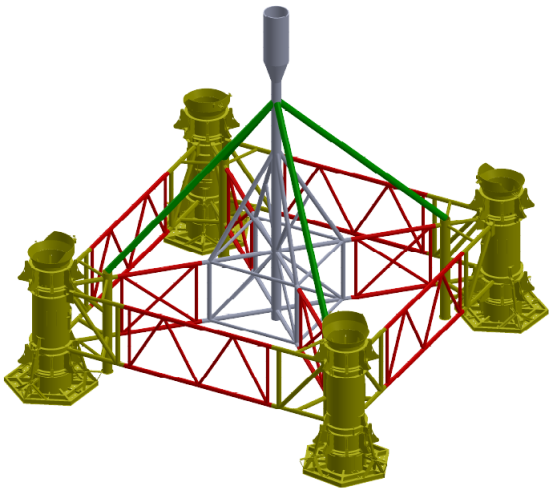

Figure 8.1: Conceptual adjustable PIF design with the maximum footprint of 32 meter

The new generated model to calculate the reaction forces from the pile onto the shims, including second order bending effect is developed and verified. From the verification, it is concluded that:

- The iteratively calculated second order bending, converges when the pile is capable to withstand the bending forces. So, the model is stable.
- The reaction forces due to the weight of the pile and the hammer are exactly equal to the model in the structural simulation software SACS.
- The environmental forces over time are within one percent difference with the SACS model. But, when the horizontal velocity component of the wave change signs in time, an offset occurs. The maximum environmental force is not at this offset. So, this will not influence the end results of the adjustable PIF integrity check.

The integrity of the conceptual PIF is checked with three models in the structural simulation software SACS. For the minimum square footprint of 20 meter, the reference footprint of 24 meter and the maximum footprint of 32 meter. From these models, it is concluded that:

- The deflections at the pile supports (shims), for the in-place condition (at the seabed with four piles and a hammer) are relatively small. This deflections are not critical for the pile installation tolerances, since these are in the same order than the current PIF.
- The ratio between the maximum stress and allowable stress of the members and braces are in the same order for the different footprint. The maximum ratio is under 0.4 for the representative reference condition, which is the Beatrice offshore wind farm.

From the analyses of the influences of variations in design conditions, it is concluded that:

- The forces in the members and braces of the frame are mainly caused by the reaction forces between the piles and shims transferred to the PIF
- The forces onto the shims in the sleeve are maximum when the hammer is at the seawater surface. This is because a section of the hammer diameter is wider than the pile.
- The pile diameter of 2.2 meter is the optimum for the reference conditions. Increasing the pile diameter gives higher force due to environmental loads, decreasing the diameter results in higher loads due to bending.
- The influence of the pile thickness is not considerable with respect to the forces onto the frame. Because the thickness is relatively small to the diameter.

8.2. Recommendations

When the footprint of the PIF should be adjusted on a regular basis, the operational costs become more important than the investment costs. In that case the conceptual design, where the sleeves can slide to all positions, should be considered. The adjustment of this concept is less time consuming during offshore operation. So, the more the frame needs to be adjusted, the more interesting this concept becomes.

Modifying the calculation pile-shims reaction forces model, by solving the offset with the SACS model. Because, the results of the second pile (pile without hammer), can be effected by the offset in the model (in some wave/ current conditions). Although, the influences of the offset in reaction forces are small with respect to the total reaction forces.

Include wind load to the model. When the wind load is in the same direction as the wave and current loads, the stresses in the frame becomes higher.

Check the on-bottom stability of the PIF. For this check another ISO load factor combination should be applied. When the overturning moment due to the environmental forces becomes high with respect to the weight of the PIF, the PIF can fall over.

Include an integrity analyses for the transport and lift scenarios. These scenarios induces other loads and therefore, the stresses in the frame becomes different.

Check the braces and the members on punching. If the check fails, connections between the members and braces should be strengthened.

When tighter installation tolerances are required for a particular project, it is recommended to reduce the gap between the pile and the shims. Because, the tilt due to the gaps between the shims and the pile induces the largest angle with respect to vertical.

A

Appendix

A.1. Adjustable PIF with Maximum Footprint on Deck of the Vessels

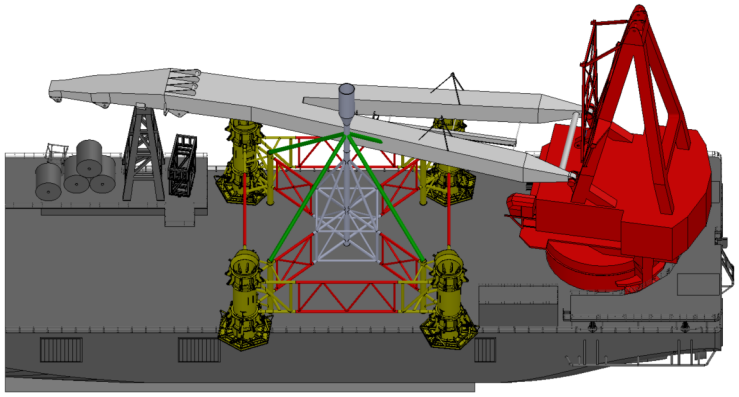

Figure A.1: Deck Stanislav Yudin with adjustable PIF maximum footprint (32x32)

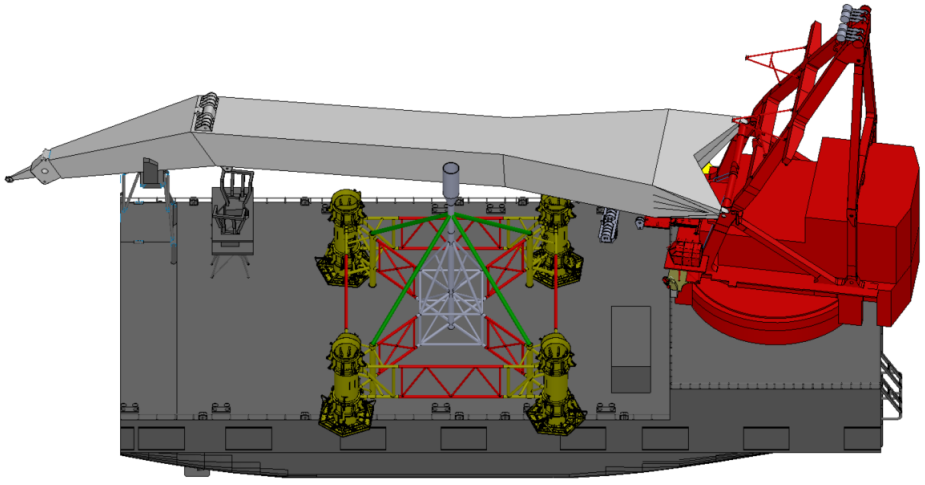

Figure A.2: Deck Oleg Strashnov with adjustable PIF maximum footprint (32x32)

A.2. Drag and Inertia Constants

Table A.1: Drag and Inertia constants per diameter tubular (ISO [2])

Diameter		**CD**	**CI (CM)**
inch	m	-	-
12	0.305	0.61	1.39
24	0.610	0.665	1.4
48	1.219	0.72	1.45
72	1.8289	0.756	1.67
96	2.438	0.781	1.67
120	3.048	0.799	1.71

A.3. Profile of Wave Velocity and Acceleration over the Water Depth

The distributions of the velocity and acceleration over the water depth are shown in figure 5.8a and 5.8b.

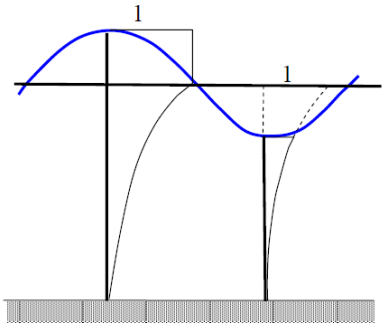

Figure A.3: Extrapolated stretching

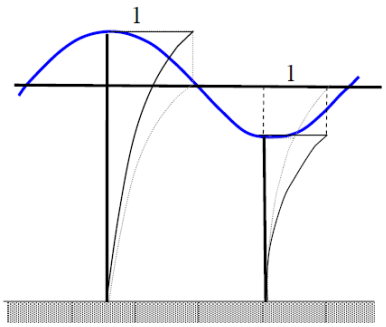

Figure A.4: Wheeler stretching

A.4. Reference Conditions

The representative reference conditions are from the Beatrice offshore wind farm project [6]. These are given in the following list:

1. Sea states:
   (a) Operational in place conditions: see table 3.2
   (b) Survival condition: $H_s = 3.5\ m$ with $t_p = 6.9\ s$
2. Design water depths:
   (a) Maximum: $d_{max} = 60.53\ m \rightarrow$ LAT + tidal + positive surge = 55.00 m + 4.66 m + 0.87 m = 60.53 m
   (b) Minimum: $d_{min} = 37.40\ m \rightarrow$ LAT + negative surge = 38.00 m - 0.60 m = 37.40 m
3. Current velocity: $u_c = 1.11\ m/s$ (different approaches of the current velocity profile over the depth are given in figure 5.9)
4. Hammer (IHC S-2500)
   : Mass: $m_{ham} = 390\ MT$
   : Dimensions hammer are given in the appendix, figure A.5
5. Pile design:
   (a) Length: $L_{pile} = 55\ m$
   (b) Diameter: $D_{pile} = 2.2\ m$
   (c) Thickness: $t_{pile} = 50\ mm$
   (d) Material: Steel S355
6. Initial pile soil penetration depth: 1.3 m

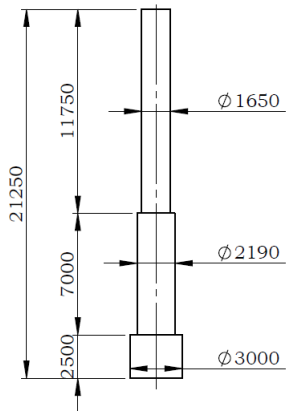

Figure A.5: Dimensions hydraulic hammer IHC S-2500

A.5. Shear Forces and Moments From Hammer on Top of Pile

Shear forces

$$-S_{H,2} = \int_b^a F_M dz \quad \text{with} \quad \begin{cases} a = z_{H,1} & \text{if } z_{H,1} \geq 0 \\ a = 0 & \text{if } z_{H,1} < 0 \end{cases} \quad \text{and} \quad \begin{cases} b = z_{H,2} & \text{if } z_{H,2} \geq 0 \\ b = 0 & \text{if } z_{H,2} < 0 \end{cases} \tag{A.1}$$

$$-S_{H,3} = S_{H,2} + \int_d^c F_M dz \quad \text{with} \quad \begin{cases} c = z_{H,2} & \text{if } z_{H,2} \geq 0 \\ c = 0 & \text{if } z_{H,2} < 0 \end{cases} \quad \text{and} \quad \begin{cases} d = z_{H,3} & \text{if } z_{H,3} \geq 0 \\ d = 0 & \text{if } z_{H,3} < 0 \end{cases} \tag{A.2}$$

$$-S_{H,4} = S_{H,3} + \int_f^e F_M dz \quad \text{with} \quad \begin{cases} e = z_{H,3} & \text{if } z_{H,3} \geq 0 \\ e = 0 & \text{if } z_{H,3} < 0 \end{cases} \quad \text{and} \quad \begin{cases} f = z_{H,4} & \text{if } z_{H,4} \geq 0 \\ f = 0 & \text{if } z_{H,4} < 0 \end{cases} \tag{A.3}$$

Moments

$$-M_{H,2} = \int_b^a F_M dz \quad \text{with} \quad \begin{cases} a = z_{H,1} & \text{if } z_{H,1} \geq 0 \\ a = 0 & \text{if } z_{H,1} < 0 \end{cases} \quad \text{and} \quad \begin{cases} b = z_{H,2} & \text{if } z_{H,2} \geq 0 \\ b = 0 & \text{if } z_{H,2} < 0 \end{cases} \tag{A.4}$$

$$-M_{H,3} = M_{H,2} + \int_d^c F_M dz \quad \text{with} \quad \begin{cases} c = z_{H,2} & \text{if } z_{H,2} \geq 0 \\ c = 0 & \text{if } z_{H,2} < 0 \end{cases} \quad \text{and} \quad \begin{cases} d = z_{H,3} & \text{if } z_{H,3} \geq 0 \\ d = 0 & \text{if } z_{H,3} < 0 \end{cases} \tag{A.5}$$

$$-M_{H,4} = M_{H,3} + \int_f^e F_M dz \quad \text{with} \quad \begin{cases} e = z_{H,3} & \text{if } z_{H,3} \geq 0 \\ e = 0 & \text{if } z_{H,3} < 0 \end{cases} \quad \text{and} \quad \begin{cases} f = z_{H,4} & \text{if } z_{H,4} \geq 0 \\ f = 0 & \text{if } z_{H,4} < 0 \end{cases} \tag{A.6}$$

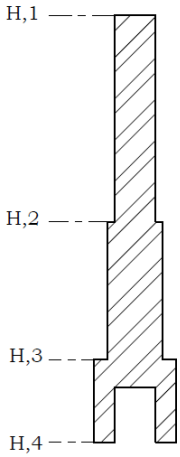

Figure A.6: Hammer sections defined

A.6. SACS Model Exposed to Individual Loads

Figure A.7: Pile with hammer on top

Figure A.8: Wave force

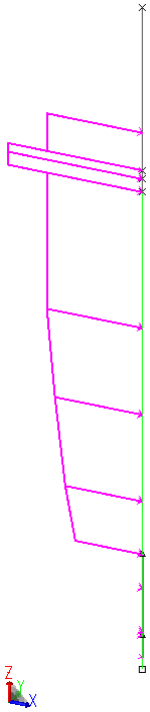

Figure A.9: current force

Figure A.10: Horizontal force component hammer

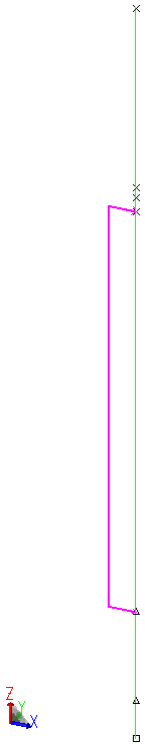

Figure A.11: Horizontal component pile

A.7. Second Order Calculation Method of Current PIF

The second order bending occurs due to the own mass of the piles. The calculation is iterative, since, due to deflection, the pile mass will create more deflection and so on.

The initial angle is depended on the initial tilt of the pile, and the initial banding because of the environmental force. The bending because of the environmental force is an output from SACS simulation software.

calculated according to:

$$\theta_{tilt} = \frac{L_A}{L_B} \cdot \Delta_{gap} \tag{A.7}$$

$$\theta_{env} = d_{env,sacs} / L_A \tag{A.8}$$

$$\theta_0 = \theta_{tilt} + \theta_{env} \tag{A.9}$$

Then the moment is calculated with the initial angle θ_0.

$$M_i = \theta_i \cdot F_{pile} \cdot \frac{1}{2} \cdot L_A + \theta_i \cdot F_{ham} \cdot L_A \tag{A.10}$$

With the calculated moment M_i of equation A.10 the new bending angle is calculated:

$$\theta_{i+1} = \theta_0 + \frac{M_i L_A}{EI} \tag{A.11}$$

The new bending angle θ_{i+1} is submitted in the moment equation A.10, and the following bending angle again calculated with equation A.11. This is the iterative process. When the difference of the calculated moment (M_{i+1}) with the previous calculated moment (M_i) is almost zero, the equilibrium is achieved.

Subsequently, the forces into the shims are calculated by:

$$F_{shim1,2} = M_r \cdot \frac{L_B}{2} \tag{A.12}$$

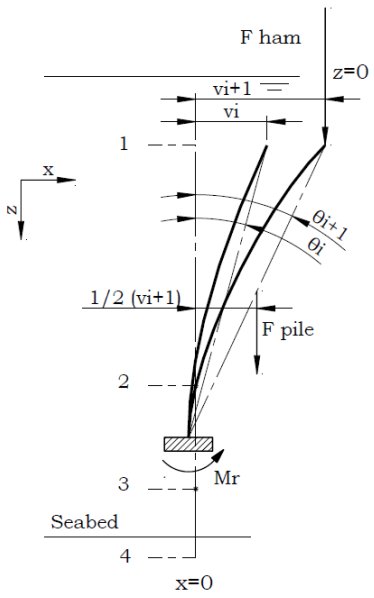

Figure A.12: FBD of current bending calculation method

A.8. On-bottom Stability

In the following is explained what influence of the mass and the buoyancy is on the stability.

Figure A.13 represents the PIF with the piles stabbed in the sleeves. Static equilibrium of moments equals zero. When this is not the case the system, in this case the PIF, is unstable.

$$\Sigma M_R = 0 \rightarrow F_e \cdot a - (F_g - F_b) \cdot \frac{1}{2} b + F_{r1} \cdot b = 0 \tag{A.13}$$

If the moments of the system do not equals zero, the system is not static. In this case the PIF is unstable and will fall over. Rewriting equation A.13 gives the force due to the mass what should be higher than the external forces due to the environmental and the reaction forces of the bottom.

$$F_g - F_b > \frac{F_e \cdot a + F_{r1} \cdot b}{\frac{1}{2} b} \tag{A.14}$$

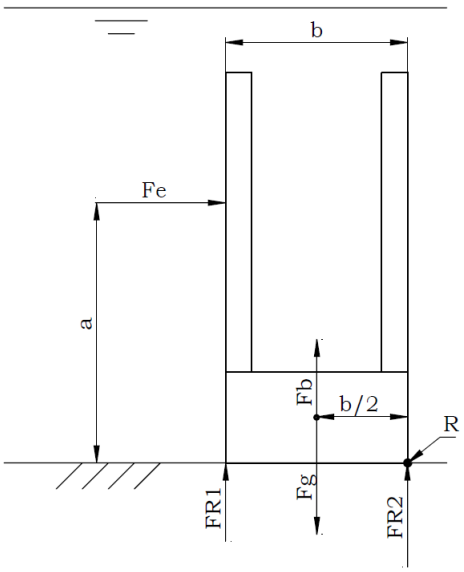

F_e = environmental force
F_g = gravitational force
F_b = buoyancy force
F_{r1} = reaction force 1
F_{r2} = reaction force 2
R = rotation point

Figure A.13: Stability of the PIF in survival condition

Structural Load on Adjustable PIF

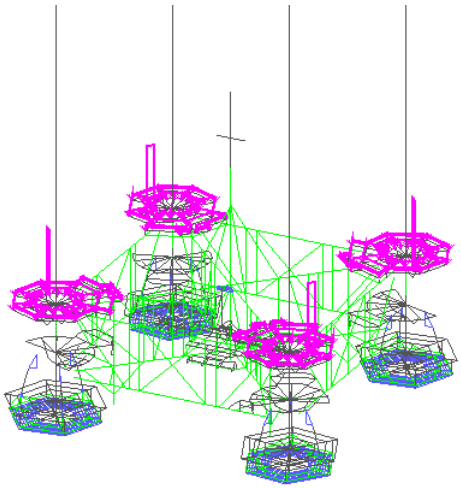

Figure A.14: Access platforms sleeve top

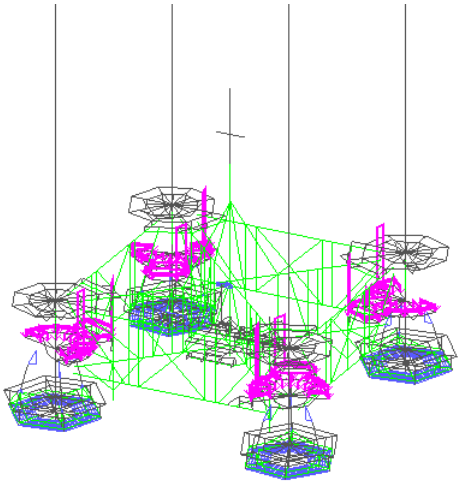

Figure A.15: Acces platforms sleeve middle

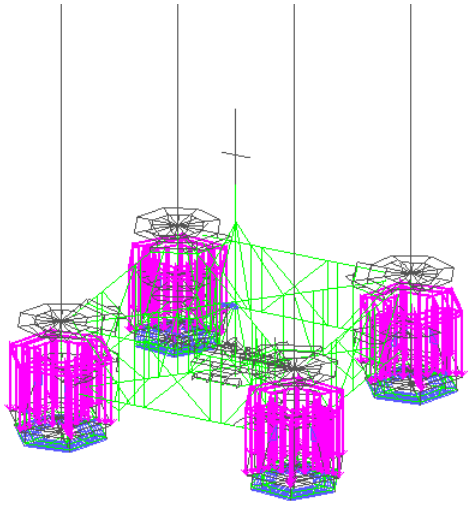

Figure A.16: Access platforms sleeve bottom

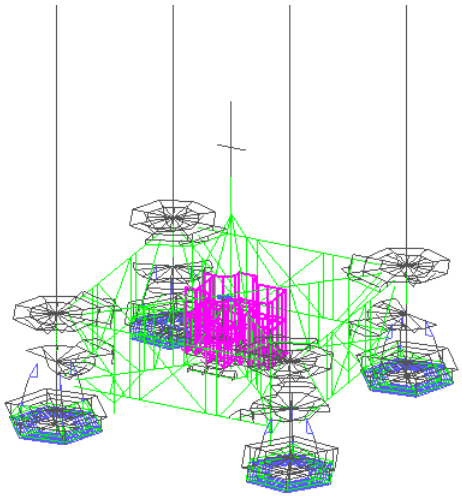

Figure A.17: Center platform

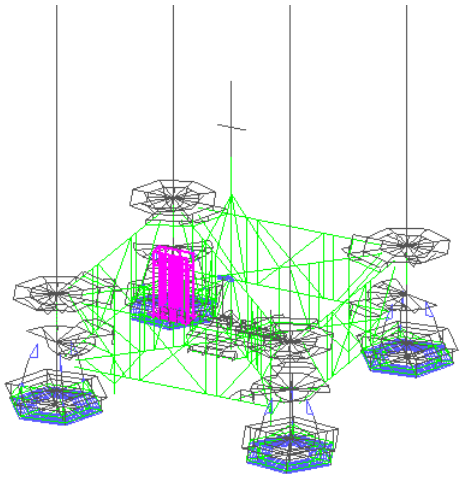

Figure A.18: Umbilical termination platform

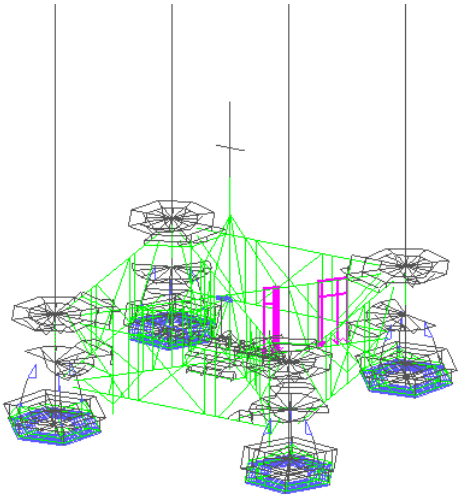

Figure A.19: Walkway

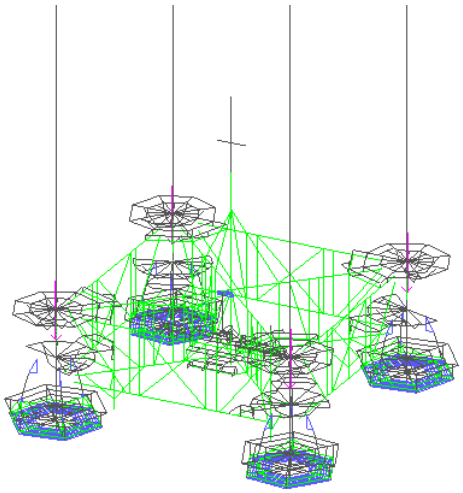

Figure A.20: Sleeve additional structural items

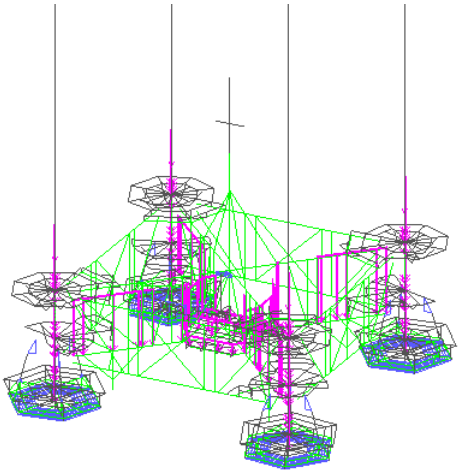

Figure A.21: Cables and hydraulics with supports

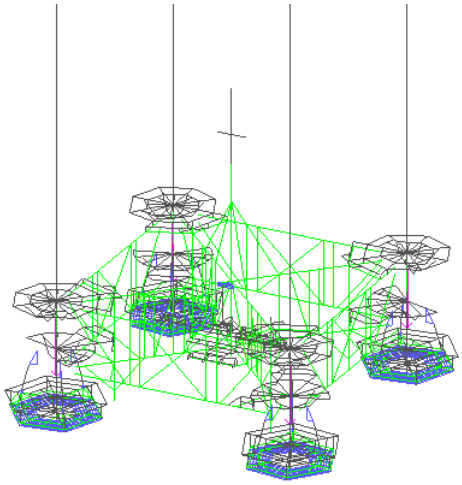

Figure A.22: Lower shims

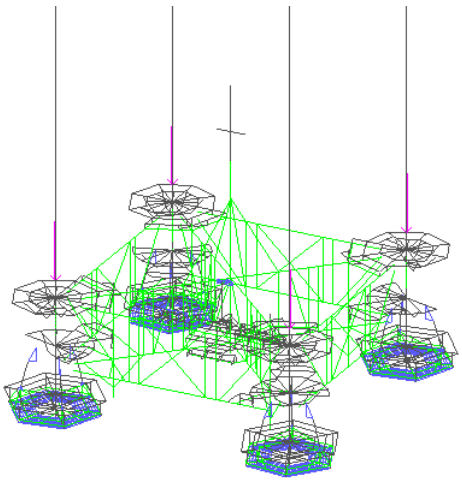

Figure A.23: Upper shims

A.9. Equipment Load on Adjustable PIF

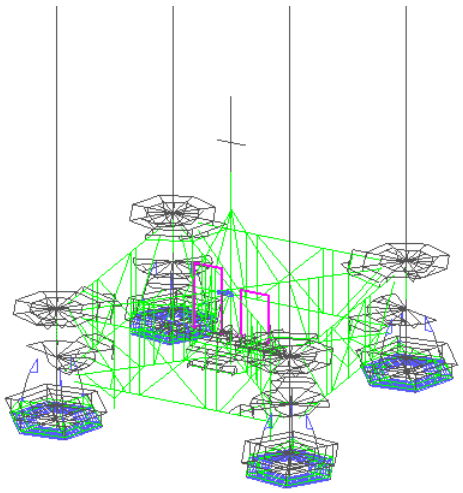

Figure A.24: Base frame

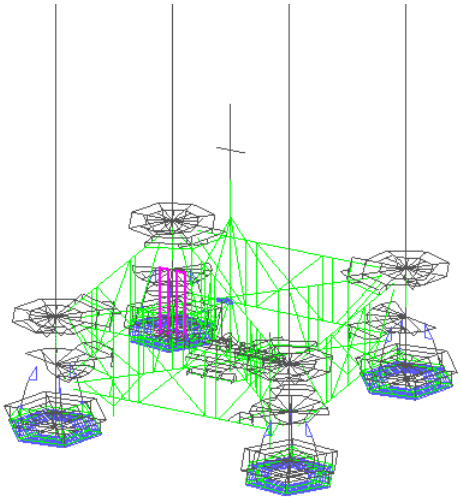

Figure A.25: Umbilical termination

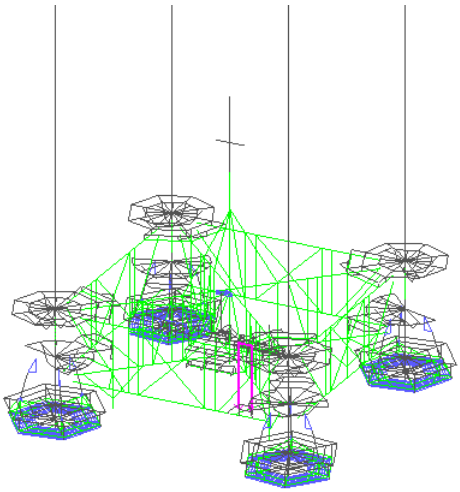

Figure A.26: Hot stab

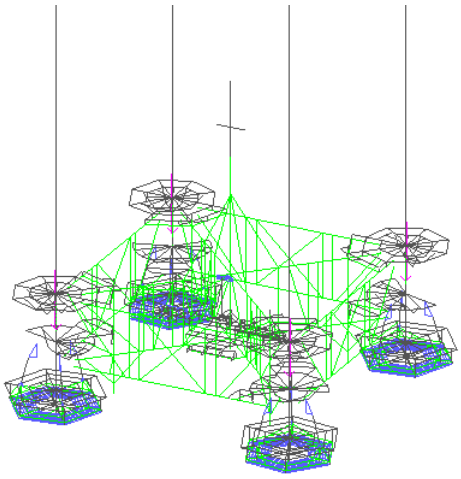

Figure A.27: Tube level sensors

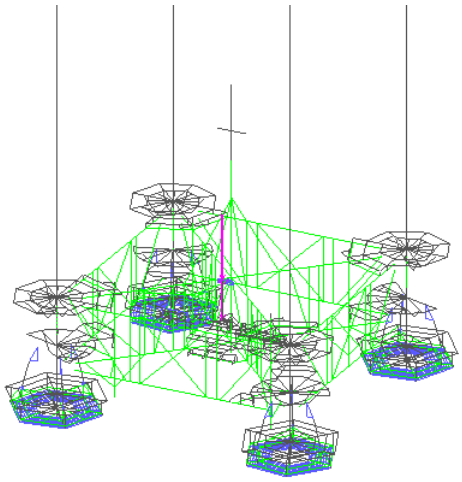

Figure A.28: Main compensator

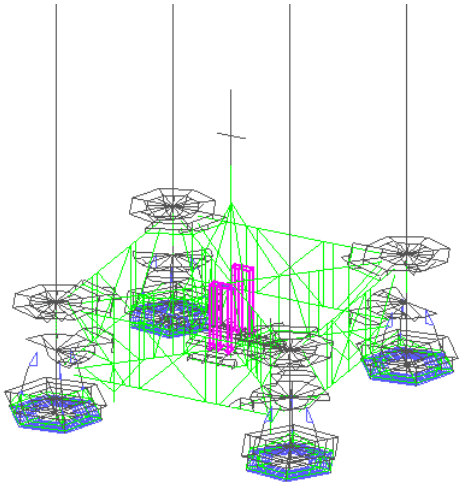

Figure A.29: PIF compensation sensor

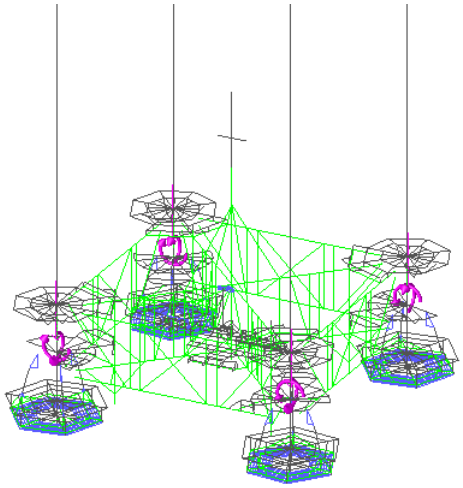

Figure A.30: PPSM

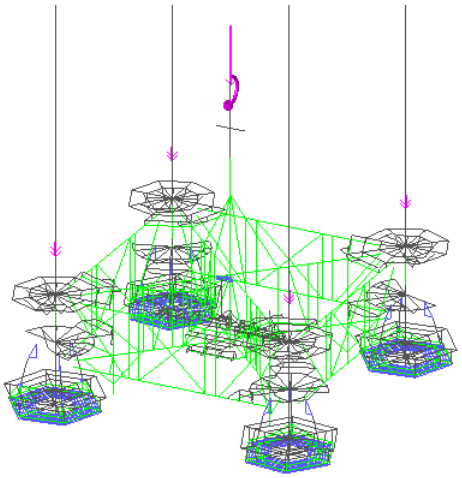

Figure A.31: Cameras, lasers at ILT and catcher

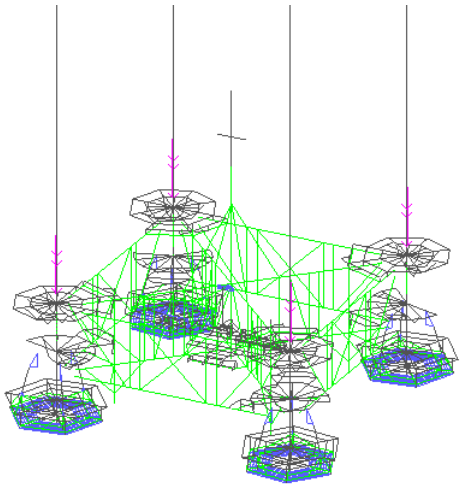

Figure A.32: Lamps at pile catchers, cameras and lasers at sleeves

A.10. Detailed Unity Check Calculation by Hand

The forces and moments are gained from the results of SACS, with these the member unity checks are calculated according to the ISO code.

Geometric Properties of the Member

Cross sectional area A:

$$A = \frac{\pi}{4}\left(D^2 - (D-2t)^2\right) \tag{A.15}$$
$$A = \frac{\pi}{4}\left(457^2 - (457-2\cdot 12.7)^2\right) = 177.3\cdot 10^2 \quad mm^2$$

Moment of inertia of the cross section I; since tubular member $I_x = I_y$:

$$I = \frac{\pi}{16}\left(D^4 - (D-2t)^4\right) \tag{A.16}$$
$$I = \frac{\pi}{16}\left(457^4 - (457-2\cdot 12.7)^4\right) = 437.8\cdot 10^6 \quad mm^4$$

Polar moment of inertia of the cross section I_p:

$$I_p = \frac{\pi}{32}\left(D^4 - (D-2t)^4\right) \tag{A.17}$$
$$I_p = \frac{\pi}{32}\left(457^4 - (457-2\cdot 12.7)^4\right) = 218.9\cdot 10^6 \quad mm^4$$

Radius of gyration r:

$$r = \sqrt{\frac{I}{A}} \tag{A.18}$$
$$r = \sqrt{\frac{437.8\cdot 10^6}{177.3\cdot 10^2}} = 157.1 \quad mm$$

Slenderness parameter λ:

$$\lambda = \frac{KL}{\pi r}\sqrt{\frac{f_{ys}A}{EI}} = \frac{r}{L} \tag{A.19}$$
$$\lambda = \frac{r}{L} \quad \rightarrow \quad \lambda = 0.000109 \tag{A.20}$$

Elastic section modules

$$Z_e = \frac{\pi}{32D}\left(D^3 - (D-2t)^3\right) \quad = \quad \left(\frac{I}{D/2}\right) \tag{A.21}$$
$$Z_e = \frac{\pi}{32\cdot 457}\left(457^3 - (457-2\cdot 12.7)^3\right) = 191.5\cdot 10^4 \quad N/mm^3$$

Plastic section modules

$$Z_p = \frac{1}{6}\left(D^3 - (D-2t)^3\right) \tag{A.22}$$
$$Z_p = \frac{1}{6}\left(457^3 - (457-2\cdot 12.7)^3\right) = 250.8\cdot 10^4 \quad N/mm^3$$

Calculating of Stresses

Hydrostatic Pressure p (γ_e from table 6.10):

$$p = \gamma_e \rho_f g H_z \tag{A.23}$$
$$p = 1.35 \cdot 1025 \cdot 9.81 \cdot 63.625 = 0.640 \quad N/mm^2$$

Axial tensile stress σ_t :

$$\sigma_t = \frac{f_x}{A} \tag{A.24}$$
$$\sigma_t = \frac{-708.9655 \cdot 10^3}{177.3 \cdot 10^2} = -39.994 \quad N/mm^2$$

Bending Stress σ_b

$$\sigma_b = \frac{M}{Z_e} \tag{A.25}$$
$$\sigma_{b,y} = \frac{-187.2461 \cdot 10^3}{191.5 \cdot 10^4} = -97.735 \quad \text{and} \quad \sigma_{b,z} = \frac{2.2139 \cdot 10^3}{191.5 \cdot 10^4} = 1.1556 \quad N/mm^2$$

Shear Stress τ_b

$$\tau_b = \frac{2V}{A} \tag{A.26}$$
$$\tau_b = \frac{2 \cdot 407.6757 \cdot 10^3}{177.3 \cdot 10^2} = 45.995 \quad N/mm^2$$

Torsional Shear stress τ_t

$$\tau_t = \frac{MD}{2I_p} \tag{A.27}$$
$$\tau_t = \frac{-9.149 \cdot 10^3 \cdot 457}{2 \cdot 218.9 \cdot 10^6} = -2.3877 \quad N/mm^2$$

Hydro hoop stress σ_h

$$\sigma_h = \frac{pD}{2t} \tag{A.28}$$
$$\sigma_h = \frac{0.640 \cdot 457}{2 \cdot 12.7} = 14.964 \quad N/mm^2$$

Capped-end stress is a compressive axial stress due to capped-end hydrostatic actions calculated using the value of pressure (p) (always positive):

$$\sigma_q = 0.5\sigma_h \tag{A.29}$$
$$\sigma_q = 0.5 \cdot 14.964 = 7.482 \quad N/mm^2$$

From the calculated stresses is concluded that the critical member has a negative stress, which means the member is in tension. Therefore, the member have not to be checked for compression.

Unity checks

The tubular members subjected independently to tension, compression, bending, shear or hydrostatic pressure shall be designed to satisfy the strength and stability requirements [2]. Also combinations are checked. This is calculated in the subsequent.

Compression

$$U_m = \frac{\sigma_t}{f_t/\gamma_{R,t}} \tag{A.30}$$

$$U_m = \frac{\sigma_t}{f_t/\gamma_{R,t}} \quad \rightarrow \quad U_m = 0.0967 \quad \rightarrow \quad U_m = 0.0967 \tag{A.31}$$

With:

$$f_t = f_t \quad \rightarrow \quad f_t = 355.00 \tag{A.32}$$

Beam Shear

$$U_m = \frac{\tau_b}{f_v/\gamma_{R,v}} \quad \rightarrow \quad U_m = 0.205 \tag{A.33}$$

With:

$$f_t = f_y//sqrt3 \quad \rightarrow \quad f_t = 204.959 \quad N/mm^2 \tag{A.34}$$

Torsional Shear

$$U_m = \frac{\tau_t}{f_v/\gamma_{R,v}} \quad \rightarrow \quad U_m = 0.008 \tag{A.35}$$

Combined Shear
The utilization of the member under torsional shear in combination with beams shear:

$$U_m = \frac{\tau_b + \tau_t}{f_v/\gamma_{R,h}} \quad \rightarrow \quad U_m = 0.2133 \tag{A.36}$$

Hoop buckling
The utilization of the member under external pressure:

$$U_m = \frac{\sigma_h}{f_h/\gamma_{R,h}} \quad \rightarrow \quad U_m = 0.1342 \tag{A.37}$$

With f_h is the representative hoop buckling strength, and since $f_{he} < 00.55 f_y$:

$$f_h = f_{he} \quad \rightarrow \quad f_h = 139.319 \quad N/mm^2 \tag{A.38}$$

The representative elastic critical hoop buckling strength f_{he} is:

$$f_{he} = 2C_h Et/D \quad \rightarrow \quad f_{he} = 139.319 \quad N/mm^2 \tag{A.39}$$

Since, $\mu > 1.6D/t$, the critical hoop buckling coefficient C_h is:

$$C_h = 0.44t/D \quad \rightarrow \quad C_h = 0.0122 \quad N/mm^2 \tag{A.40}$$

Where μ is a geometric parameter:

$$\mu = \frac{L}{D}\sqrt{\frac{2D}{t}} \quad \rightarrow \quad \mu = 7.611 \tag{A.41}$$

Bending and Hydrostatic
The utilization of the member bending and hydrostatic pressure shear in combination with beams shear:

$$U_m = \frac{\sigma_b}{f_b/\gamma_{R,b}} \quad \rightarrow \quad U_m = 0.225 \tag{A.42}$$

Since, $f_y D/(Et) = 0.0623$ which is in between 0.0517 and 0.1034:

$$f_b = \left(1.13 - 2.58 \cdot \frac{F_y D}{Et}\right) \frac{Z_p}{Z_e} f_y \quad \rightarrow \quad f_b = 450.37 \tag{A.43}$$

Tension ,Bending and Hydrostatic
The representative *yield strength* f_y is given in table 6.8.

Unity check for axial tension, bending and hydrostatic pressure

$$U_m = \frac{\gamma_{R,t}\sigma_{t,c}}{f_{t,h}} + \frac{\gamma_{R,b}\sqrt{\sigma_{b,y}^2 + \sigma_{b,z}^2}}{f_{b,h}} \quad \rightarrow \quad U_m = 0.302 \tag{A.44}$$

Since the tension stress is higher than the cabbed end stress, the combined tensile stress $\sigma_{t,c}$ is:

$$\sigma_{t,c} = \sigma_t - \sigma_q \quad \rightarrow \quad \sigma_{t,c} = -40.171 \quad N/mm^2 \tag{A.45}$$

The axial tensile strength in presence of external hydrostatic pressure $f_{t,h}$:

$$f_{t,h} = f_y\left(\sqrt{1 + 0.09B^2 - B^{2\eta}} - 0.3B\right) \quad \rightarrow \quad f_{t,h} = 340.989 \tag{A.46}$$

The axial bending strength in presence of external hydrostatic pressure $f_{b,h}$

$$f_{b,h} = f_b\left(\sqrt{1 + 0.09B^2 - B^{2\eta}} - 0.3B\right) \quad \rightarrow \quad f_{b,h} = 432.594 \tag{A.47}$$

With:

$$B = \frac{\gamma_{R,h}\sigma_h}{f_h} \quad \rightarrow \quad B = 0.134 \tag{A.48}$$

And:

$$\eta = 5 - 4\frac{f_h}{f_y} \quad \rightarrow \quad \eta = 3.430 \tag{A.49}$$

A.11. Detailed Unity Check Results From SACS

```
>>>>>>>>>>>>>>>>>>>>>>>>>>>>>>>>>>>>>>>>>>>>>>>>>>>
   Detailed review report of member  B073 - 0062

<<<<<<<<<<<<<<<<<<<<<<<<<<<<<<<<<<<<<<<<<<<<<<<<<<<


Units: Length -(cm)          Force -(kN)         Stress -(N/mm2)

Design Code - ISO 19902:2007(E)
   (Ultimate limit state)

- Resistance Factors

Tension    1.0500     Compression    1.1800

Bending    1.0500     Shear          1.0500

Hoop Buckling    1.2500

------------------------------------------------------------------------


****** Member Infomation ******

Group                                 A1

Section Name                          Tubular

Total Length                              0.41   (m)

Location                                  0.00   (m)

Segment                               1 of 1

LC Option                             List

Critical LC                           D315

------------------------------------------------------------------------
```

```
****** Basic Properties ******

Section Type                          Tubular

Outer Diameter                        45.70

Wall Thickness                         1.27

Elastic Modulus                      205.00   1000(N/mm2)

Shear Modulus                         82.00   1000(N/mm2)

Yield Strength                       355.01   (N/mm2)

Axial Area              A            177.27

Mom. of Inertia         Iy         4.4E+004

Mom. of Inertia         Iz         4.4E+004

Shear Area Y                          88.63

Shear Area Z                          88.63

Tors. Constant          J          8.8E+004

-------------------------------------------------------------------------


****** Member's Properties ******

Slenderness Ratio     (KL/r)y          2.59

Slenderness Ratio     (KL/r)z          2.59

Radius of Gyration      ry            15.71

Radius of Gyration      rz            15.71

Eff. Length Factor      Ky             1.00

Eff. Length Factor      Kz             1.00

Overall Buck. Length    Ly             0.41   (m)

Overall Buck. Length    Lz             0.41   (m)

              Final (K*L)y             0.41   (m)

              Final (K*L)z             0.41   (m)

TUB Ring Spacing                       INF

Reduction Factor        Cmy            0.85

Reduction Factor        Cmz            0.85

-------------------------------------------------------------------------
```

****** End Forces and Moments ((kN), (kN-m)) ******

Tor. Moment	Mx	-9.1490
Bending Moment	My	-187.2461
Bending Moment	Mz	2.2139
Axial force	fx	-708.9655
Shear force	fy	1.8068
Shear force	fz	407.6757

****** Acting Stresses (N/mm2) ******

Axial stress	fa	-39.9940
Bending Major	fby	-97.7352
Bending Minor	fbz	1.1556
Shear	fv	45.9959
Torsional Shear	fvt	-2.3877
Hydro Hoop Stress	fh	14.9589

```
****** Basic Allowable Stresses (w/o. Rsist Fact.) (N/mm2) ******

Axial Tension                   Ft          355.0002     (Eq 13.2-1)

Shear                           Fv          204.9595     (Eq 13.2-16)

Axial Compression               Fc          354.8840     (Eq 13.2-5,6)

                          (Lambda)            0.0343     (Eq 13.2-7)

Local Buckling                  Fyc         355.0002     (Eq 13.2-8,9)

Elastic Local Buckling          Fxe        3418.1636     (Eq 13.2-10)

Bending                         Fb          450.3694     (Eq 13.2-13~15)

Euler Buckling Y                Fey      301637.0000     (Eq 13.3-5)

Euler Buckling Z                Fez      301637.0000     (Eq 13.3-6)

--- Reported Allowable Stresses (with Resist. Factors)

Axial                                 300.8476

Major Axis Bending                    412.0003

Minor Axis Bending                    412.0003

Shear in Local Y                      195.1995

Shear in Local Z                      195.1995

Euler Buckling                     301637.0000

------------------------------------------------------------------------------
```

****** Hydrostatic Analysis ******

--- Parameters

Water Depth	d	63.6250	(m)
Water Depth at Member	z	63.6250	(m)
Wave Height	Hw	0.0000	(m)
Wave Length	L	N/A	
Hydrostatic Pressure	p	0.6396	(N/mm2)
Load Factor	Lh	1.3000	
Hydro Hoop Stress	fh	14.9589	(N/mm2)

--- Applied Stresses (N/mm2) (Not including Capped-end Actions)

Capped-end Stress	fq	7.4795	
Axial Stress	fa	-39.9940	
	fa,c	-47.4735	
Bending Stress Y	fby	-97.7352	
Bending Stress Z	fbz	1.1556	
Max Comb. Comp. Stress	fx	145.2155	

```
--- Hydro-related Allowable Stresses (N/mm2)

Hoop buckling                Fh       139.3194     (Eq 13.2-23~25)

Elastic hoop buckling        Fhe      139.3194     (Eq 13.2-26)

Reduced Axial Tensile        Ft,h     340.9990     (Eq 13.4-8)

Reduced Axial Compressive    Fc,h     347.4070     (Eq 13.4-15,16)

Reduced Bending              Fb,h     432.6003     (Eq 13.4-9)

Local Buckling               Fyc      355.0002     (Eq 13.2-8,9)

          - Parameter        CH   0.0122      (Eq 13.2-27~30)
                             AM  57.5748
                              B   0.1342      (Eq 13.4-10)
                            Eta   3.4302      (Eq 13.4-11)
                          Alpha   0.8000      (A.13.2.6.2)


--- Unity Checks with Hydro Pressure

Hoop Buckling                    (Eq 13.2-31)   0.1342

Compression + Bending            (Eq 13.4-19)   0.3950

                                 (Eq 13.4-20)   0.3375

Euler Buckling                                  0.0001

Max Combined Compressive         (Eq 13.4-21)   0.0495


Combined Shear             (Eq 13.2-17,19)   0.2479

-------------------------------------------------------------------------


-------------------------------------------------------------------------

********    Reported Unity Ratios     ********

Critical Unity Ratio                  0.3950     (C 13.4.3       )     CB+Hydro

Combined Unity Ratio                  0.3950

Axial Component                       0.1578

Bending Major Y-Y                     0.2372

Bending Minor Z-Z                     0.0000

Shear                                 0.2479

Torsional Shear                       0.0122

Euler Buckling                        0.0001
```

Bibliography

[1] Beatrice offshore wind farm. URL https://www.4coffshore.com/windfarms/beatrice-united-kingdom-uk53.html.

[2] Petroleum and natural gas industries - fixed steel offshore structures. Technical report, International Organization for Standardization.

[3] Beatricewind. URL https://www.beatricewind.com/.

[4] The engineering design process: Specify requirements. URL https://www.sciencebuddies.org/science-fair-projects/engineering-design-process/engineering-design-requirements.

[5] Paris agreement - climate action - european commission, 2017.

[6] Dimitris Chrysafopoulos. Beatrice offshore wind farm pif structural design report. Technical report, Seaway Heavy Lifting.

[7] Russell C. Hibbeler. *Sterkteleer*. Pearson.

[8] Andrew Ho and Ariola Mbistrova. The european offshore wind industry - key trends and statistics. Technical report, Wind Europe, January 2017.

[9] LEO H. Holthuijsen. *Waves in Oceanic and Coastal Waters*. Cambridge.

[10] A.V. Metrikine. *Dynamics, Slender Structures and an Introduction to Continuum Mechanics*. Faculty of Civil Engineering and Geosciences.

[11] Frances Robles, Kirk Semple, P. Vivian Yee, and C. Thomas. Caribbean devastated as irma heads toward florida. *The New York Times*, 2017.

Glossary

CAPEX Capital Expenses.

COG Center of Gravity.

env environmental.

EPCI Engineering, Procurement, Construction and Installation.

HLV Heavy Lift Vessel.

ILT Internal Lifting Tool.

LAT Lowest Astronomical Tide.

LRFD Load Resistance Factor Design.

MSL Mean Sea water Level.

OPEX Operating Expenses.

OWF Offshore Wind Farm.

PIF Pile Installation Frame.

SHL Seaway Heavy Lifting.

T&I Transport and Installation.

tot total.